SANDIA REPORT
SAND2017-XXXX
Unlimited Release
Printed Month and Year

Arc-Fault Primer: Numerical, Analytical, and Experimental Characteristics of Initiation and Sustainment of Arc Plasmas (DRAFT).

Kenneth M. Armijo, Jay Johnson, Richard K. Harrison, Salvador Rodriguez, Olga Lavrova and Eric J. Schindelholz

Prepared by
Sandia National Laboratories
Albuquerque, New Mexico 87185 and Livermore, California 94550

Sandia National Laboratories is a multi-mission laboratory managed and operated by Sandia Corporation, a wholly owned subsidiary of Lockheed Martin Corporation, for the U.S. Department of Energy's National Nuclear Security Administration under contract DE-AC04-94AL85000.

Issued by Sandia National Laboratories, operated for the United States Department of Energy by Sandia Corporation.

Available to DOE and DOE contractors from
U.S. Department of Energy
Office of Scientific and Technical Information
P.O. Box 62
Oak Ridge, TN 37831

Telephone: (865) 576-8401
Facsimile: (865) 576-5728
E-Mail: reports@osti.gov
Online ordering: http://www.osti.gov/scitech

Available to the public from
U.S. Department of Commerce
National Technical Information Service
5301 Shawnee Rd
Alexandria, VA 22312

Telephone: (800) 553-6847
Facsimile: (703) 605-6900
E-Mail: orders@ntis.gov
Online order: http://www.ntis.gov/search

SAND2017-XXXX
Unlimited Release
December 2016

Arc-Fault Primer: Numerical, Analytical, and Experimental Characteristics of Initiation and Sustainment of Arc Plasmas (DRAFT)

Kenneth M. Armijo, Jay Johnson, Richard K. Harrison, Salvador Rodriguez, Olga Lavrova and Eric J. Schindelholz

Sandia National Laboratories
P.O. Box 5800
Albuquerque, New Mexico 87185-1127

Abstract

While arc-faults are rare in electrical installations, many documented events have led to fires that resulted in significant damage to energy-generation, commercial and residential systems, as well as surrounding structures, in both the United States and abroad. Arc-plasma discharges arise over time due to a variety of reliability issues related to cable material degradation, electrical and mechanical stresses or acute conductive wiring dislocations. These may lead to discontinuity between energized conductors, facilitating arcing events and fires. Arc-flash events rapidly release significant energy in a localized volume, where the electric arc experiences a reduction in resistance. This facilitates a reduction in electrical resistance as the arc temperature and pressure can increase rapidly. Strong pressure waves, electromagnetic interference (EMI), and intense light from an arc pose a threat to electrical worker safety and system equipment. This arc-fault primer provides basic fundamental insight into arc-fault plasma discharges, and an overview of direct current (DC) and alternating current (AC) arc-fault phenomena. This primer also covers pressure waves and EMI arc-fault hazard analyses related to incident energy prediction and potential damage analysis. Mitigation strategies are also discussed related to engineering design and employment of protective devices including arc-fault circuit interrupters (AFCIs). Best practices related to worker safety are also covered, especially as they pertain to electrical codes and standards, particularly Institute of Electrical and Electronics Engineers (IEEE) 1584 and National Fire Protection Agency (NFPA) 70E. Throughout the primer various modelling and test capabilities at Sandia National Laboratories are also covered, especially as they relate to novel methods of arc-fault/arc-flash characterization and mitigation approaches. Herein, this work describes methods for producing and characterizing controlled, sustained arcs at atmospheric pressures as well as methods for mitigation with novel materials.

ACKNOWLEDGMENTS

Sandia National Laboratories is a multi-mission laboratory managed and operated by Sandia Corporation, a wholly owned subsidiary of Lockheed Martin Corporation, for the U.S. Department of Energy's National Nuclear Security Administration under contract DE-AC04-94AL85000. This work was primarily funded by the US Department of Energy Solar Energy Technologies Office. This material is also based upon work partially supported by the US Department of Homeland Security under Grant Award Numbers 2012-DN-130-NF0001-0202 and HSHQDC12X00059. The views and conclusions contained in this document are those of the authors and should not be interpreted as representing the official policies, either expressed or implied, of the US Department of Homeland Security.

CONTENTS

FIGURES

TABLES

1. INTRODUCTION

1.1 Arc-Discharge Overview

Electrons are the negatively charged particles that make up the outer shells of an atom. In materials that are good conductors (i.e., most metals like copper, gold, silver) the electrons in the outermost orbit can easily be knocked out and travel to another atom to facilitate electron movement or current. Electrical current is the measure of electrons flowing through a wire (measured in amps, symbolized by A), which can be analogous to water flowing in a pipe, where water molecules represent moving electrons. Voltage is a measure of the capability to push electrons through a wire (measured in volts, symbolized by *V*) though also commonly prescribed in some mathematical equations by *E*. Voltage can be analogous to water pressure, where pressure pushes water through a pipe, and as it increases, the amount of water flowing too increases. All batteries and generators provide direct current (DC), where current only flows in one direction and the voltage is constant. Within utility connections however, voltage and current takes on an alternating form (i.e., alternating current (AC)), where the voltage will build up to a maximum, then fall to a minimum, and then back to a maximum, Figure 1-1.

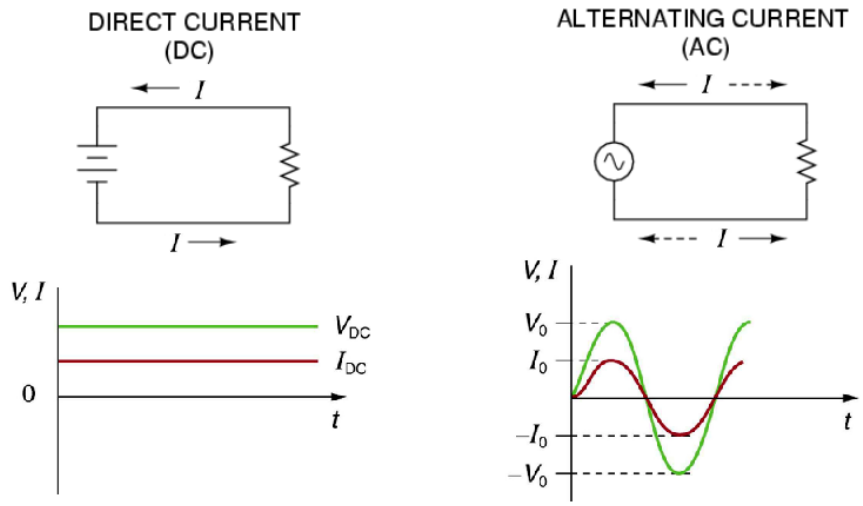

Figure 1-1. Direct current (DC) circuit vs. Alternating current (AC) circuit

For both DC and AC systems, when a break, or fault between two current-carrying conductors exists, arc discharges can arise as sustained electrical current propagates through a conductive plasma created by the breakdown of a gaseous dielectric medium (typically air), between the two conductors or electrodes. The dielectric strength of air is large until the arc ionizes the atmosphere, where the characteristic shape of an arc-discharge is facilitated as hot air rises rapidly. Physically, an arc is initiated by ionization as current increases between two electrodes. The potential for an arc being facilitated between two electrodes is the breakdown voltage, which is a function of the gap size, pressure in the discharge space, and the type of gas surrounding the electrodes. Given the right conditions, the current will continue to flow unabated until it is interrupted by an upstream over-current protective device or energy absorbing body. Such arcs release enormous energy, resulting in high temperatures, sound levels, pressures, as well as ejection of high-speed molten debris, shown in Figure 1-2. Arc-faults that do not fall into thermal equilibrium, can continue to expand in air facilitating an arc-flash event that can cause blasts in electrical transmission, distribution and utilization systems. This can lead to injuries and fatalities of electrical workers,

with estimated costs of hundreds of millions of dollars each year in downtime and damaged equipment [29].

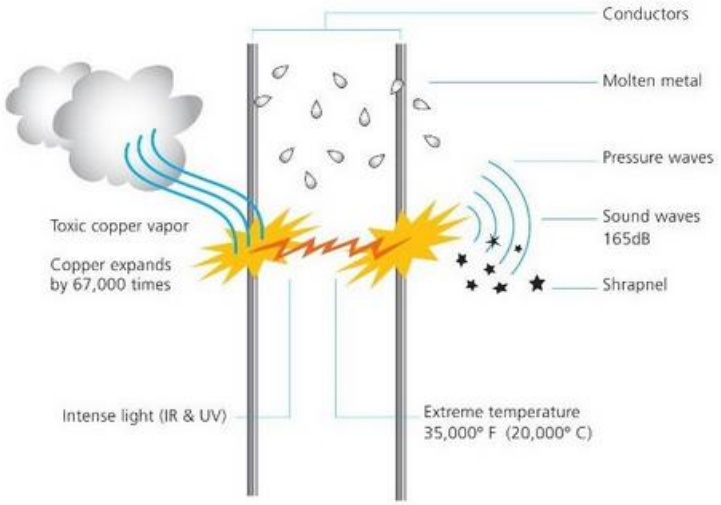

Figure 1-2. Potential damage from an arc-plasma discharge [1]

Electrical arcs experience incremental negative resistance, which causes the arc temperature to increase. Therefore, as the arc develops and gets hotter the resistance drops, drawing more current ("runaway") until some part of the system melts, trips, or evaporates, providing enough distance to break the circuit and extinguish the arc [2].

Although there are many types of electrical injuries, a ten-year study involving over 120,000 employees performed by Electricite de France found that electrical arc injuries accounted for 77% of all recorded electrical injuries [3]. This statistic has facilitated the relatively recent emphasis on arc-fault and arc-flash hazards research. The arcing phenomenon constitutes a unique hazard, because, unlike electric shock, serious injury and death can occur at some distance from the actual current path. The most frequently identified consequences of arc-flash incidents are:

1. Thermal burn injury
2. Blast pressure wave injury
3. Hearing loss injury
4. Harmful electromagnetic emissions
5. Release of highly toxic gases
6. Shrapnel injury

Thermal burn injuries are caused by direct heat exposure and ignition of clothing material. Strong pressure waves from an arc blast can throw workers or knock them off ladders or scaffolding. The blast sound waves emanating from an arc blast can cause hearing loss while the generated intense light can impair vision and cause blindness [3]. The temperatures generated by arc-flash events can vaporize all known materials, producing some highly toxic byproducts as a result in plasma clouds that may contain molten electrode material and the byproducts of burned insulation. Copper oxides, particularly deadly compounds, are formed when cooling copper vapor combines with oxygen that results in the formation of toxins that may cause damage to the lungs, skin, and eyes [3]. Rapidly expanding gases cause shrapnel to be propelled from an arc blast resulting in severe wounds. Electrical arcs produce some of the highest temperatures known to occur on earth, up to

19,426 °C—four times the temperature of the sun's surface—which is ~4,980 °C. These temperatures could also be high enough to super heat the air medium, as well as melt and/or vaporize the materials the plasma contacts [3]. During arc-faults, when electrode materials vaporize, they greatly expand in volume, notably Copper—67,000 times (compared to water at 1,670 times). The intense heat from an arc causes sudden expansion of air resulting in a blast with resultant high pressure waves. Arc discharges can spray droplets of molten metal at a high speed, where blast pressure waves can exceed measured values of higher than 2,000 lbs/ft^2 [3]. In confined spaces, such as a small room or an electrical cabinet, the blast can become more directed, magnified and more severe. In addition, the consequences of an arc-flash event can have a significant financial, impact which can lead to lost production from downtime and potential litigation costs. Further, a company's reputation may be affected by such incidences through the loss of ISO ratings and poor safety records [4].

Arc-faults are generally limited to systems where electrical bus voltage levels are in excess of 120 volts [5], where lower voltage levels normally will not sustain an arc and self-extinguish. The cause of an arc-fault electrical short normally burns away during the initial flash, where the arc-fault is then sustained by the establishment of a highly-conductive plasma. This plasma will conduct as much energy as is available, and is only limited by the impedance of the arc. This massive energy discharge can burn bus bars and wiring, vaporizing the electrodes and causing explosive volumetric increases, where an arc blast can facilitate an expansion of approximately 40,000 to 1 [5].

1.2 System Reliability and Arc-Faults

Arc-plasma discharges arise over time due to a variety of reliability issues related to cable material degradation, electrical and mechanical stress, wiring breakage or conductor separation, seen in Figure 1-3.

a. b.

Figure 1-3. a. Arc-plasma discharge between two conductors [6] and b. PV structure fire [7]

In general, there are two types of faults. The first type is a contact (or bolted) fault, characterized by a solidly connected fault path, which causes high levels of current to flow through a solid connect. Conversely, a second type of fault is facilitated as current flows through ionized air causing an arc. The significant difference between these two is that energy in a bolted fault condition is dissipated within faulted equipment while an arcing fault releases energy out into the surrounding environment. According to Jones [5] electrical arcs are typically facilitated by:

1. Inadvertent contact
2. Loose connections
3. Insulation failure
4. Poorly maintained equipment
5. Voltage transients
6. Unsuccessful short circuit interruption
7. Corrosion buildup on the conductor
8. Animal damage

Series arc-faults often occur in electrical systems due to corrosion or other conductor discontinuities [11]. Factors like humidity, contaminants, temperature, enclosure type, and material consumed in the arc can also affect the radiated energy level. Other factors like power factor, conductor gap distance, arc impedance, and arc duration also impact its severity [8]. According to Ammerman et al., [9] arc-flash incidents that arise from arc-faults, may occur in the workplace when tools are dropped, wiring errors occur, or physical connections are made between two energized conductors. Arcs may also be initiated without human intervention by mechanisms such as insulation breakdown and the buildup of conductive dusts [9].

1.3 Arc-Fault Characteristics

1.3.1 Types of Arc-Faults

Phenomenologically, arc-fault discharges (terminology defined in Appendix 4) may be established in three ways: 1. transition from a low current stable discharge such as a glow, 2. transient nonsteady spark discharge, and c. physical initiation. Additionally, arc-faults are facilitated by either series or parallel arc discharges, where a series arc discharge occurs when a conductor in series with the load breaks. In a series, configuration arc current cannot be greater than the load current that the conductor serves [10]. Traditionally, series wires and electrodes have historically received much attention regarding arc-faults as this configuration is often used to design power-system protective devices like circuit breakers and fuses. As shown in Figure 1-4. series arc-faults are created when there is a discontinuity in a conductor and the current bridges this gap. Conversely, parallel arc-faults are facilitated when an arc is established between conductors at different potentials [11]. Although there are many potential parallel arc-fault paths, there are three generic types of parallel arc-faults. To use a PV array as an example system, the three types of parallel arc-faults are:

1. Parallel Arc-Fault to Grounded Conductor–This parallel arc-fault could result from the negative DC cable (often grounded in the USA) shorting to a positive conductor due to wear, rodent bites, or damage to cables in conduit runs. In the case of the Mount Holly, NC fire [12] and the Bakersfield, CA fire [13], the fault path was established through the grounded current-carrying conductor via two faults to the conduit.
2. Cross-String Parallel Arc-Fault–This fault occurs when conductors on different strings at different potentials arc.
3. Intra-String Parallel Arc-Fault–This parallel arc-fault can occur anywhere in the string where a short occurs (e.g., junction boxes) [14].

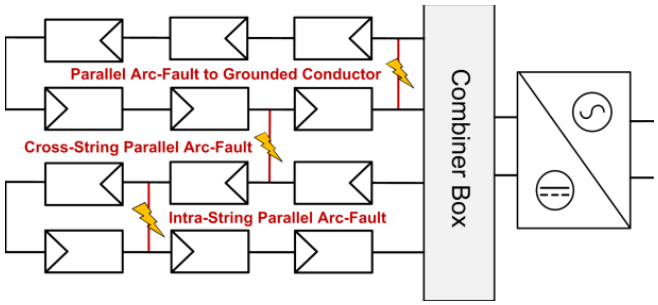

Figure 1-4. Parallel arc-faults on the DC-side of a photovoltaic (PV) array [11]

The differentiators between series (Figure 1-5) and parallel arc-faults are that current and voltage only vary slightly from normal operation [15], and that the location of the arc-fault does not change the current or voltage [11]. Another observation that has been made at Sandia National Laboratories (SNL) is that during both parallel and series arcs, although electrical devices such as inverters may turn off during an arcing event, the arc itself may not extinguish where it remains energized until the current flow stops, or when the arc burns through its conductor electrodes [11].

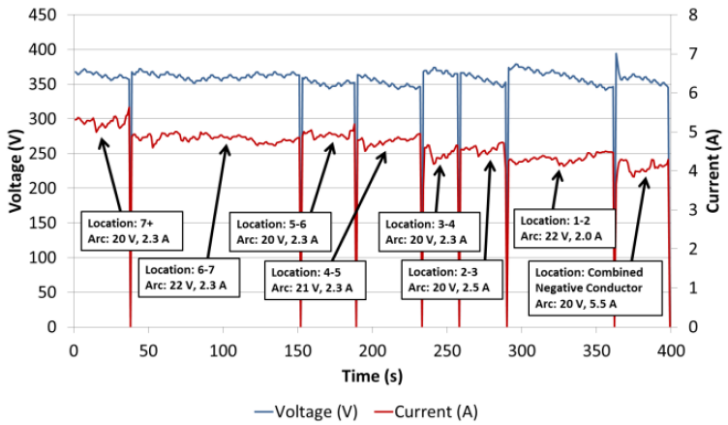

Figure 1-5. Series arc-faults at different locations within an inverter where current and voltage vary slightly from normal operation [11]

Parallel arc-faults tend to be more dangerous than series arc-faults, where they can be facilitated from a short circuit or a ground-fault. A ground-fault can facilitate a parallel arc-fault only when a ground path is present where this arc-fault type can be cleared by a ground fault circuit interrupter (GFCI) or an arc-fault circuit interrupter (AFCI). The RMS current value for parallel arc-faults can be considerably less than that of a solid, bolted-type fault. Therefore, even a commercial 15 A breaker might not clear this type of fault before a fire can ignite. An arc from a short circuit decreases the dielectric strength of insulation separating the conductors. This allows a high-impedance, low-current arc-fault to develop that carbonizes the conductor's insulation, further decreasing the dielectric strength of the insulation separating the conductors [10]. The result is an increased current, where thermal energy can be exponentially increased potentially increasing the likelihood of a fire. The current flow in a short circuit, parallel arc-fault is limited by system impedance and the impedance of the arc-fault itself [10].

1.3.2 Arc-Discharge Phenomena

As shown in Figure 1-6, an arc discharge arising from an arc-fault event, consists of three regions: the anode region, the plasma column, and the cathode region, where the electrode boundaries form

the transition regions between the gaseous plasma and the solid conductors. Also illustrated in the figure is a characteristic voltage profile for arc discharges, where the voltage gradient across the arc depends on the actual arc distance, where variability in the voltage can occur due to the arc deviating from the electrode gap [16]. This can arise due to rapid thermal and magnetic fluctuations, in addition to buoyancy impacts. Previous observations however have shown less deviation for shorter gap distances ("length"), as well as less turbulent conditions for these reduced configurations [16].

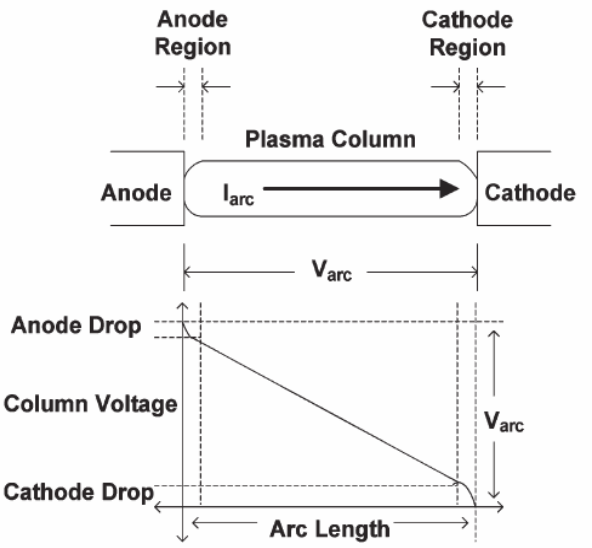

Figure 1-6. Arc-Plasma Discharge Characteristics [16]

A number of investigators have postulated that the voltage gradient in the plasma column of an arc is nearly independent of the arcing current [16], where Browne found that the voltage gradient in the arc column is nearly independent of the arc current for magnitudes above 50 A. His results also found that it is approximately 12 V/cm for arcs in open air [17] during his investigations of both AC and DC circuits. An open-air arc is one that radiates the heat in all directions [8]. From his investigation, Strom determined that although the voltage gradient in the arc is affected to a small extent by current magnitude [18] his results suggested that arc length, too, had an impact, where for arc lengths between 0.32 to 122 cm, resultant arc voltages averaged 13.4 V/cm during tests, which produced peak AC currents ranging from 68-21,750 A [16].

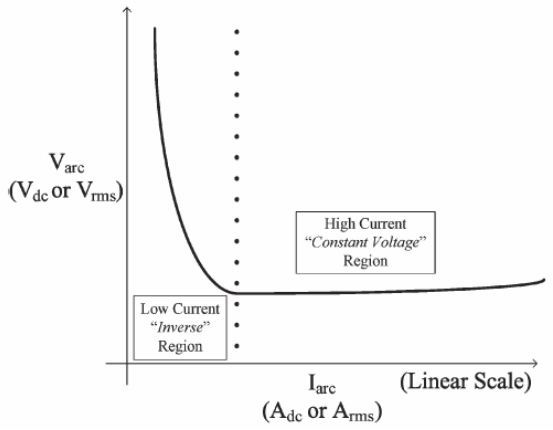

Figure 1-7. Arc-plasma high/low current and voltage phenomena [18].

For DC systems, the arc risk is generally evaluated based on the potential power of the circuit. Although the power may maintain a relatively constant value, respective current and voltage values may fluctuate relative to each other, where many investigators evaluate the characteristics of an arc based on a voltage-current (V-I) curve [16]. Figure 1-7 illustrates a DC V-I curve under quasi-static conditions, characteristic for an arc of "fixed" length. In the low-current region (left of the dotted line), arc voltage drops as arc current increases, thus facilitating a relatively constant arc power in this region. Conversely, high current arc-faults are commonly viewed as being quasi-stationary because the large thermal inertia in the arc discourages changes in arc temperature and conductance [16]. Even though the dynamic nature of the arc generates a time-varying arc length, arc voltage equations are commonly developed from the quasi-stationary V-I characteristics [16]. The majority of arc-plasma discharge literature is based on single-phase opposing electrodes, where the current comes from one side and flows across to the other side [19]. Consequently, arcs are often considered axisymmetric and nonaxisymmetric. As shown in Figure 1-8, an axisymmetric arc burns uniformly, while nonaxisymmetric arcs are either in a "state of dynamic equilibrium or continuous motion" [20].

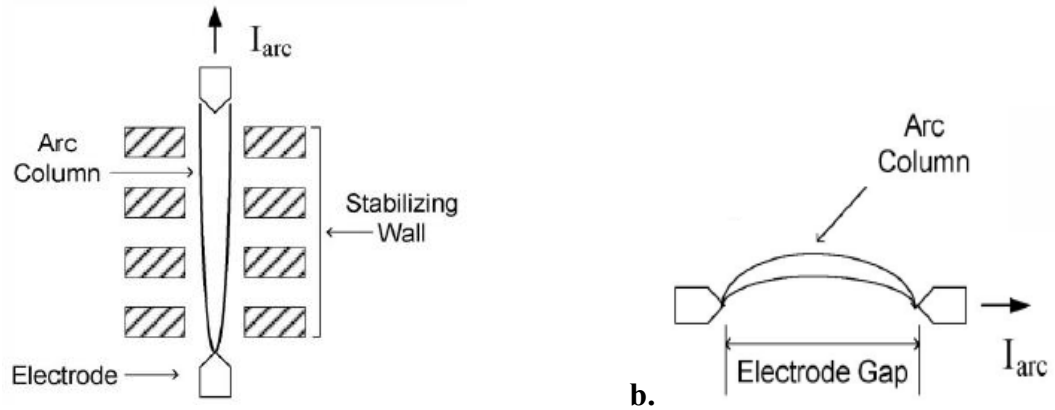

Figure 1-8. Series-electrode arc classification for a. vertical, axisymmetric wall stabilized arc, and b. horizontal, non-axisymmetric free-burning arc [19]

Under thermodynamic equilibrium conditions, a "wall-stabilized" arc can become evident, where the arc is constrained to a cylindrical shape. At low currents (< 10 A), the geometry of a free-burning arc would look similar to the diagram on the right side of the figure. With wall-stabilized arcs, the arc plasma is only partially ionized in the low-current region, whereas the plasma becomes fully ionized above a threshold current [20]. A similar transition in the level of ionization is observed for free-burning arcs in air [16]. In industrial applications, high-current free-burning arcing faults are extremely chaotic in nature where the arc can move so rapidly that its length and geometry are in constant dynamic motion. According to Gammon et al. [16] contributing factors to the dynamic nature of high-current free-burning arcs are the following:

1. Thermal convection
2. Electromagnetic forces
3. Burn back of electrode material
4. Arc-discharge extinction and restriking
5. Plasma jets

2. ARC-FAULTS IN AC SYSTEMS

Arc discharges in AC electrical systems can be described physically as the flow of current through an atmosphere between two phase conductors, or between a phase conductor and neutral, or between a phase conductor and a ground. Although all arc-faults can be hazardous, they can be extremely dangerous in some locations and less capable of significant damage in others depending on maximum fault current, X, Y, and Z. [21]. Arc-faults tend to release most energy at main distribution panels, which have high available fault current and least energy at the branch, which tends to have the lowest available fault current [21]. Historically, engineers have associated high level of available fault current and high reactance to resistance ratio (or X/R based on impedance used to determine peak asymmetric fault current) at the main distribution panel with arc-faults that are likely to be self-sustaining and capable of great destruction [22]. Arc-fault risks also depend on the presence of current-limiting fuses [23] and on whether a ground-fault-protective system has been installed, as well as the threshold ground-fault current that will activate the system. A GFCI system installed inside a main distribution panel does not protect branch circuits [23].

For transformers, grounded transformer systems provide high fault currents on its secondary side, which lead to faster protective device trip times, resulting in lower incident energy at the fault [9]. Low-resistance grounding however can provide much lower fault currents on the secondary side, which leads to slower trip times and higher incident energy at the fault. High-resistance grounding configurations provide extremely low fault currents and traditionally do not trip for the first ground fault. An ungrounded system will also not trip for the first ground fault, where their trip times in high-resistance and ungrounded systems can depend upon the activation and timing of respective phase protective devices [9].

In AC systems, one should note that bolted fault current and arc-fault currents are not the same in systems rated less than 1,000 V [25]. A bolted fault has essentially no fault impedance while arc-fault current has impedance associated with the arc, and therefore has a higher voltage drop and therefore lower fault current magnitude. Many common protective devices in low-voltage systems are coordinated to trip for higher bolted fault current and not necessarily with respect to arc-fault current or its current signal. Because protective device clearing time is an important factor in the calculation of incident energy, one must understand that it is the trip time to clear the arc current that is used in calculations and not the delay time for clearing of a bolted fault [25]. Additionally, programming relays for faster trip times based on arcing current sacrifices relay coordination and may put a large portion of the system out of service under an arc-fault [25].

From research performed by Wilkins et al., [26] orientation of electrodes directly dictates arc propagation between them and to the surroundings [27], as illustrated by Ammerman, [9]. Figure 2-1 shows three-phase parallel electrode configurations encountered in industrial applications.

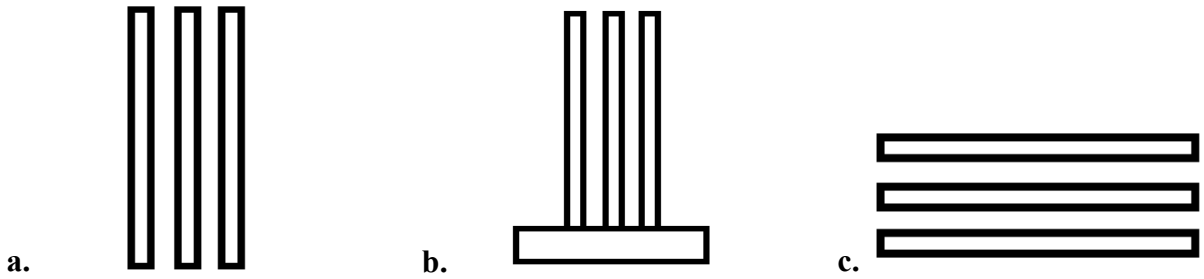

Figure 2-1. Parallel electrode (Three-Phase) configurations for a. vertical electrodes, b. vertical electrodes terminating into an insulating barrier and c. horizontal electrodes [9]

As demonstrated by Shea [28], there are general situations in which overheated utility wiring can lead to arcing and conversely, where arcing can lead to overheating and subsequent ignition of wire insulation, of decomposed gases produced from insulation, or of nearby materials. Shea demonstrated how arcing leads to overheating wire insulation, which can decompose and produce ignitable gases, and eventually ignition. Figure 2-2 illustrates one of the tests performed by Shea for an AC arc-plasma discharge, over an approximate 5 second test window, where temperatures over 1100 °C were reached [28]. Also illustrated within the inset plot are characteristic voltage and current waveforms that can be observed during an AC arc-fault.

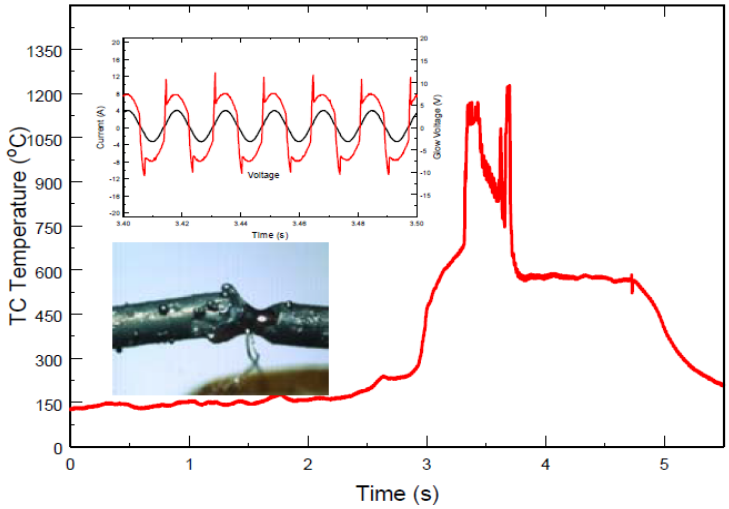

Figure 2-2. Temperature for a 2.5 Amp glowing filament induced arc discharge [28], where inset plot illustrates characteristic current (black inset lines) and voltage (red inset lines) waveforms

It is generally accepted that the vast majority of line-to-line or single-line-to-ground faults in a three-phase AC system will quickly escalate into three phase faults due to the propagation of arc-fault current that passes through the conductive plasma and the vaporized conductive material [29]. The energy radiated by the arc is a function of its current, which depends on the short circuit current (SCC) available at the fault location. The available SCC is defined as the maximum current that will flow from all sources in the system to a bolted, or zero impedance fault, which occurs during the first half cycle after the fault begins [29]. It is important to understand that the available SCC at a particular node in the system is independent of the steady-state current drawn by the downstream load, and is a function of the sources of SCC. These can include impedances from generators and motors as well as the impedance of conductors and transformers in the system.

Because of the load independence, Smith [29] suggests that the equivalent impedance tends to be predominantly inductive, where the fault current waveform will lag the voltage approximately by 90 degrees. This indicates that the symmetry of the current waveform about the zero axis will depend on the point in the voltage cycle at which the fault occurs. If the voltage is at its peak value when the fault occurs, then the current will start at a zero magnitude and follow the voltage down through the zero-crossing and be symmetrical about the zero axis. However, if the voltage is at zero when the fault occurs, the current will again start at zero, however, because it must follow the voltage by 90 degrees, the current will rise above the zero axis and vary as a sinusoid about a DC offset value. These phenomena can be illustrated by Figure 2-3 by [30].

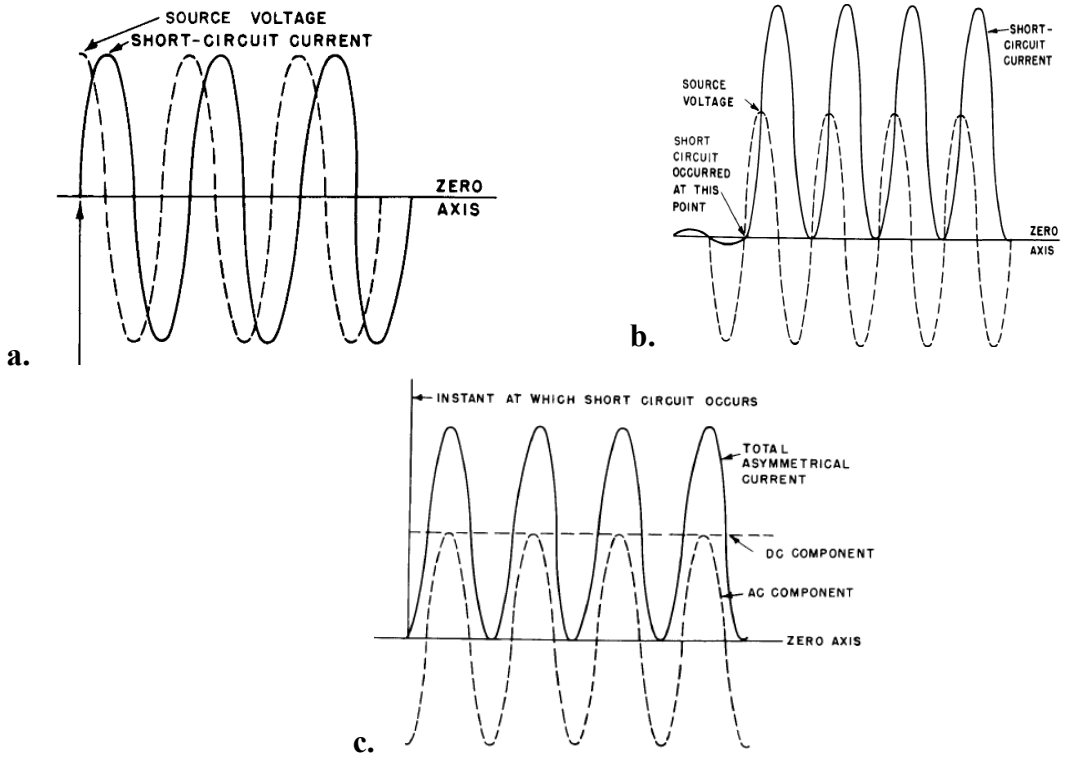

Figure 2-3. Power factor circuit a. symmetrical current and voltage, b. asymmetrical current and voltage, and c. AC vs. DC voltage under the influence of a short circuit [30]

Additionally, it is common to assess asymmetrical fault current as the sum of a symmetrical sinusoid and a DC component that decays as a function of the circuit's X/R impedance ratio, shown by Figure 2-4.

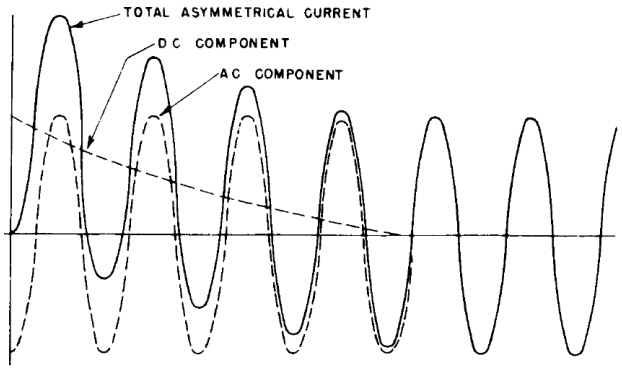

Figure 2-4. Impact of asymmetric current, and subsequent decay of DC component [30]

The maximum asymmetrical SCC can be found theoretically by analyzing the transient response of an equivalent series RL circuit just after the time a fault begins [29]. However, these calculations can be very complex in real systems. Therefore, simplified approaches have been developed where the steady-state symmetrical SCC is adjusted by a table of multiplying factors based on relative X/R ratios at the fault location, along with the test X/R ratio of the interrupting device. These methods are described in several IEC and ANSI standards for different interrupting devices, most notably ANSI C37.04 [126] and ANSI C37.010 [127] for high voltage circuit breakers rated on a symmetrical basis [29]. However, these standards are intended to guide the proper selection of an interrupting device capable of opening under worst-case fault conditions, for which the maximum asymmetrical SCC must be known. For purposes of estimating arc energy, the symmetrical RMS SCC value would be sufficient because the power of an arc is found as the product of the effective (RMS) voltage across the arc and the effective current through the arc [29]. The current through the arc will be lower than the available symmetrical SCC due to arc impedance; however, this approach is started by first finding the symmetrical SCC and then adjusting it accordingly. This is done by reducing the system to a per-unit impedance network at a common base power rating and a common driving voltage. Next, available symmetrical SCC at each node can be calculated simply as I=V/Z, where V is the system driving voltage and Z is the equivalent impedance of the network as found at the fault location [29].

As previously described, arc impedance prediction is important for predicting the energy radiated by an AC electric arc. Because arc power is the product of the driving voltage and arc current, arc impedance would need to be known to calculate the difference between a bolted fault current and the arc current. In applications where arcs are deliberately formed, such as in welding applications, the arc gap, pressure and chemical composition of the dielectric can be precisely determined. However, for inadvertent arcs, these parameters may vary greatly where accurate predictions can be difficult at best. Here, impedance is defined as the proportionality constant relating phasor voltage and current in linear, two-terminal elements [31]. Herein, a phasor is defined as a complex number representing the magnitude and phase of a sinusoidal AC voltage or current. Therefore, electrical impedance extends the concept of DC resistance to AC circuits, where it possesses both magnitude and phase [31]. Conversely, a DC resistance has only encompassed magnitude with a zero phase angle. Additionally, impedance is defined as the frequency domain ratio of the voltage to the current. [32] Therefore, it is the voltage–current ratio for a single complex exponential at a particular frequency ω. The impedance for the three passive circuit elements is listed in Eqns. 1-3 for respective resistors, inductors, and capacitors:

$$\text{Resistors:} \quad Z_R = R \tag{1}$$

$$\text{Inductors:} \quad Z_L = j\omega L \tag{2}$$

$$\text{Capacitors:} \quad Z_C = \frac{1}{j\omega C} = -\frac{j}{\omega C} \tag{3}$$

where j can be defined by the following identities for the imaginary unit and its reciprocal:

$$j \equiv cos\left(\frac{\pi}{2}\right) + jsin\left(\frac{\pi}{2}\right) \equiv e^{j\frac{\pi}{2}} \tag{4}$$

$$\frac{1}{j} \equiv -j \equiv cos\left(-\frac{\pi}{2}\right) + jsin\left(-\frac{\pi}{2}\right) \equiv e^{j\left(-\frac{\pi}{2}\right)} \tag{5}$$

To gain a more comprehensive fundamental overview of AC circuits, the reference by Thomas and Rosa is recommended [31]. According to Ammerman et al., [9] arc energy calculations currently fall into three general categories: (1) theoretical models developed from arc physics, (2) statistical models developed from statistical analysis, and (3) semi-empirical models developed from known observations and numerical analysis. Subsequently, to determine the power generated in AC circuits, the circuit diagram illustrated in Figure 2-5 by Papallo [33] is typically considered, where respective power and time-averaged power can be determined according to Eqns. 6 and 7:

$$P_{Arc} = V_{Arc} I_{Arc} = I_{Arc}^2 R_{Arc} \tag{6}$$

$$P_{Avg} = \frac{1}{T}\int_0^T V(t)I(t)dt \tag{7}$$

where T is the arc duration. Low voltage (LV) arcs are susceptible to self-extinction as they do not pass through current zero every half cycle [21]. In turn, the energy for DC or single-phase AC arc discharges can be expressed in terms of the power released by a short circuit and other heating effects from:

$$E_{Arc} \approx I_{Arc}^2 R_{Arc} t \tag{8}$$

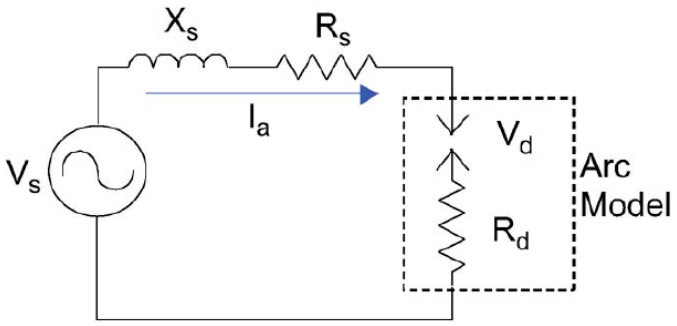

Figure 2-5. Simple AC circuit diagram for arc damage analysis [33].

According to Eqn. 8, the energy released by the arc is directly proportional to the RMS arc current [21]. In a study by Stanback [34] the author developed a damage indicator that states the level of system damage, tolerable under the following criterion:

$$I_{Arc}^{1.5} \cdot t < 250 \cdot I_{rated} \tag{9}$$

According to Gammon [16] because AC arc current and arc voltage contain harmonics, this equation is not precisely accurate. Arc energy may be precisely calculated from digitally sampled waveforms from the following equation:

$$E_{Arc} = \frac{\sum v_{Arc} \cdot i_{Arc}}{number\ of\ samples} \cdot t \tag{10}$$

where v_{Arc} and i_{Arc} are instantaneous arc voltage and current. One should note that E_{Arc} is associated with an arc voltage limiting current flow so that the instantaneous trip mechanisms in

overcurrent devices may not be initiated; in such events, the arc continues to release energy.

Incident energy from an arc-flash event can be directly related to the amount of thermal energy that is impressed on a surface at a certain distance from the source. Traditionally one of the most commonly used theoretical models for predicting arc incident energy in AC systems is a method developed by Lee [29], which relies on basic circuit theory and the maximum power transfer theorem. In his research investigations, Lee [35] assumed that short circuit current (SCC) sources in electrical systems are primarily inductive and that the impedance of an arc is primarily resistive, such that again the source voltage and arc current would be shifted by 90 degrees. Therefore, the voltage would drop across the source inductance where arc resistance can be illustrated by a quadrature, Figure 2-6.

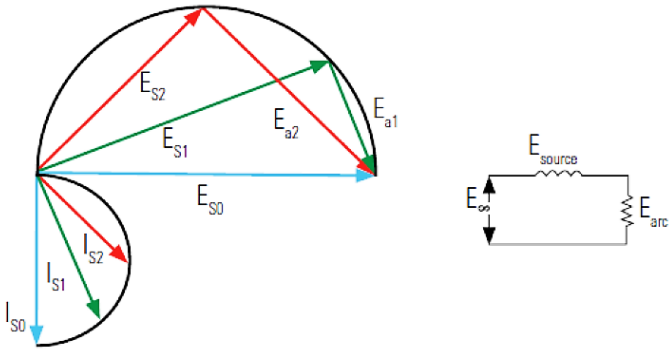

Figure 2-6. Lee's Method Quadrature Vector Diagram [35]

Lee developed a theoretical model for predicting arc-flash incident energy as a function of time, available SCC, and distance from the arc. By treating the arc as a spherical radiant heat source, the fraction of energy absorbed by a spherical surface per-unit area will be inversely proportional to the square of the distance between the arc and the respective surface according to Eqn. 11:

$$E = 5.12 \times 10^5 I_{bf} \left(\frac{t}{D^2}\right) \tag{11}$$

where E is the incident energy (J/cm^2), I_{bf} is the bolted 3 phase fault SCC (kA), t is the arc time (s) and D is distance from the arc to a potential bystander (mm). This method is limited however, because at the maximum power point, arc energy will increase linearly despite the non-linear nature of arc V-I characteristics. Past a certain point, the voltage across the arc is primarily a function of arc length, and current through it are equal to 70.7% of the system voltage and the bolted fault current. This results in predicted arc energy increasing linearly with system voltage and available bolted fault current. Therefore, the real non-linear nature of arc V-I characteristics is problematic, because the voltage across the arc is primarily a function of arc length, where current through the arc may increase almost independently of arc voltage. A further issue is that the maximum power prediction method does not provide a way to accurately predict the arc current, which may be significantly different than the 70.7% of bolted fault current present at the maximum power point. Lee's method, along with various but relatively minor refinements, was the accepted methodology until the publication of the IEEE 1584 Standard in 2002, which presented empirically-derived equations based on extensive laboratory test data. It should be noted that Lee's method is still the consensus standard when the system to be evaluated falls outside of the scope of the IEEE 1584 standard or tests up to 13.8 kV [36].

For the IEEE 1584 standard, arc-flash energy equations incorporate many variables, including equipment-bolted fault current values, arc-fault current values, and upstream protective device clearing times. These calculations are also dependent upon factors such as operating voltage, gap length, and type of grounding. These last three items are very difficult to change in an existing facility, [37] however. The most impactful parameters on these calculations is the time the upstream device operates, followed by working distance, and then available fault current. The IEEE 1584 Eqns. 12-13, for normalized incident energy (J/cm^2), can also be used to establish the flash boundary distance for workers and appropriate personal protective equipment guidelines.

$$E_n = 10^{K_{E1}+K_{E2}+1.081I_{arc}+0.0011l_{arc}} \tag{12}$$

For V_{sys} < 1000 V: $$I_{arc} = 10^{K_{I1}+0.662I_{bf}+0.0966V_{sys}+0.000526l_{arc}+0.5588I_{bf}-0.00304l_{arc}I_{bf}} \tag{13}$$

For 1000 V < V_{sys} < 15,000 V: $$I_{arc} = 10^{0.00402+0.983I_{bf}} \tag{14}$$

where:

I_{arc}	Arcing Current (kA)
K_{I1}	-0.153 for open configurations, and -0.097 for box configurations
I_{bf}	Bolted 3-phase fault current (kA)
V_{sys}	System voltage (V)
l_{arc}	Arc gap length (mm)
K_{E1}	-0.792 for open configurations, and -0.555 for box configurations
K_{E2}	0 for ungrounded and high-resistance systems, and -0.113 for grounded systems

For arc flash considerations, the incident energy (cal/cm^2) between the source of an arc and a bystander can be determined according to Eqn. 15.

$$E_f = C_f E_n \left(\frac{t}{0.2}\right)\left(\frac{610^x}{D^x}\right) \tag{15}$$

where:

C_f	1.0 for voltages above 1 kV, and 1.5 for voltages below 1 kV
t	Arc duration time (s)
D	Distance from an arc to a bystander
x	Distance exponent constant, defined by Table 2-1.

Table 2-1. IEEE 1584 incident energy factors for equipment and voltage classes [36].

System Voltage (kV)	Equipment Type	Gap length between conductors (mm)	Distance Exponent
0.208 - 1	Open Air	10-40	2.000
	Switchgear	32	1.473
	MCC and Panels	25	1.641
	Cable	13	2.000
> 1 - 5	Open Air	102	2.000
	Switchgear	13-102	0.973
	Cable	13	2.000
> 5 - 15	Open Air	13-153	2.000
	Switchgear	153	0.973
	Cable	13	2.000

The IEEE 1584 standard includes empirical equations for arc energy, derived from extensive laboratory test data using curve-fitting techniques [36]. The group created arcs at several common system voltages (208, 400, 450, 480, 600, 2300, 4160 and 13800 V) over a range of bolted fault currents up to 106,000 amperes while varying electrode gap and composition, enclosure size and distance from the arc. Here, the IEEE 1584 data came from measured current delivered by the system under a variety of configurations and provided equations for predicting arcing current as a function of system voltage, arc gap, and bolted fault current [36]. The test results demonstrated that arcing current as a percentage of bolted fault current increased quickly as the system voltage was increased. Figure 2-7 a. by Smith [29] illustrates the relationship between arc current and bolted fault current using the 1584 equation at the five voltages under 1000V that the group tested at, with all other variables held constant. Additionally, results are also shown in Figure 2-7 b. for 2.3KV, 4.16KV and 13.8KV, where the arc current was almost entirely a function of bolted fault SCC. The equation provided for arcing current is the same for all three system voltages, where the arc current is almost equal to the bolted fault current.

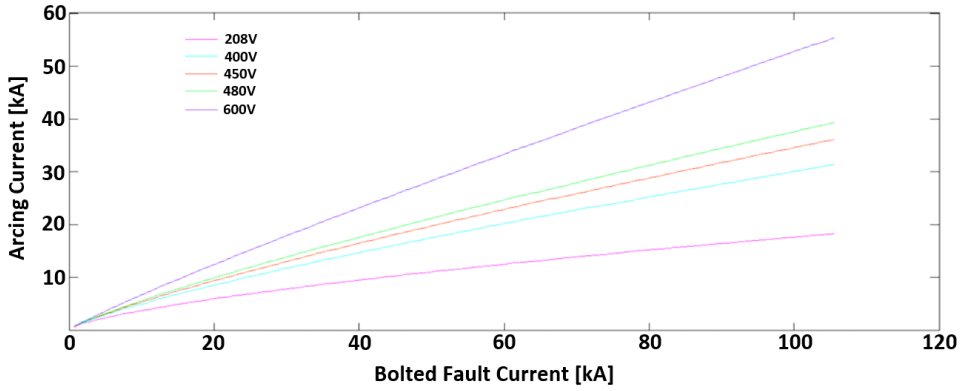

a.

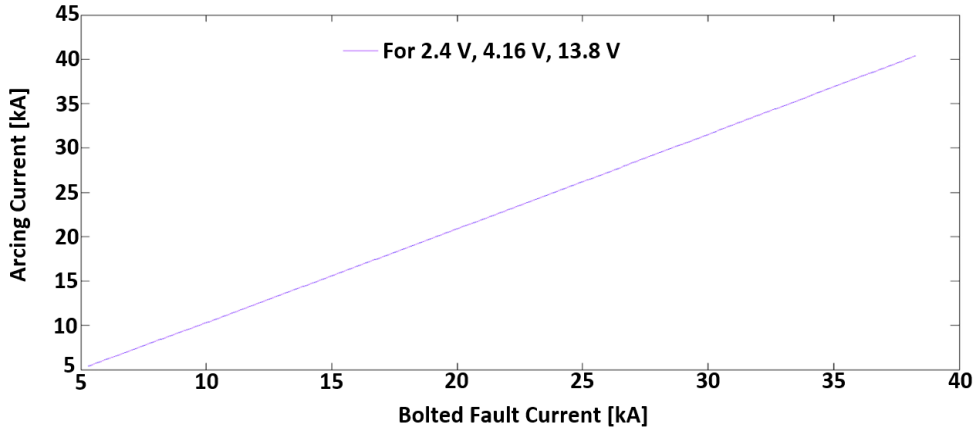

b.

Figure 2-7. Analytical arc current vs. bolted current for a. < 1000 V system and b. > 1000 V system [29]

In comparison to Lee's method, Smith's analysis with IEEE 1584 [29], shown in Figure 2-8 a., that incident energy is consistently conservative at lower system voltages.

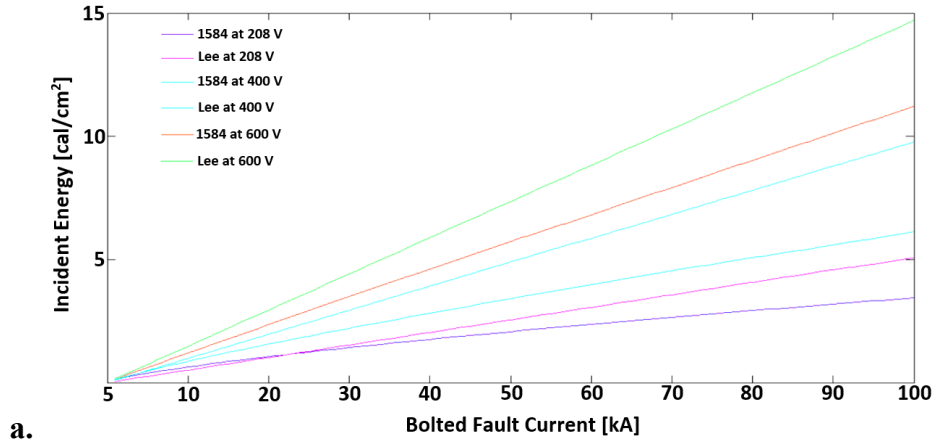

a.

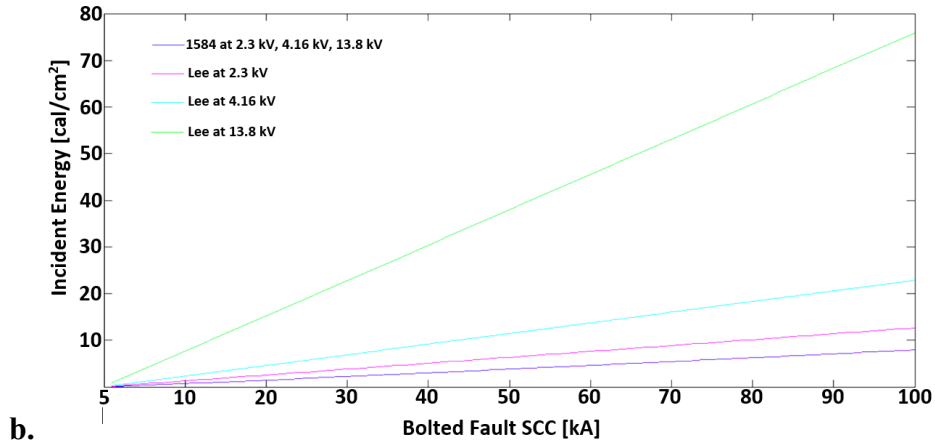

b.

Figure 2-8. Analytical bolted fault SCC versus incident energy for a. < 1000 V system and b. > 1000 V system [29], where the arc time is 0.1 sec.

From these test results a simplified version of the IEEE 1584 incident equations are provided:

For $V_{sys} \leq 480\ V$ $$E_f = 1.5(0.258 I_{bf})\left(\frac{t}{0.2}\right)\left(\frac{610}{D}\right)^x \quad (16)$$

For $480\ V \leq V_{sys} \leq 600\ V$ $$E_f = 1.5(0.344 I_{bf})\left(\frac{t}{0.2}\right)\left(\frac{610}{D}\right)^x \quad (17)$$

For $V_{sys} > 1000\ V$ $$E_f = (0.57 I_{bf})\left(\frac{t}{0.2}\right)\left(\frac{610}{D}\right)^x \quad (18)$$

However, Lee's method does not provide a way to predict arcing current. In systems where over-current devices have inverse time-current characteristics (i.e. time it takes for the device to open decreases as the current through the device increases), an accurate estimate of the device clearing time is essential to properly predict incident energy [35]. Because Lee's method calculates the maximum power in an arc using the bolted fault SCC/square root of 2, this is the amount of current we must logically assume is present in the arc, and hence is the amount of current sensed by the clearing device [29]. As the 1584 test results show, the arcing current is a strong function of system voltage under 1000 V, and on these systems, Lee's method may overestimate the arc current which could result in an underestimation of the arc clearing time and arc incident energy [36].

From the respective arc-flash incident energy equations, Figure 2-9and Figure 2-10 (a. and b.) present experimental test data against equations provided by Lee [35] and the IEEE 1584 standard [36], for an open-air arc in a 600 V system [8]. As can be seen in all three figures, the IEEE 1584 data matches well with the IEEE 1584 equations, however deviate from Lee's equation with increasing voltage.

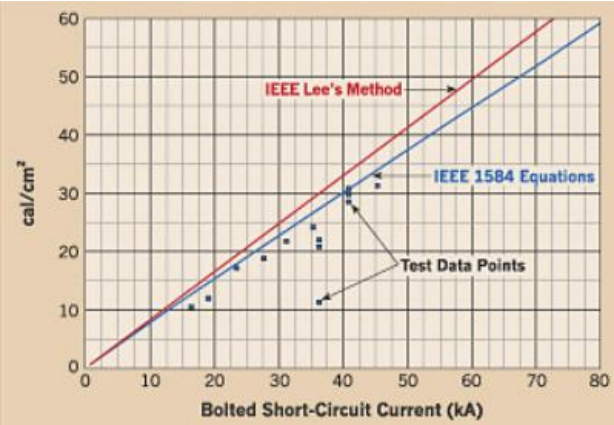

Figure 2-9. IEEE 1584 standard [36] vs. Lee paper [35] incident arc energy equation comparison for a 600 V system voltage [8]

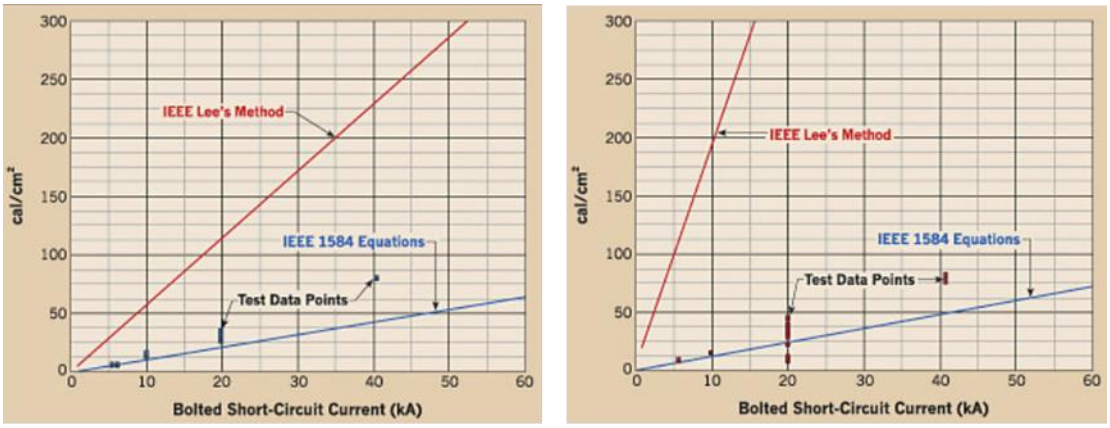

Figure 2-10. IEEE 1584 standard [36] vs. Lee paper [35] incident arc energy equation comparison for a system voltage of a. 4,160 V and b. 13.8 kV [8].

Another standard that prescribes methods, based on analysis of a flash protection boundary and incident energy, is the national fire protection agency (NFPA) 70E standard [106]. Figure 2-11 shows the relationship between arc-flash energy and bolted fault capacity. Note that this relationship can be linear for the IEEE 1584 equations and conversely somewhat logarithmic for the NFPA 70E equations. Further examination of this figure indicates that for values above 16kA the NFPA 70E is more conservative than IEEE 1584 [93].

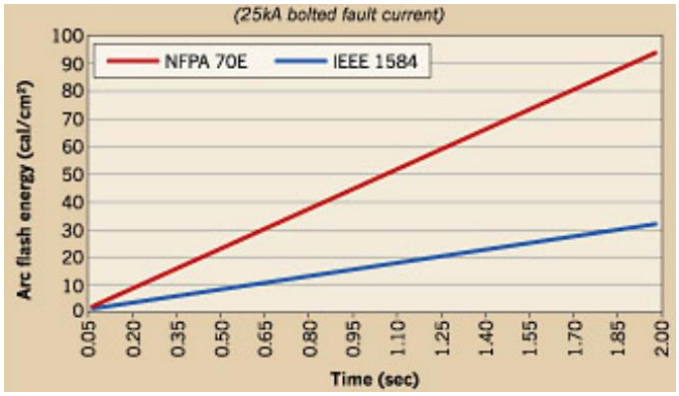

Figure 2-11. IEEE1584 and NFPA 70E standards comparison for a 25kA bolted fault current [93]

With regard to arc gap length in AC circuits, Stokes and Oppenlander performed an extensive investigation of free-burning vertical and horizontal arcs between series electrodes in open air [38]. Here, current and voltage signals were recorded for arcs burning with exponentially decaying currents from 1000 to 0.1 A, and 50-Hz arcs for sinusoidal currents with amplitudes decaying from 20 kA to 30 A [38]. Their results shown in Figure 2-12, for gap widths ranging from 5 to 500mm (from bottom to top), suggest that the minimum voltage needed to maintain an arc depends on current magnitude, gap width, and orientation of the electrodes.

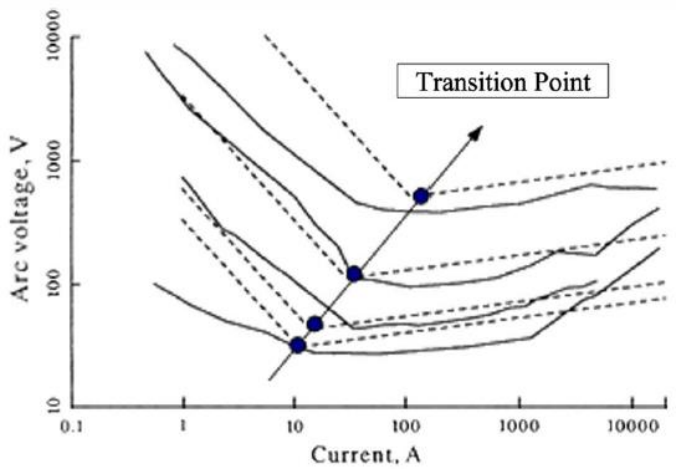

Figure 2-12. Minimum arc voltage for vertical arcs facilitated between copper electrodes, where continuous lines are for measured values and dashed lines are for calculated values. The arc gap widths for curves from bottom to top are 5, 20, 100, and 500 mm [38].

The transition current is defined as $I_t = 10+0.2z_g$, where the arc gap length, z_g is in units of millimeters [38]. The curves show the inverse V–I characteristic for an arc with a current that is lower than the transition point, however for current values above this transition point, the arc voltage has a slow rise. Stokes and Oppenlander modeled arc voltage for arc current values above a transition point, where data set included approximately two million current and voltage points, producing Eqns. 19 and 20:

$$V_{Arc} = \left(20 + 0.534z_g\right)I_{Arc}^{0.12} \tag{19}$$

$$R_{Arc} = \frac{20+0.534z_g}{I_{Arc}^{0.88}} \tag{20}$$

During their tests, copper electrodes were tested in a horizontal configuration, while aluminum electrodes were tested in a vertical configuration. The authors also defined instantaneous arc power [38] by Eqn. 21, where it is assumed to be quasi-static near the peak of an AC current.

$$P_{Arc} = (20 + 534g)i_{Arc}^{1.12} \quad for\ i_{Arc} > 10 + 200g \tag{21}$$

This equation applies only to arc currents above the transition level [21], which is usually surpassed in most low-voltage systems. This equation was developed based on free-air arcs generated between both copper and aluminum, hemispherical-tipped electrodes [38]. Subsequently, the investigators formulated an instantaneous power equation which has been used to develop an arc model incorporating a current-dependent arc voltage defined by Eqn. 22.

$$V_{Max}sin(\omega t) = Ri_{Arc} + L\frac{di_{Arc}}{dt} + (20 + 534g)i_{Arc}^{0.12} \tag{22}$$

When assessing differences between vertical and horizontal arcs, Paukert [39] compiled data sets, which included those by Stokes and Oppenlander, where the best agreement was found in the higher current range, (> 100 A) [16]. Paukert concluded that the approximation formulas for minimal arc voltage and minimal arc resistance were found to be in good agreement with other authors' results as well, however mentioned that without the ability to measure actual arc length, the ability to obtain the exact V-I curve values will be impacted [39].

Additionally, when modeling AC arc-faults it is important to be mindful of proper characterization of source impedance per each device in a respective electrical system. Fault current sources like power generators cannot supply faults in a power system indefinitely [25], where the fault current magnitude is limited by the generator's internal reactance, transmission line impedance, transformer impedance, and series reactors. From an engineering controls perspective, it is important to not model the source as an infinite source, where the assumption of an infinite source can result in high fault currents, which can lead to faster tripping of protective devices (i.e. "nuisance tripping"). This, in turn, leads to less incident energy at the fault location, as well as to trip times that are misleading, and incorrectly identifying a hazardous location [25].

3. ARC-FAULTS IN DC SYSTEMS

Arc-fault characterization experiments (Appendix A2) at Sandia National Laboratories, Figure 3-1, demonstrated for DC arc-faults that plasma discharge temperatures can exist well above 1000 °C, with electrode temperatures above 500 °C. Like AC arcs, the localized temperatures caused by DC arcs have the potential to cause extensive damage to personnel and equipment in the surrounding environment.

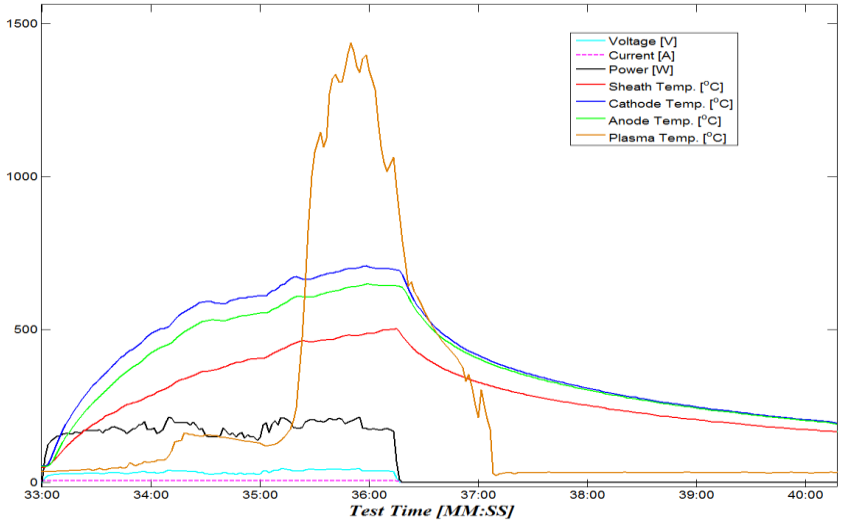

Figure 3-1. DC arc-fault experimental measurements made at Sandia National Laboratories, which include plasma and electrode temperatures

The 2012 edition of the NFPA 70E standard [40] references papers that offer theoretical and semi-empirical methods for estimating DC arc discharge energy. For a fault in a DC circuit, the prospective available SCC is the final constant value VDC/R, where VDC is the source voltage and R is the resistance of the circuit. To determine the peak (and worst case) SCC, Mendenhall [41] developed Eqns. 23 through 26 where the rise and decay time constants are defined by τ_{Rise} and τ_{Decay} respectively, in units of milliseconds.

SCC:
$$i_{pD} = \kappa_D I_{kD} \tag{23}$$

$$\kappa_D = 1 + \frac{2}{\pi} e^{-\left(\frac{\pi}{3}+\varphi_D\right)cot\varphi_D} sin\phi_D \left(\frac{\pi}{2} - arctan\frac{L_{DBr}}{L_N}\right) \tag{24}$$

$$\tau_{Rise} = 2 + (\kappa_D - 0.9)\left(2.5 + 9\frac{L_{DBr}}{L_N}\right) \tag{25}$$

$$\tau_{Decay} = \frac{2}{\frac{R_N}{X_N}\left(0.6+0.9\frac{R_{DBr}}{R_N}\right)} \tag{26}$$

From these equations, L_{DBr} and L_N are the respective load and line side inductance, R_{DBr} and R_N are the resistances and I_{kD} is the quasi steady-state current. A DC source can be simply modeled as a system voltage and impedance [33]. For test validation, Figure 3–2 provides a typical test

circuit used to measure the characteristics of a DC arc, where the gap width, *L* is not to be confused with the actual arc length. Although short gap lengths can be good approximate estimations for the gap length between series arc electrodes for low currents, the arc length may be considerably longer than the gap width for higher currents. It is important to remember that the impedance of the arc is governed by the actual arc length. The arc's physical processes are complex and chaotic in nature, and can be very difficult to develop accurate theoretical models using pure fundamental arc physics equations (Appendix A1). Figure 3-2 shows the simplified DC equivalent-circuit representation of the arc used in obtaining empirical and semi-empirical data sets.

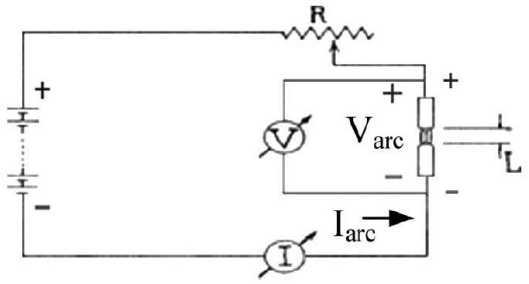

Figure 3-2. DC arc-fault test circuit diagram [16].

An arc discharge is often represented with an even more simplified equivalent electrical circuit ("black-box" approach), Figure 3-3, especially for objectives in determining an approximate arc current, power or energy level [16].

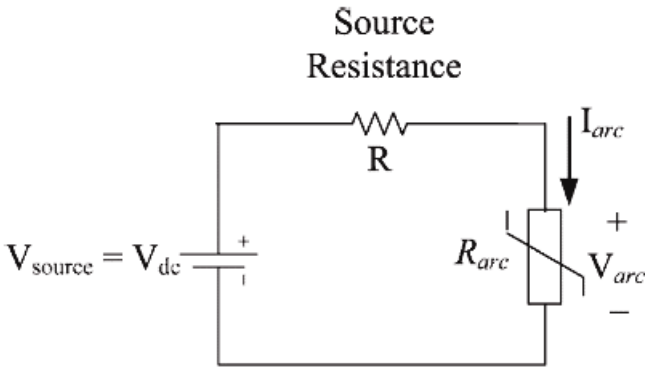

Figure 3-3. Simplified DC equivalent "Black-Box" circuit model [16].

During an DC arc-fault circuit analysis one can begin with the assumption of steady state current passing through the arc where any inductance in the system would tend to reduce the available power in the arc [42]. Therefore, this should be a conservative assumption. Also, the inductances in the system and in the arc would tend to reduce the average power during the fault, because it would limit arc current at its inception [42]. Doan's theoretical model presents a maximum power approach to determining arc energy very similar to that by Lee for AC circuits [42]. His approach is based on an initial consideration of only the resistive portion of the impedances in the simple model, where the arc power can be calculated by Eqn. 27.

$$P_{Arc} = V_{Arc}^2 / R_{Arc} \tag{27}$$

One can determine the maximum power released in the arc at the point where the resistance in the arc is equal to the resistance of the system, or when the arc voltage is half of the system voltage,

as prescribed by Eqn. 28.

$$P_{Max} = \left(V_{Sys}/2\right)^2 / R_{Sys} \tag{28}$$

To convert this to the maximum energy, Eqn. 28 is multiplied by time:

$$E_{Power,Max} = P_{Max} * t_{Arc} \tag{29}$$

which determines the total arc energy in joules. To convert to calories/Joule, which is often the units to characterize arc flash energy, the unit conversion factor of 0.239 cal/J is multiplied further in Eqn. 30.

$$E_{Power,Max} = 0.239 * \left(V_{Sys}/2\right)^2 / R_{Sys} * t_{Arc} \tag{30}$$

Here, $E_{Power,Max}$ is the energy released at the maximum power point, V_{Sys} is the system voltage, R_{Sys} is system resistance and t_{Arc} is the duration of the arc:

$$IE_{Max\ Power} = 0.005 \left(\frac{V_{sys}^2}{R_{sys}}\right) \frac{t_{Arc}}{D^2} \tag{31}$$

where $IE_{\text{Max Power}}$ estimated incident energy at the maximum power point, V_{Sys} and R_{Sys} are respective system voltage and resistance values and D is the distance from the arc. In his paper, Mendenhall [41] outlined a basic approach for performing arc heat and blast analysis for a nuclear research facility, specifically for a concentrated load that included eight 1050 HP DC drives with 1 MW silicon controlled rectifiers (SCRs) regulating +/-300 VDC outputs to tightly arranged terminations at a load. The work included an arc flash hazard analysis for the AC electrical system components that were to be installed. The employed resistive heater loads could generate nearly 1.4 MW of heat. Within the analysis values for relatively low strand count conductors were found in sources like the Standard Handbook for Electrical Engineers [43].

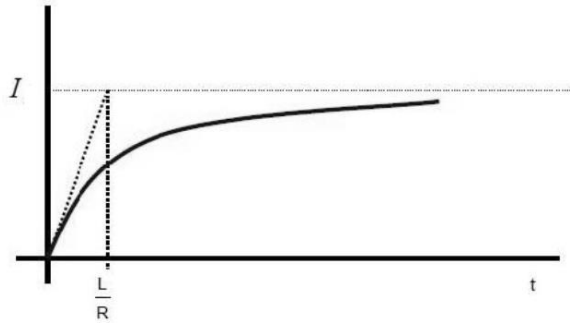

Figure 3-4. DC fault short circuit current time profile, illustrating L/R time-constant [45].

As outlined by J.C. Das [44], the first step in computing the DC arc hazard potential is to determine available current at the fault, where one can determine incident energy from the current of an arc-fault. This method was validated by several years of DC arc empirical measurements [41]. After a fault occurs, the current in the circuit increases exponentially, as shown in Figure 3-4, with a circuit time-constant (L/R), where L and R are the respective circuit inductance and resistance values [45].

During a DC fault the current rise (di/dt) is dependent on the circuit time constant (L/R), where for a simple DC motor circuit, the L/R time constant can be on the order of 40 ms, which yields a lower current rise under short circuit conditions as compared to an AC short circuit. With the lower

d*i*/d*t*, the fuse takes longer to melt compared with an equivalent AC circuit, which also leads to a relatively long arc-discharge duration. These conditions, together with the absence of natural current zeroes, make the interruption of a DC fault more difficult for a fuse than for AC faults if *L*/*R* is high. However, as the *L*/*R* time constant increases, the DC voltage capability of the fuse decreases. However, although it can be difficult to obtain a precise value for *L*/*R* in practice, various investigators provide some typical guideline values as shown in Figure 1-1 [45]. When assessing potential DC faults for a respective circuit and *L*/*R*, there exists a maximum breaking current, minimum breaking current, which provides maximum arc energy, where minimum breaking currents for DC circuits are published in separate ratings tables.

Table 3-1. Suggested DC fault (*L*/*R*) time constants [45].

Type of Equipment	Typical L/R, (ms)
Battery Supply or Capacitor Bank	< 10
Bridge Circuit	< 25
DC Motor Armature Circuit	20 - 60
DC Traction Systems	40 -100
DC Motor Field	1000

For a series equivalence circuit, Doan [42] illustrated the effect of *L*/*R* on current rise in a protective device, against an AC waveform, along with the current rise for DC systems time constants equal to 2 and 10 ms. From Figure 3-5 it can be seen that for AC system fuse or circuit breakers, the opening times can be from 4 ms to a few cycles, however for DC systems, it may take longer for the current to reach a steady-state value where a protective device will take longer to sense the fault current and open the circuit [42].

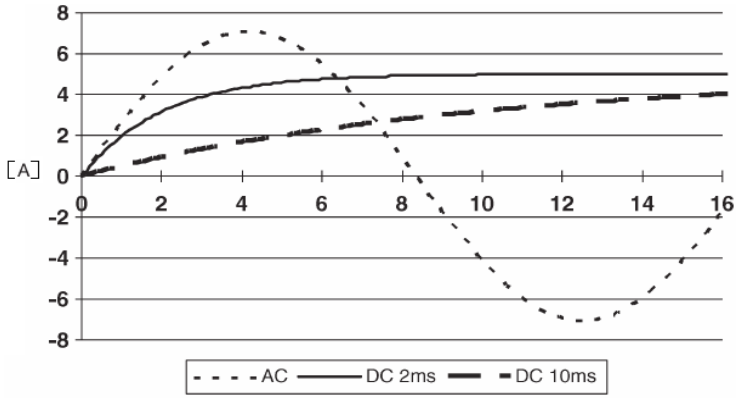

Figure 3-5. Effect of L/R on current sensing [42].

For DC systems where *L/R* is under 10 ms, fuses operate under a curve similar to that published for AC operation but with minor changes at the high current portion of the curves [42]. For *L/R*

values above 10 ms, there will be a slow increase in fault current and a correspondingly slower opening of the circuit by the fuse. In most cases for battery banks, such as in a UPS device, where inductance is relatively low, 2 to 5 ms would be a good range of values to use. In his investigation, Cline illustrated the effect of DC circuit inductance on a 30 A fuse (Figure 3-6) where the most pronounced impact on current occurred for an L/R of 10 ms [46].

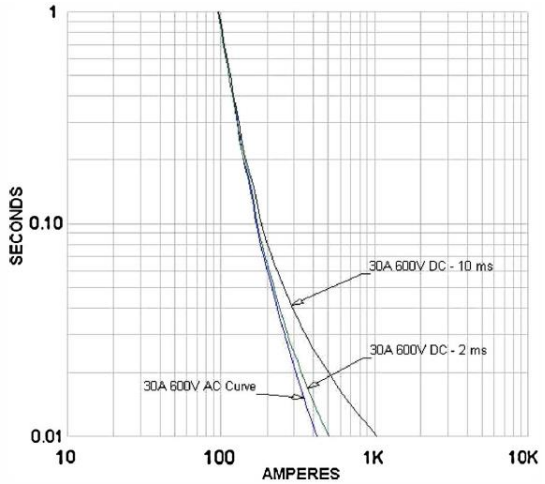

Figure 3-6. Effect of L/R on a Fuse [46].

DC arcs in an industrial setting are likely to be initiated between parallel electrodes, which are characterized by longer arc lengths and higher arc voltages. For determining arc voltage, Nottingham conducted arc research that produced a corresponding inverse representation [58]:

$$V_{Arc} = A + \frac{B}{I_{Arc}^{n}} \tag{32}$$

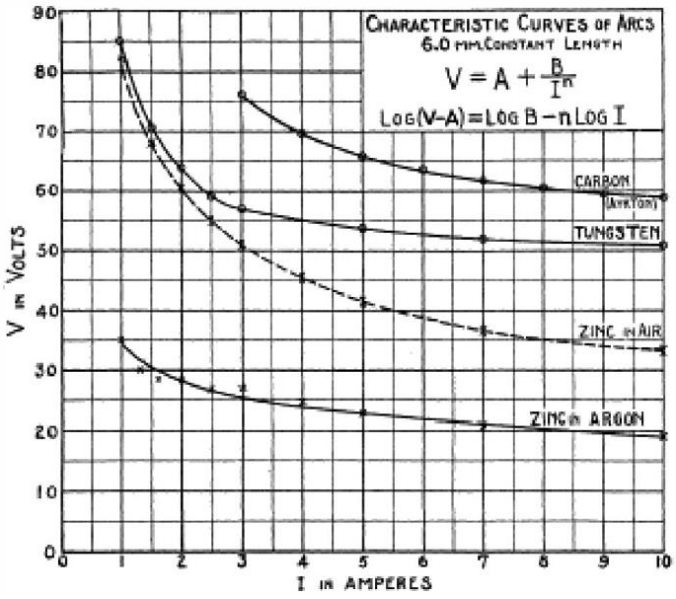

Figure 3-7. Sample V-I curves based on electrode material by Nottingham et al. [16]

The constants *A* and *B* are dependent on the arc length, electrode material, and based on imposed

current values up to 10 A. For example, for arc lengths ranging from 1.0 to 10.0 mm, the respective *A*, *B* and *n* values for copper electrodes are 27.5, 44 and 0.67 [41]. Figure 3-7 shows a sample of some typical V–I characteristics of arcs with 6-mm arc lengths and different electrodes. Van and Warrington performed several tests on high-voltage AC systems for arc current levels between 100 and 1000 A, with electrode distances which spanned several feet [47]. The V-I prediction of a stable arc was determined as:

$$V_{Arc} = \frac{8750L}{I_{Arc}^{0.4}} \tag{33}$$

From their results, Van and Warrington confirmed research results obtained by Ayrton [124] and Steinmetz [125], demonstrating arc voltage proportionality to arc length and its reduction with increasing arcing current. In 1978, a group of researchers conducted tests to evaluate faults on DC trolley systems [48] where over 100 DC arc tests were conducted using a 300 V DC power supply. Arc currents ranged between 300 to 2,400 A, with electrode gap lengths ranging between 4.8-152 mm. The relationship between the arc current and voltage in the DC trolley system was determined to match the form defined by the Nottingham equation.

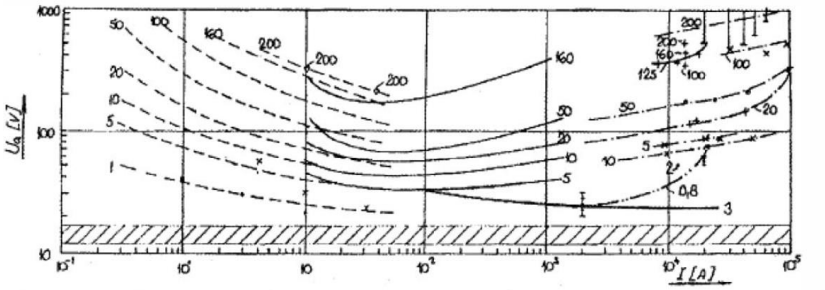

Marking	Author	Electrodes	Current	Arc
– – – –	Rieder [2]	Cu ø 6	DC	vertical
——— V	Amft [3]	Mo	DC	vertical
— · — · —	Rybář [4]	Cu horns 10x30...500	50 Hz	horizontal
— · — · —	Paukert [5]	Cu horns 10x30...500	50 Hz	horizontal
——— +	Harča [6]	Cu 30x5	50 Hz	not stated
———	Burkhard [7]	Fe, Cu plated, 2 mm	50 Hz	horizontal
— · · — · ·	Gremmel [8]	ø 8, Ag, Cu, CuCr	impulse	vertical

Figure 3-8. DC Arc-fault data compiled by Paukert [39].

In comparing DC and AC arc-plasma discharges, Paukert published arc-fault data over a wide range of DC and AC arc tests. The configurations were for both vertical and horizontal configurations where arc currents ranged between 0.3 A to 100 kA, while electrode gaps lengths between 1-200 mm [39]. The results, as illustrated in Figure 3-8, provided formulated arc-voltage and arc-resistance equations for various electrode gap lengths as listed in Table 3-2 and Table 3-3. While Table 3-2 presents an inverse V–I characteristic for low-current arcs, Table 3-3 presents positive V–I characteristics for currents above 100 A [39].

Table 3-2. Empirical data by Paukert for I_{Arc} < 100 A [39]

Electrode Gap (mm)	Arc Voltage (V)	Arc Resistance (Ω)
1	$36.32\ I_{arc}^{-0.124}$	$36.32\ I_{arc}^{-1.124}$
5	$71.39\ I_{arc}^{-0.186}$	$71.39\ I_{arc}^{-1.186}$
10	$105.25\ I_{arc}^{-0.239}$	$105.25\ I_{arc}^{-1.239}$
20	$153.63\ I_{arc}^{-0.278}$	$153.63\ I_{arc}^{-1.278}$
50	$262.02\ I_{arc}^{-0.310}$	$262.02\ I_{arc}^{-1.310}$
100	$481.20\ I_{arc}^{-0.350}$	$481.20\ I_{arc}^{-1.350}$
200	$662.34\ I_{arc}^{-0.283}$	$662.34\ I_{arc}^{-1.283}$

Table 3-3. Empirical Data by Paukert for 100 A < I_{Arc} < 100 kA [39]

Electrode Gap (mm)	Arc Voltage (V)	Arc Resistance (Ω)
1	$13.04\ I_{arc}^{0.098}$	$13.04\ I_{arc}^{-0.902}$
5	$14.13\ I_{arc}^{0.211}$	$14.13\ I_{arc}^{-0.789}$
10	$16.68\ I_{arc}^{0.163}$	$16.68\ I_{arc}^{-0.837}$
20	$20.11\ I_{arc}^{0.190}$	$20.11\ I_{arc}^{-0.810}$
50	$28.35\ I_{arc}^{0.194}$	$28.35\ I_{arc}^{-0.806}$
100	$34.18\ I_{arc}^{0.241}$	$34.18\ I_{arc}^{-0.759}$
200	$52.63\ I_{arc}^{0.264}$	$52.63\ I_{arc}^{-0.736}$

Additionally, experimental results by Sölver, Fig. 3-9, for arc gap lengths up to 200 mm, illustrated the inverse relationship between arc voltage and current, whereas arc current increases, arc voltage decreases toward a nearly asymptotic constant respective value. This proved that arc resistance was nonlinear and dependent on arc current magnitude [49].

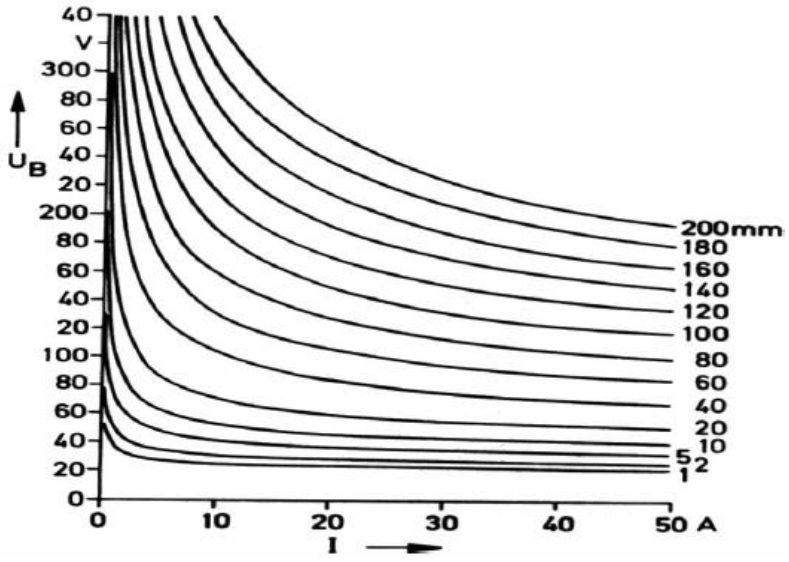

Figure 3-9. Current-voltage IV characteristics in air with copper electrodes by Sölver [49]

or a more detailed examination of arc discharges under thermodynamic equilibrium conditions, theoretical models have been formulated to predict arc properties for any given current from basic material properties of the arc plasma [50, 51]. However, these methods have been found to be problematic [53] from the disadvantage that current density needs to be specified at the cathode as a boundary condition. This boundary condition requirement is a problem because free burning arc properties, such as arc radius and central plasma temperature are largely dominated by convective flow. Here, for current levels greater than 40 A, convective flow, is mainly driven by the pinch pressure of the self-magnetic field of the arc, which in turn is determined by the current density at the electrodes, in particular the cathode [53].

However, various research papers by Lowke [53-56] have developed theoretical formulations of free-burning arcs in air that enable arc radius, temperature, central plasma velocity, electric field and voltage to be predicted as a function of axial position from the cathode to the anode, using simple formulae involving the material functions of the arc plasma [53]. In the majority of the models by Lowke, the arc was treated as a channel, and isothermal with respect to radius, so the predictions are necessarily approximate. At low currents, (< 30 A), the controlling physical process was natural convection, where it was assumed that the arc was vertical and that the input electrical energy produced an arc plasma discharge which was carried upwards by natural convection. The integrated flow of enthalpy across any arc cross-section was taken to be equal to the total input electrical energy upstream of the axial position being considered, where the arc radius increased as a function of distance from the lower electrode. The plasma velocity was obtained approximately from the pressure drop over which any element of plasma was accelerated.

For his general model, Lowke et al., [54, 55] described that within the plasma gas space, $\dot{Q}_{Plasma}$ includes Ohmic heating due to electron and ion currents, as well as losses due to radiation.

$$\dot{Q}_{Plasma} = jE - U(T) \tag{34}$$

His model is illustrated by Eqn. 34 where $\boldsymbol{E}$ is the electric field, j is the current density, and $U(T)$ is the radiation loss. For this study two power levels of 100W and 300W were analyzed, with current levels below 15 A. For low current plasmas, previous studies [53, 55] of atmospheric discharges in air found that radiation losses from the arc column were generally small for currents less than approximately 30 A. From Ohm's law, the electric field in terms of current can be described by Eqn. 35, where σ is the electrical conductivity and A the cross-sectional area.

$$\mathrm{E} = \frac{\partial \mathrm{V}}{\partial \mathrm{z}} = \frac{\mathrm{I}}{\sigma \mathrm{A}} \tag{35}$$

At the cathode/plasma interface, special treatment is required to account for cooling by thermionic emission of electrons and heating by ion bombardment of the electrode [56]. At this interface the additional energy flux provided by Eqn. 36 is included in Eqn. 30, where:

$$F = j_i V_i + j_e \left(\phi_w + \frac{2k_b T}{e} \right) \tag{36}$$

ϕ_w is the work function of the cathode material, Vi is the ionization potential of the gas, k is the Stefan-Boltzmann constant, j_i the ion current density, j_e the electron current density due to

thermionic emission. At the anode/plasma interface Eqn. 37 is set to:

$$F = j_e \phi_w \tag{37}$$

where ion current density is approximated to be zero and j_e is positive as electrons at this location are absorbed at the anode. Theoretical thermionic current is provided by the Richardson equation where ξ is a measured material constant [57]:

$$j_{Rich} = \xi T^2 e^{\frac{-\phi e}{k_b T}} \tag{38}$$

Because the imposed current density j is typically larger than the theoretical current for thermionic emission [55] j_{Rich}, it is assumed that at the cathode/plasma interface the excess current is carried by the ions where $j_i = j - j_{rich}$. In Eqn. 36, j_e accounts for thermionic cooling by electrons overcoming the work function by removing energy as they leave the cathode [55]. At this interface j_e is calculated based on the expression provided by Morrow and Lowke [55] where j_i for a uniform discharge is negative, whereas j_e and E are positive. Further details for the determination of j_i and j_e can also be found in their work.

$$j = j_e - j_i \tag{39}$$

Although the various analyses conducted at Sandia was for arc-plasma discharge currents under 30 A, for higher applied currents above 30 A, Stokes and Oppenlander suggest that magnetic forces are dominant where correlation with Eqns. 40 and 41, which were found to be higher for electrode gap distances between 5-10 mm [38]:

$$V = 0.52 \left(\frac{hx}{\sigma}\right)^{1/2} (\mu j_0 \rho)^{1/4} I^{1/4} \tag{40}$$

$$I = \frac{12kT(\sigma/h)^{1/2}(x/\rho\rho_w g)^{1/4} + 0.9UI}{h(x/\rho\rho_w g)^{1/4}} \tag{41}$$

where T is determined by iteration and U is defined as the net radiation emission coefficient [28]. Results of Lowke's [54] formulations in two dimensions, for high current arcs of approximately 200 A are illustrated in Figure 3-10, where cathode temperatures, as well as bulk plasma temperatures of up to 3,500 K and 22,000 K were predicted respectively. The 200 A arc was predicted with respect to an Argon atmosphere, using 3.2 mm diameter tungsten cathodes with a gap distance of 5mm [54].

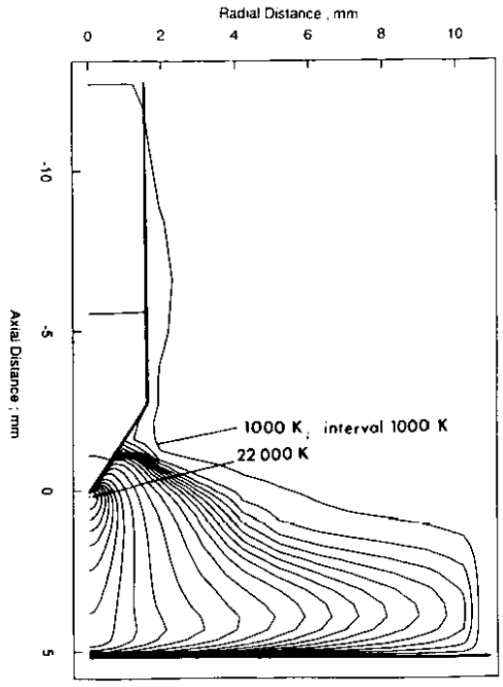

Figure 3-10. Calculated temperature contours for free burning arc win Argon atmosphere, for a 200 A arc at a pressure of 100 kPa [54]

In a more recent publication by Ammerman et al. [16], the investigator compared the previous studies, by Stokes and Opplenlander [38] and Paukert [39], against theoretically-formulated equations by Lowke [53], Figure 3-11. Here, the best agreement between the respective data sets and the model formulations was found for higher current values (> 100 A). The authors concluded from these results that uncertainty with respect to actual arc length determination will likely result in unsuccessful exact calculation of these V-I trends [16].

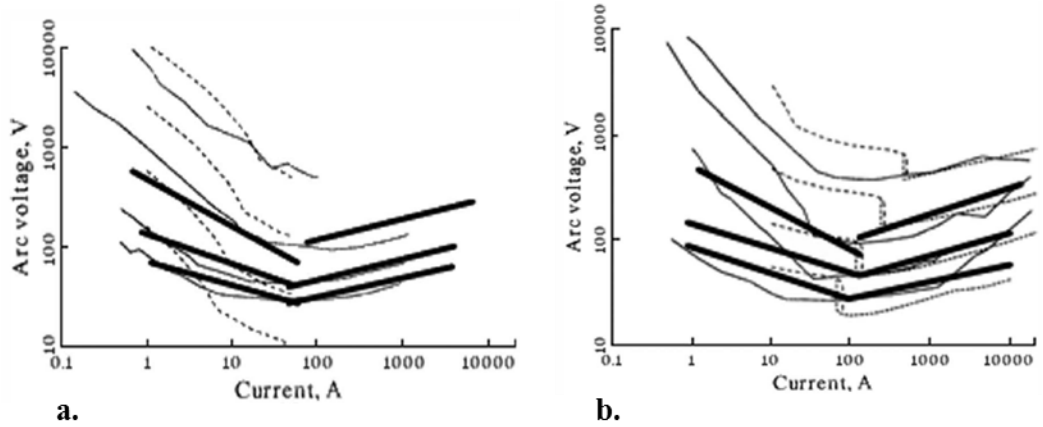

Figure 3-11. a. V–I comparison of characteristic formulas for vertical arcs [39], where full lines are measurements of Stokes and Oppenlander [38], very full thick lines—Paukert [39], and broken lines are provided by the theory of Lowke [53]. (b) V–I comparison of characteristic formulas for horizontal arcs [39], where full lines are measurements of Stokes and Oppenlander [38], thick lines by Paukert [39], and broken lines by the theory of Lowke [53].

Ammerman [16] also compared arc-resistance formulas by Paukert, Stokes and Oppenlander and Nottingham, shown in Figure 3-12 a. and Figure 3-12 b. Figure 3-12 c. shows a comparison of the three approaches for a gap length of 10 mm, where the Nottingham formula is only applicable to electrode gaps in the range of 1 to 10 mm. This illustration shows that the three models are mostly in agreement, especially within the low-current region. Figure 3-12 c. shows the relationship between arc resistance, gap length, and sensitivity to arc current. Figure 3-12 b. shows that the V–I relationships developed by Paukert and by Stokes and Oppenlander exhibit more deviation with large gap widths. Additional observations include the following [16]:

1. Arc resistance is nonlinear.
2. Arc resistance decreases with increasing arc current.
3. Arc-resistance drop approaches a constant value at high current magnitudes.
4. Arc resistance changes rapidly at low current magnitudes (< 1 kA).
5. Paukert predicts larger arc resistances (almost by a factor of 1.5) than what Stokes and Oppenlander predict.
6. For a given arc current, the arc resistance increases linearly with the electrode gap.

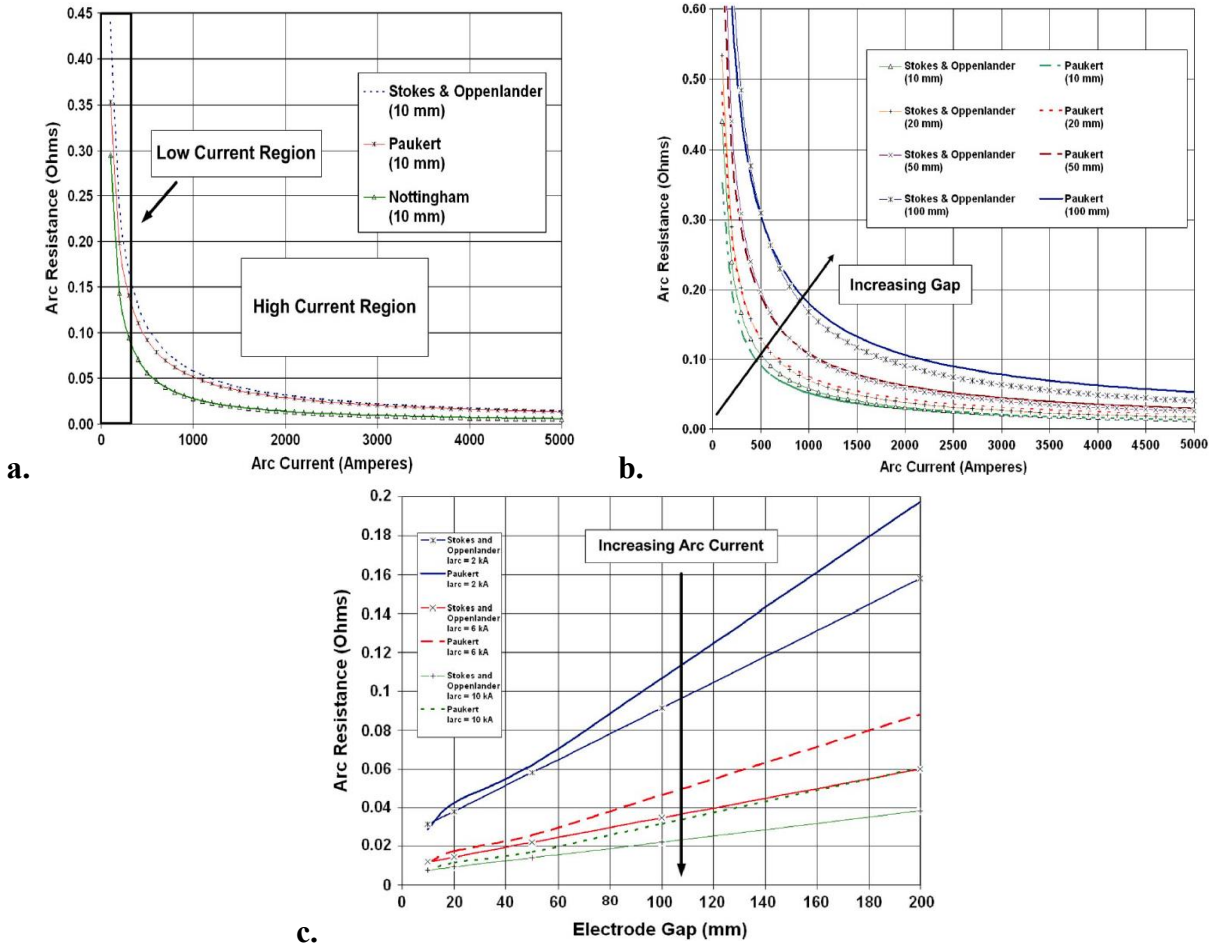

Figure 3-12. a. DC-arc resistance comparative study (10-mm electrode gap) b. DC-arc resistance comparative study (sensitivity to electrode gap) and c. DC-arc resistance comparative study (Stokes and Oppenlander/Paukert formula comparison) [16].

4. PHYSICAL DAMAGE EVALUATION OF AN ARC DISCHARGE

4.1 Overview

The potential arc heat and blast energy from AC and DC sources may be significant where electric arcs involve extremely complex processes of specific thermo-magnetic modelling parameters and environmental conditions. An arc-flash releases large levels of energy rapidly due to arc-faults from low-impedance connections, as the electric arc resistance decreases with time. This reduction in electrical resistance as the arc temperature increases draws more current until a portion of the system melts, trips, or evaporates. This thereby provides enough gap distance to break the circuit and extinguish the arc. In addition to an explosive blast, arc-discharges emanating from metal electrodes can produce very high levels of light energy from far infrared to ultraviolet [59]. Surfaces of nearby objects, including people, absorb this energy and are instantly heated to vaporizing temperatures, where the effects of can be seen on adjacent walls and equipment where they can become ablated and/or eroded from radiant effects [59].

AC arc-fault damage (expressed in units of kW-cycles) is typically proportional to the arc current, fault duration, and the RMS arc voltage, where minimal damage occurs anywhere from 1,800 to 2,000 kW-cycles, limited damage occurs below 6,000 kW-cycles, and more extended damage occurs above 10,000 kW-cycles [60]. According to Gammon and Mathews [21] faults that release 10,000 kW-cycles of energy are likely to destroy system equipment and endanger human life. Stanback's [61] method for assessing damage of a single-phase-to-ground arcs avoids the built-in error associated with assuming an arc voltage [21]. In the authors' investigations, single-phase arc-faults were initiated on a 277 V single-phase system from phase (copper or aluminum bus bars) to ground (steel housing) to quantify the damage that occurred to bus bars and steel housing. The amount of material burned was related to the arc current, the time span during which the arcing occurred, and material type. The rate of material burning, Y (m^3/s) can be determined from the following equations [61]:

$$\begin{aligned} Y &= 1.076 \cdot 10^{-11} \cdot I_{Arc}^{1.5} t \quad for\ Steel \\ Y &= 1.185 \cdot 10^{-11} \cdot I_{Arc}^{1.5} t \quad for\ Copper \\ Y &= 0.249 \cdot 10^{-11} \cdot I_{Arc}^{1.5} t \quad for\ Aluminum \end{aligned} \tag{42}$$

From these equations, if a 5,000 A arc current was discharged in 0.35 s, 0.082 m^3 of steel housing would burn along with 0.089 m^3 of copper bus or 0.188 m^3 of aluminum bus material [61].

Arc-faults in an industrial environment may be initiated under a wide range of conditions, where an arc discharge is a dynamic process, which can be more dynamic, random, and turbulent than constrained arcs initiated in a controlled, thermodynamic-equilibrium environment. One of these cases is an open-air exposure environment, such as those found in nuclear energy systems. Here, semi-empirical formulations can be an effective way of modeling arcing faults in power systems and calculating incident energy, especially for high-voltage situations. In his investigation, Ammerman highlighted two types of DC incident energy estimates for assessing hazard limits and the potential for damage: Open-air arc exposures and arc-in-a-box exposures [16]. For open-air arc exposures, Ammerman provided the example of a nuclear plant, large battery-bank installation where for this type of exposure, the heat transfer depends on the spherical energy density, as described by Eqn. 43, where d represents the distance from the arc (in mm).

$$E_{Inc.} = \frac{E_{Arc}}{4\pi d^2} \tag{43}$$

For an arc-in-a-box exposure (i.e., a confined space), for a DC arc initiated within a piece of switchgear, the enclosure tends to have a focusing effect on the incident energy [16]. Wilkins proposed an approach for three-phase AC arcs where the spherical energy density component is replaced by a value E_1 that takes into account the focusing effect of an enclosure [62]. Here, the term E_1 also represents the additional energy reflected by the back and sides of the enclosure as prescribed by Eqn. 44.

$$E_1 = k\frac{E_{Arc}}{a^2+d^2} \tag{44}$$

Table 4-1 lists Wilkins' optimum values of a and k constant for the three equipment classes described in the IEEE 1584 guide [36]. Ammerman concluded that the employment of Eqns. 43 and 44 to compare arcs initiated in enclosures with those in open-air arc exposures shows that the arc-in-a-box case results in an increase of incident energy directed toward a worker [16].

Table 4-1. Optimum values of DC semi-empirical formulation constants [62]

Enclosure Type	Width (mm)	Height (mm)	Depth (mm)	a (mm)	k (mm)
Panelboard	305	356	191	100	0.127
LV Switchgear	508	508	508	400	0.312
MV Switchgear	1143	762	762	950	0.416

From Eqns. 43 and 44, Figure 4-1 a. and Figure 4-1 b. approximate incident energies associated with DC arc-faults of 2, 6, and 10 kA were assessed across a gap spacing of 32 mm. The arc power was calculated from arc-resistance Eqn. 20 where the incident energy at 457 mm was determined [16]. The LV switchgear values for a and k in Table 4-1 were used to calculate the incident energies associated with an enclosure. The resulting incident-energy levels are compared with the hazard risk categories defined in NFPA 70E [40]. For the selected enclosure type and test distance, incident energies calculated for enclosures are 2.2 times larger than the incident energies calculated for open air [16].

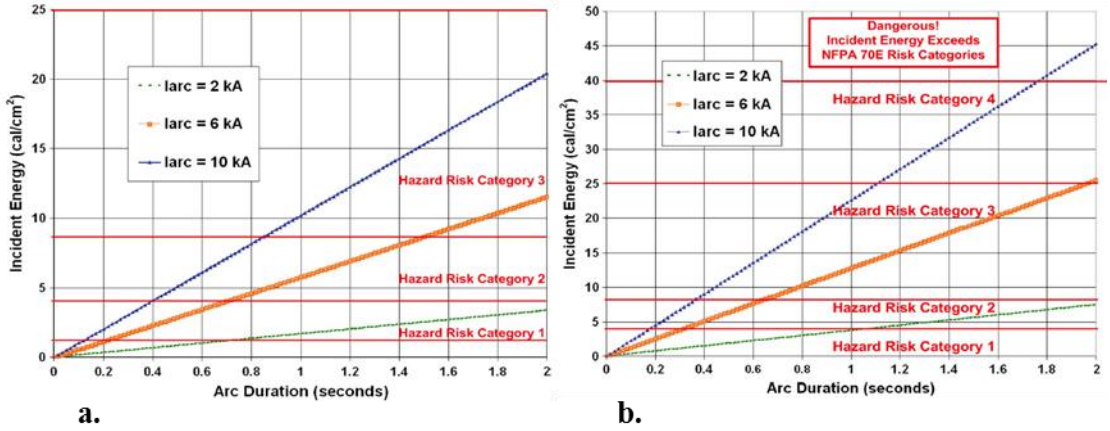

Figure 4-1. Incident energy versus arc duration for 32 mm arc gap and 457 mm working distance for a. open air configuration and b. arc-in-a-box configuration [16]

For industrial applications, arc-fault current is usually much less than the available bolted fault current, and below the rating of most circuit breakers [21]. Unless these devices have been selected to handle respective system arc-fault conditions, they will not trip, which could increase the for potential for an arc-fault and subsequent arc-flash. The transition from arc-fault to an arc-flash takes a finite period of time, increasing in intensity as the pressure wave develops. The detrimental effects of an arc flash incident all depend on the energy conversion that take place during an arc-fault. Most investigators often try to relate arc damage to the time duration and magnitude of the arc current, where some measure of potential arc damage has previously [21] been used to determine the appropriate time and current settings for ground-fault-protective devices in coordination with phase-over current protective devices. Another common approach to arc power and damage assessments uses standardized industrial power system calculations. In an analysis by Gammon and Mathews [21], shown in Figure 4-2, the locations A, B, and C correspond to the main distribution panel (MDP), a subpanel (panel), and a branch circuit (branch), respectively [16].

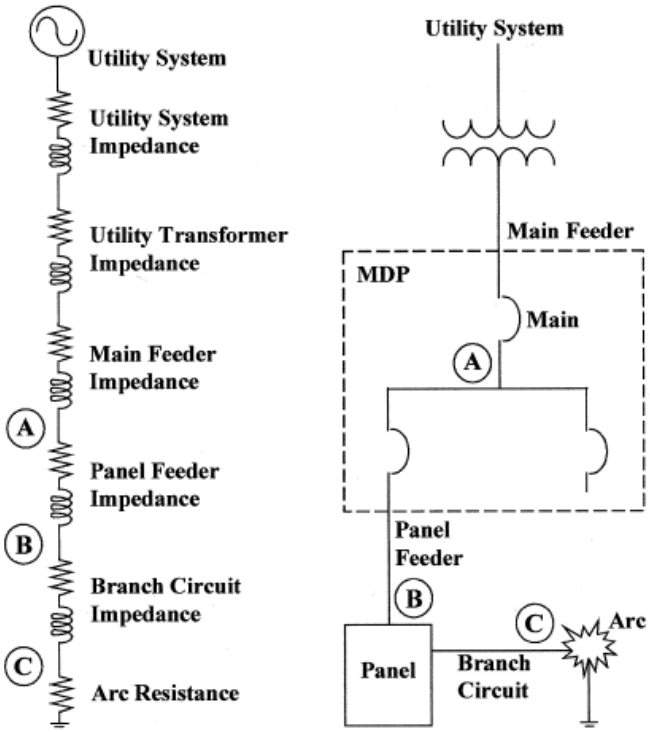

Figure 4-2. Arc-Fault test circuit [21]

From their analysis, results by Gammon and Mathews [21] suggested that in comparison with the current-dependent arc model, a 100 V arc voltage and an arc current equal to 38% of the bolted-fault, predicted a lower arc power with a greater number of cycles before a 10,000 kW-cycles threshold of energy could be released. When arc power is assumed to equal 50% of the bolted-fault VA, a larger power value is predicted that results in reaching the 10,000-kWcycle damage threshold in a smaller number of cycles than the current-dependent arc model. Their results also found that arc power at the main distribution panel is greater than the time-average power released by a short circuit [21].

4.2 Arc-Flash Pressure Impacts

4.2.1 Previous Research

Arc-flash pressure waves experienced by electrical workers as well as pressure-sensitive equipment, can be detrimental to occupational safety and also to costs. In a study by Lee [63] the author cites several case histories, where in one instance an electrician was somersaulted 25 feet away from the arc when an approximate 100 kA bolted fault occurred on a 480 V system. For this case, Lee calculated an approximate initial impulse force at 24 inches (100 kA bolted fault, or approximate 42 kA arc) to be approximately 260lb/ft^2 [8].

The force exerted from an arc-plasma discharge has also been studied to some detail, by Capelli-Schellpfeffer et al., [64] who developed a two-dimensional computational simulation of an electrical arc explosion where temperature and acoustic force propagation was assessed across the geometry of a hypothetical workroom from 0 to 50 ms after arc initiation. Theoretical results were compared to experimental findings of staged tests involving a mannequin worker monitored for electrical current flow, temperature, and pressure, and reported data regarding neurologic injury thresholds. The results of their study found that the blast temperature (Figure 4-3) is inversely proportional to distance from the ignition source, where over time, the temperature from a

simulated electrical arc ignition is attenuated sooner than the acoustic force intensity, Figure 4-4

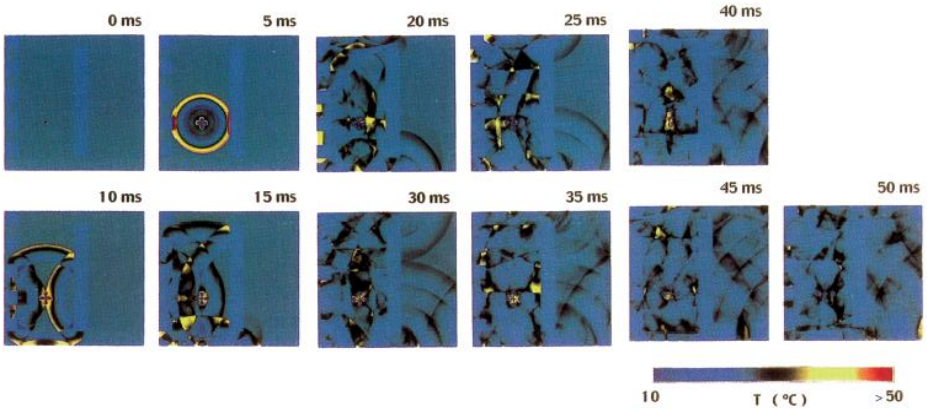

Figure 4-3. Simulated temperature in a hypothetical space following a 20 kJ arc ignition [64].

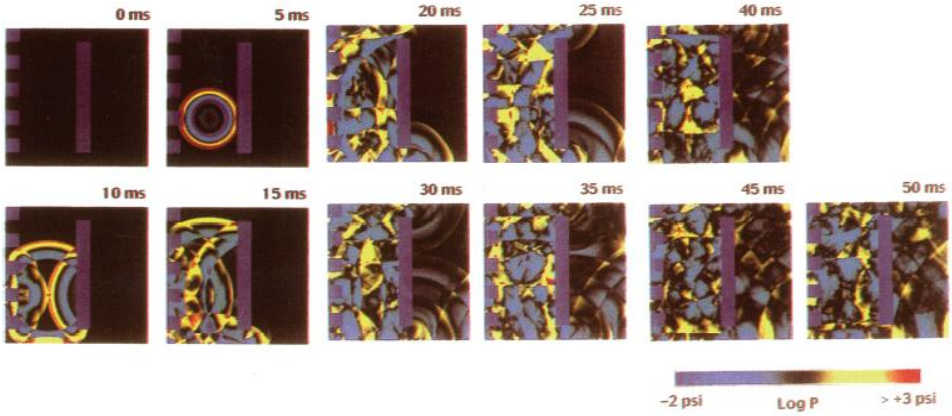

Figure 4-4. Simulation of an acoustic shock waves propagating through a hypothetical space following a 20 kJ arc ignition [64].

An analysis by Mendenhall [41] considered the potential damage of cascading faults on an electrical system where the author expounded on the high possibility that a fault at one end of a resistor termination could potentially cascade to adjacent terminations. His calculations were performed for the vectorial contributions of adjacent faults up to the maximum for contributions from all devices considered. Mendenhall found that arc heat and blast pressures were directly proportional to the square of the voltage where the heat and pressure were reduced by a factor of four. Because arc heat and blast pressures were inversely proportional to the square of the distance from an initiating arc to a shield blanket, doubling the distance to 28 cm reduced the arc heat to a maximum of 44 cal/cm^2–well within the validated testing range of a seven-layer arc suppression blanket [41]. The customized blanket was suspended by carabiner clips through grommets to a steel structure and the lower portion of the blanket was cinched by straps below the resistor array structure; thus it would deflect an arc blast upward without rupturing, and would be flexible enough to maneuver for maintenance activities.

In 2009 the international council of large electric systems (CIGRE) established working group A3.24 who provided pre-standardization input to the IEC based on a set of tests for developing tools for the simulation of internal arc effects in medium voltage (MV) and high voltage (HV)

switchgear [65]. Here, the group collected and performed internal fault tests with SF6 and air arc mediums. Their developed validated mathematical models took the approach illustrated in Figure 4-5 for assessing the pressure rise from an arc-fault.

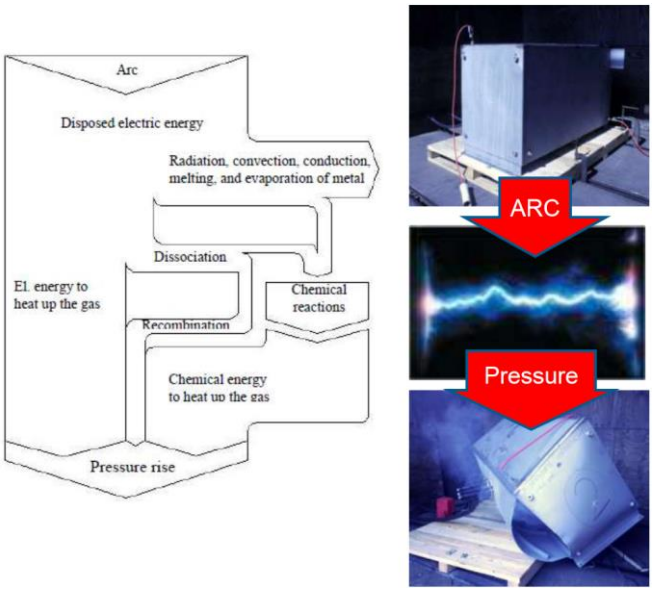

Figure 4-5. Energy/pressure development when an arc is burning between aluminum electrodes [65, 66].

The group results found that the pressure rise was directly dependent on arc voltage and current, where larger blast volumes took longer to facilitate significant blast damage. Additionally, the results showed that burn-through time for steel was four times larger than for aluminum. As illustrated in Figure 4-6, for arc-flash models of subsequent pressure waves, as well as exhaust component pressures, the results illustrate an arc-flash pressure peak that can be greater than 3.5 times that of the exhaust pressure. Although these results provide a great estimation for arc pressures, several approximations were applied that could limit its employment and scalability.

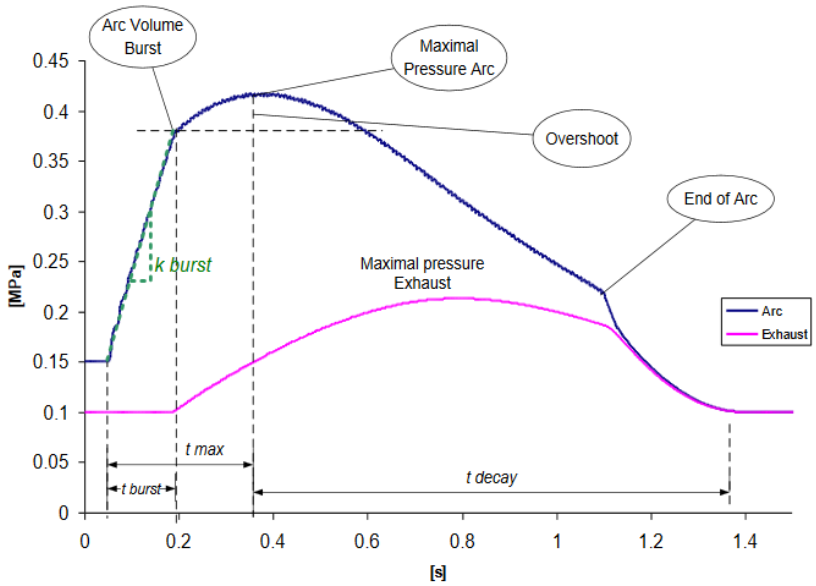

Figure 4-6. Arc characteristic values determined from calculated/measured pressures of the CIGRE A3.24 working group [65]

The blast energy or pressure from subsequent arc-flash shock waves are not presently addressed in NFPA 70E or IEEE 1584, however future plans by the IEEE arc-flash working group call for measurements of these forces, which can be significant and highly detrimental to worker safety, causing burns, and even falls and injuries that may be more severe than the burns themselves [8]. However, research at Sandia National Laboratories (SNL) is currently underway to model pressure waves from arc blasts to provide a quantitative measure for evaluating safety.

4.2.2 Sandia National Laboratories Arc Pressure Physics Modelling

Given the rapid advancement in computational power and multiphysics modeling, computational mechanics are now providing significant insights into arc-fault/arc-flash safety, design, and experiments of complex nuclear reactor systems [67, 68].

An in-house SNL code, ALEGRA, is a 2D/3D shock and multi-physics code being developed at SNL [69]. It performs multi-material arbitrary Lagrangian-Eulerian (ALE) calculations and includes circuit models (e.g., resistors, capacitors, and inductors). The ALEGRA-MHD version includes a magneto hydrodynamics (MHD) package suitable for magneto-solid mechanics, magnetic field diffusion, and many magnetic forces and phenomena, such as Lorentz forces, Joule heating, thermal conduction, and radiation [70]. This allows the ALEGRA-MHD to characterize materials experiencing shock and large deformation rates under magneto-hydrodynamic forces, which can provide a strong potential for nuclear safety, validation, and design analysis. In addition to advanced computational methods, SNL has a host of experimental facilities that are suitable for Arc-Fault/Arc-Flash experiments (Appendix A2). This includes the ignition of H_2 gas released during a severe nuclear accident, instrumentation and control panel safety, containment damage from combustible gas explosions (e.g., H_2), as well as igniter research for simulation of the oxy-combustion of natural gas mixed with CO_2.

The goal in this section is to investigate spark propagation damage to nuclear reactor facilities, as well as investigate ways to mitigate their impact for enhanced reactor safety, led to our desire to investigate ALEGRA-MHD's capability. For this capability-demonstration research discussed in this document, investigation considered two distinct systems that underwent an arc transient. One

considered an arc propagating with respect to time through an air environment, and the other considered an arc through a water environment.

4.2.2.1 MHD Arc Capacity-Demonstration Model–Air Medium

To conduct rapid capability-demonstration simulations on a small number of processors, we selected a 2D domain, as shown in Figure 4.7. The domain is five times longer in the horizontal direction (x) than the vertical direction (y), to allow a shock and spark to propagate from left to right with a sufficient span that facilitates simulation of the spark's lifetime: initiation, growth, and subsequent decay. The domain consisted of air initially at 300 K, where a spark originated at time zero at the bottom left hand side of the domain. The spark was able to grow, propagate, and decay with respect to space and time. Note that the mesh was sufficiently discretized to allow at least four computational nodes through the shock front.

Although, the domain could run in 3D, running in 2D significantly decreased the required computational time; note that the millimeter-sized domain required less than 10 minutes to run on 64 processors in parallel. However, this indicates the significant computational potential when hundreds to thousands of processors are used on a system, even if it is multiple meters in size.

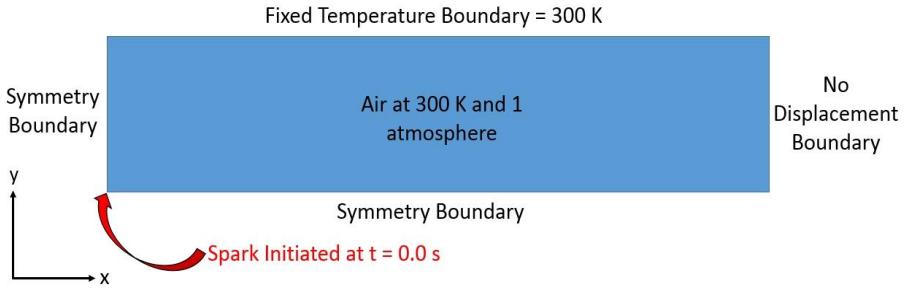

Figure 4-7. ALEGRA-MHD arc-flash model.

Key parameters from the simulation are shown in Figure 4-8, Figure 4-9, and Figure 4-10; these include temperature, pressure, and shock wave velocity. Figure 4-8 shows the spark temperature at 3.0×10^{-10}, 1.0×10^{-9}, and 2.0×10^{-9} s, respectively, as the arc-flash propagated from the bottom left to the right. As the arc-flash was initiated, the surrounding air temperature rose within a few nano-seconds from 300 to 25,300 K, and propagated throughout the domain.

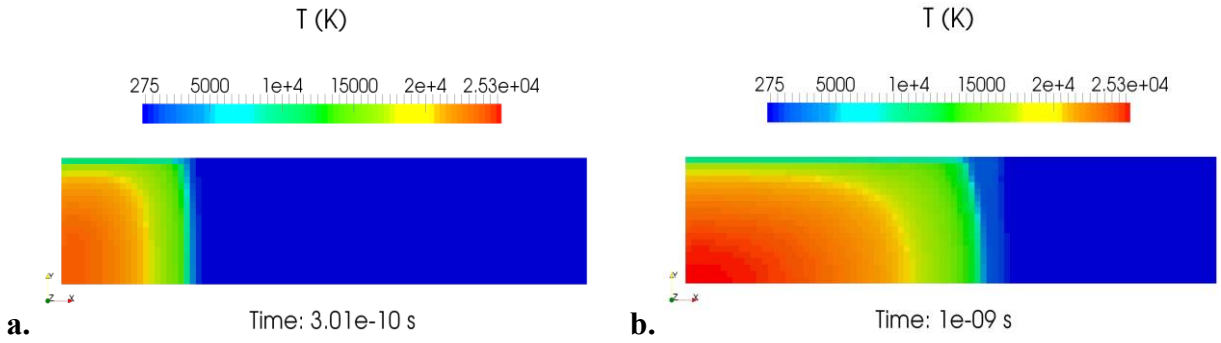

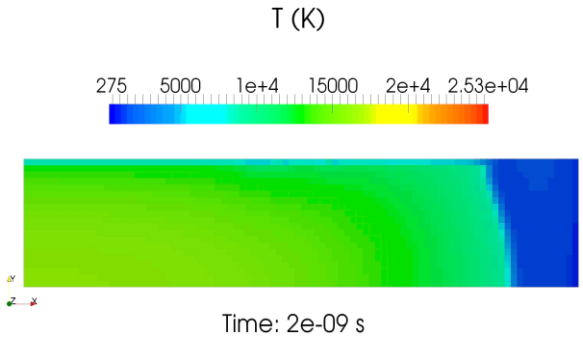

c.

Figure 4-8. a. Arc temperature at a. 3.0x10^{-10} s, when the arc had just initiated, b. 1.0x10^{-9} s, when the arc continued to grow and propagate, and c. 2.0x10^{-9} s, when the spark was decaying and reaching the opposite end of its domain.

Additionally, Figure 4-9 shows the arc shock wave pressure progression at 3.0x10^{-10}, 1.0x10^{-9}, and 2.0x10^{-9} s, respectively, as it propagated from the bottom left to the right. As soon as the spark was initiated, the surrounding pressure rapidly rose from 103,500 to 1.64x10^{6} Pa, as the spark continued to propagate through the air.

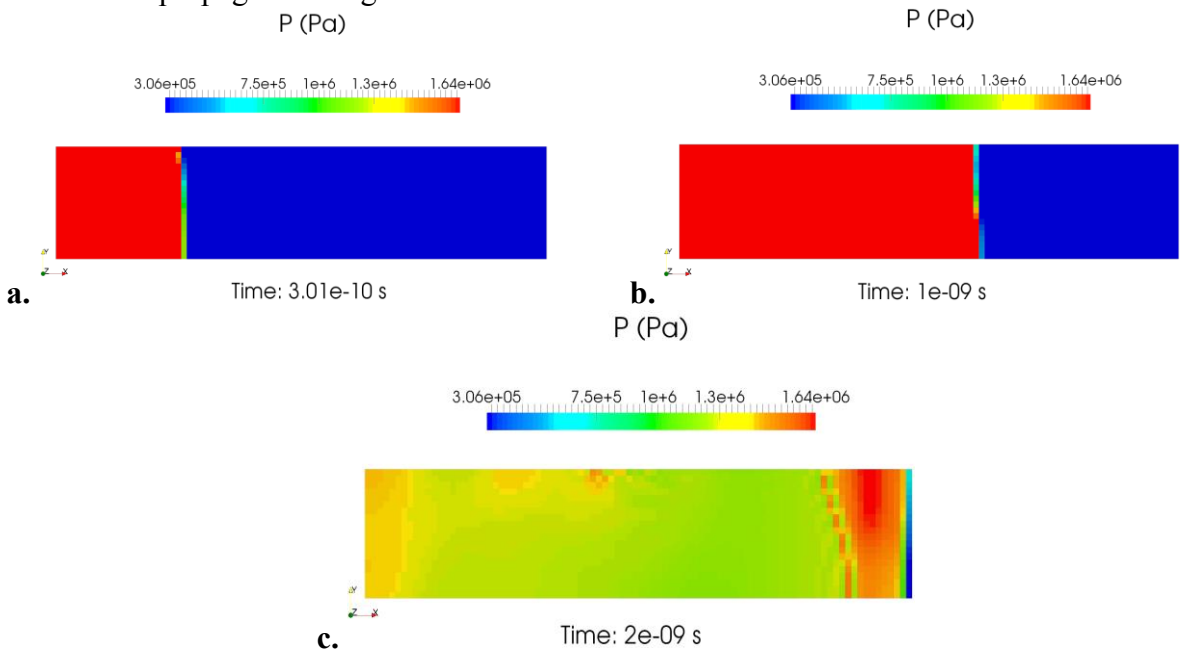

a. b. c.

Figure 4-9. Arc pressure wave distribution at a. 3.0x10^{-10} s, when the spark had just initiated, b. 1.0x10^{-9} s, when the arc continued to grow and propagate and c. 2.0x10^{-9} s, when the arc was decaying and reaching the opposite end of its domain

Accordingly, Figure 4-10 illustrates the shock wave induced by the arc at 3.0x10^{-10}, 1.0x10^{-9}, and 2.0x10^{-9} s, respectively. As the arc initiated, the surrounding velocity rapidly rose from stagnant to 1.69x10^{3} m/s, and the shock front moved rapidly to the right. As the shock wave travelled further to the right, it started to disperse and its velocity was dropped, as expected.

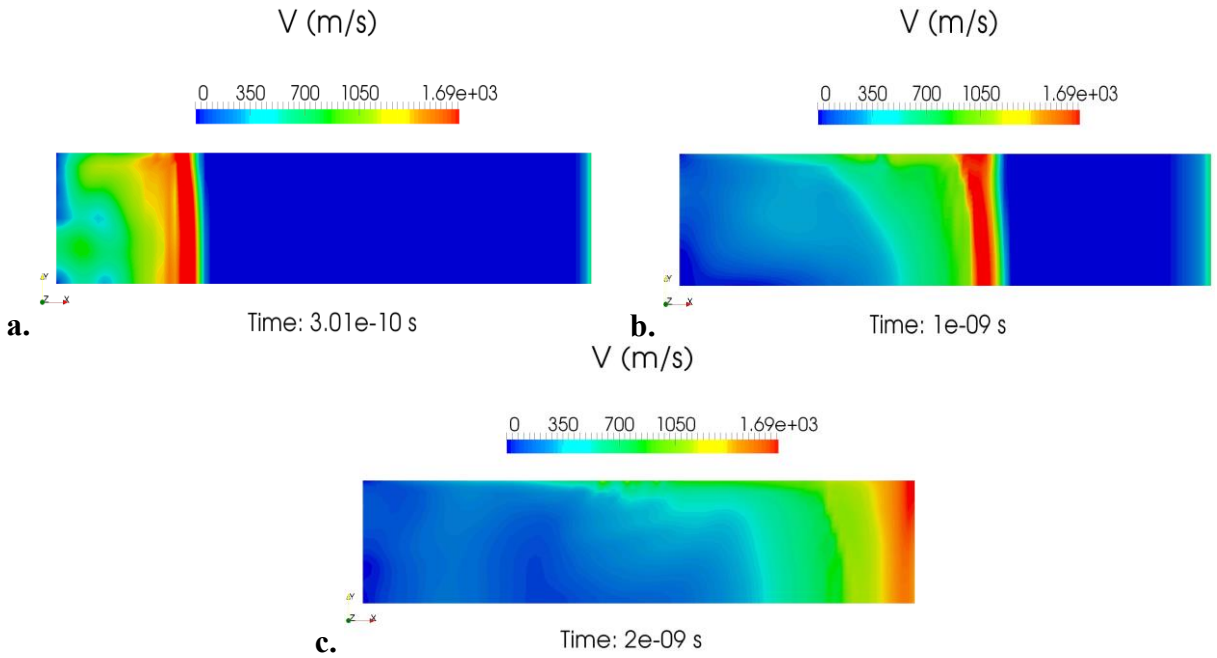

Figure 4-10. a. Arc shock wave velocity at a. 3.0×10^{-10} s, when the spark had just initiated, b. 1.0×10^{-9} s, when the spark continued to grow and propagate and c. 2.0×10^{-9} s, when the arc was decaying and reaching the opposite end of its domain

4.2.2.2 MHD Arc Capacity-Demonstration Model - Water Medium

As a further capabilities' demonstration, we briefly include a calculation conducted by the SNL ALEGRA team, where a spark occurred in a water domain. Figure 4-11 a. shows the spark temperature propagation with respect to time and space, while the pressure and density are shown in Figure 4-11 b and Figure 4-11 c, respectfully. Note the units shown in Figure 4-11 a. through Figure 4-11 c. are in electron-Volts (eV) and mm.

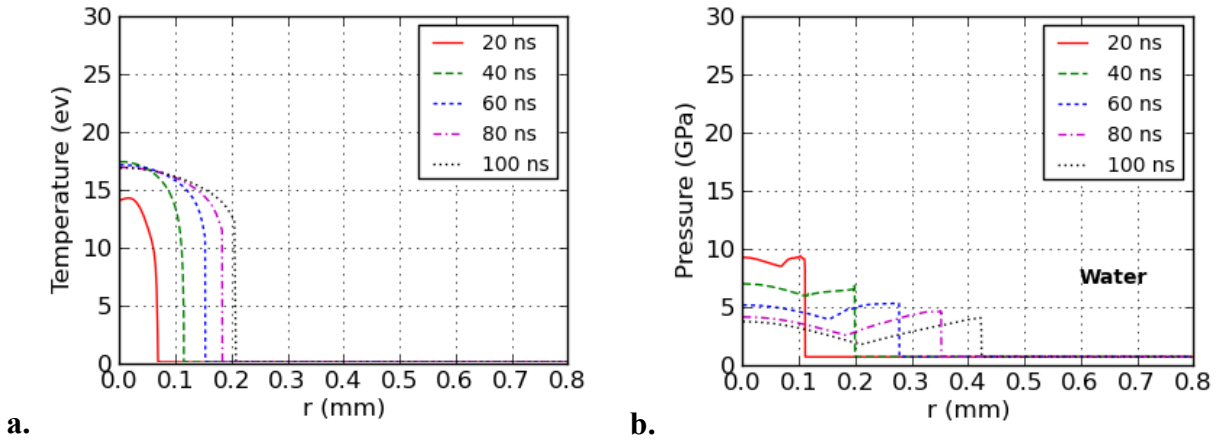

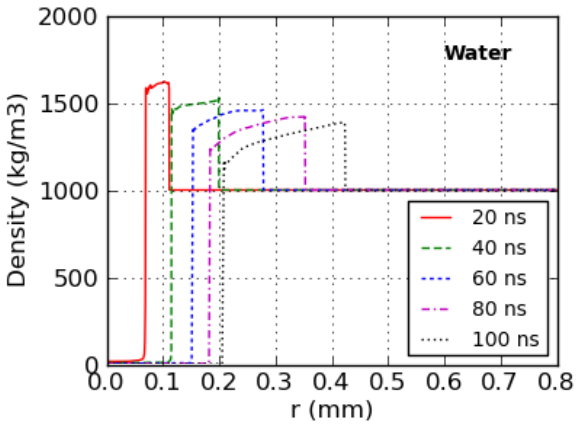

c.

Figure 4-11. a. Temperature propagation in space and time for an arc in a water environment, b. pressure propagation in space and time for a spark in a water environment, and c. density distribution in space and time for an arc in a water environment

The simulations required less than 10 minutes to run on 64 processors in parallel. This indicates the computational potential when hundreds to thousands of processors are used; our capability-study demonstrates that we can capture a spark's shock front for large systems within a reasonable amount of time. The research conducted shows a strong potential for the ALEGRA-MHD model to conduct safety, design, and validation analysis. Being able to capture a spark's shock front allows the calculation of the total force imposed on the nuclear system, and therefore addresses any potential damage and provides mitigation recommendations. Moving forward, validation simulations are needed to compare with experimental data, which will help increase confidence in the analysis of complex systems. An overview of the SNL arc-fault generator can be found in Appendix A2, which can be used to generate this data. ALEGRA-MHD can be used to plot dozens of key parameters for validation of experimental data.

4.3 EMI Impacts of Arc-Flash on Equipment

4.3.1 Overview

As a result of an arc-flash event, equipment can also be damaged including primary switch gear, transformers, and low voltage distribution equipment, where an arc-flash can generate an enormous explosive force where even a relatively small 10,000A arc at 480V can create an explosion equivalent to 8 MW of power [71]. Concerns about the effect of electromagnetic interference (EMI) events on the power grid have been the subject of a large body of research. Historically, geo-magnetic storms have created ground induced currents in long electrical conductors, which can then damage or destroy components such as power line transformers [72] or capacitors, even on properly protected equipment. For example, in March 1989, a solar storm caused a complete collapse of the Hydro-Quebec power system. This precipitated the development of new NERC reliability standards for geomagnetic disturbance [73, 74].

Electrical systems, especially those connected to the grid, routinely experience disruptions where the cause is typically attributed to the failure of one or a small number of components. EMI events can lead to widespread failures; however, models that predict failures resulting from EMI events have not been validated in enough detail [72]. Causes of EM events include naturally occurring solar flares, solar wind, lightning and P-static discharge caused by triboelectric effects [72]. EM events could also be man-made, such as microwave pulse sources and arc-plasma discharges of

various effective coverage areas and directivity.

Some high level EM effects occur naturally, and are experienced occasionally in our every-day environments. For example, electrostatic discharge (ESD) is a "mini-lightning." ESD is a serious issue for micro-electronics industry, but we will not address this issue here due to significantly lower energies involved. Low EMP (LEMP) refers to the EM environment associated with standard lightning (not a direct strike), and is generally easiest to protect against through the use of surge protectors. Plasma-discharge (e.g., lightening) susceptibility can vary widely by region, depending on flash density of lightning strike events as well as other characteristic properties (e.g., effective "touchdown area" on the ground or equipment). Damage to a utility asset may vary from a "puncture" to a much broader impact caused by a strike with larger "touchdown" area.

There are strong similarities in the types of damage resulting from EM events, as well as similarities in the mitigation measures necessary to reduce vulnerability. Expected damages can be classified into two major categories:

- Permanent damage (immediate or latent)—The damage can cause immediate failure, accelerated degradation or latent failure. Such latent reliability effects are hard to predict, and high-level laboratory tests should be used to detect and quantify such vulnerabilities.
- Temporary upset of normal operation—Upset is considered a disruption of the normal operation of the system. This might be a minor glitch from which the system quickly recovers and continues working, or a more serious problem that requires a system restart. The effect might be immediate, or be discovered only later. Inverter settings (which may be customized by individual operators) may be lost, thus leading to improper settings and sub-optimal or erroneous operation. For sparsely manned facilities, such as utility-scale DC systems, detection may be delayed. This can leave the system working at improper settings, potentially compromising the lifetime of the equipment.

4.3.2 Relevant International Specifications

- IEC 61000-2-5: Electromagnetic compatibility (EMC)—Part 2-5: Environment-Description and classification of electromagnetic environments;
- IEC 61000-4-1: Electromagnetic compatibility (EMC)—Part 4-1: Testing and measurement techniques—Overview of immunity tests;
- IEC 61000-4-6: Electromagnetic compatibility (EMC)—Part 4-6: Testing and measurement techniques—Immunity to conducted disturbances, induced by radio-frequency fields

4.3.3 Susceptibility of Utility and Power System Equipment

We can divide susceptible equipment into several broad categories: High power transformers, high power utility substations including SCADA (Supervisory Control and Data Acquisition) and similar control equipment, switches and relays, and finally, transmission and distribution lines.

There are two primary ways that EMI-induced damage may be delivered to a system. One is through the propagation of externally radiated fields, and the other is through conduction along cables and wires. These two methods of delivery are consistent with the general treatment of electromagnetic disturbances in the field of electromagnetic compatibility where nearly all environments and tests are defined in terms of radiated or conducted environments (e.g., IEC

61000-2-5).

For radiated fields, frequencies above 100 MHz are of primary concern in that they are able to penetrate unshielded or poorly protected buildings very well, and yet couple efficiently to the equipment inside of the building. The externally incident fields are characterized by the direction of incidence, polarization, amplitude (V/m), and waveform (rise time and pulse width). Fields of amplitudes as low as single Volts/m have been shown to have a potential to induce damage to the electric and electronic circuit elements via breakdown of individual components. While the electromagnetic fields fall off as $1/r^2$, the conducted current and voltage pulses may be propagated over long distances.

4.3.3.1 Transformers

Several prior studies have investigated possible EMI damage on step-down distribution classes of transformers [75]. This testing included 19 samples of 7.2 kV/25 kVA power distribution transformers. Damage that occurred was usually from dielectric breakdown within the windings–pinhole damage. Additionally, it was noted in the test results that failures occurred when the peak fast pulse voltage was between 264 and 304 kV. No damage occurred for EM peak pulses of 290 and 296 kV, so there appears to be some variability within the group of 19 transformers, although the variation is not that great. When lightning surge arresters were added to the transformers, no damage was noted up to 1000 kV.

4.3.3.2 High Power Utility Substations: SCADA and Other Control Equipment.

Within the substation, it is generally the SCADA and other control equipment that may be most vulnerable to the EMI effects. And, specifically, these devices may be most sensitive to voltage and current pulses coupled from outside EMI environment, and carried via either low voltage or communications (such as CAT-5/6) cabling. Previous studies have shown that voltage and current pulses up to 1000 V and tens to hundreds of Amps may be induced on the communication lines. It is then quite possible to expect immediate and/or latent damage on equipment that may only be rated to handle a 12 to 24 V logic switching operations.

4.3.3.3 Switches and Relays

Relays, switches, and fuses may also malfunction or reduce their functionality, due to EMI. Most of the modern switches and relays are communications-enabled (Modbus, Ethernet or other), so the same high voltage and current pulses coupling into communications ports may lead to damage, malfunction or loss of function of relays and switches. As a result of voltage and current coupling on transmission and distribution lines (see 4.3.3.4), fuses may also be damaged, and therefore may need to be manually replaced. This may result in an extended outage to an electrical system or utility customers.

4.3.3.4 Transmission and Distribution Lines.

EM effects may couple substantial amounts of energy onto long stretches of transmission and distribution lines. Any line's configuration (underground, aerial, and overhead) can be susceptible to EM fields, the coupling strength will of course vary and will be dependent on multiple parameters. For example, if an underground cable is installed under a protective layer of concrete, this will of course act as a shielding medium, and will reduce coupling effects. Aerial lines, on the other hand, may experience worse cases of coupling. Each of the cases will be different, depending on the EM fields' frequency ranges and directivity. Previous studies have shown that low ambient electric field (as low as single Volts per kilometer) may result in significant geomagnetically induced currents and result in significant damage to substation equipment and, specifically,

transformers [76].

SNL's Electromagnetic, Pulsed Power and Electrical Sciences Group is a multidisciplinary research and development team that conducts a broad range of experimental and theoretical research impacting electrical systems. This work includes EM pulse coupling into components and systems supported by large volume transverse EM, reverberation, and anechoic test cells; lightning protection of components and systems; and high-voltage sciences including electrical breakdown, advanced power, and power electronic systems.

The reliability group at SNL also has extensively studied reliability and inverter physics of failure modes under different stresses, as well as failure modes of individual components, such as electrolytic and thin film capacitors, metal–oxide–semiconductor field-effect transistors, insulated-gate bipolar transistor, and even soldering joints.

5. ARC-DISCHARGE MITIGATION SOLUTIONS

5.1 Overview

To reduce the potential of an arc-flash event, Dargatz suggest the following considerations [77]: proper design; preventative maintenance on electrical equipment; established goals and objectives; and performance and maintenance of short circuit study, arc-flash analysis, and coordination study. System design philosophy has a significant impact on both prevention and suppression of arc-fault related fires, with an increasing preference being given to AC-based systems that mitigate the risk of fire by avoiding distribution of high DC voltage and high DC current. Overall, there are two main elements to AC and DC arc-fault safety [77]:

1. Prevention–Engineering mechanisms and factors necessary to reduce the creation of an arc, especially one that is capable of becoming the source of ignition of nearby combustible materials. Here, preventative measures are necessary to minimize the risk of starting the fire altogether.
2. Suppression–These are approaches for extinguishing fires after they have started. Various means related to arc-fault circuit interrupters as well as a new class of self-extinguishing materials recently developed at SNL can be used to address this approach. Here, the presence of relatively high DC voltage and high DC current presents a significant risk to firefighters, where built-in methods of suppression can be highly desirable within design.

5.2 Prevention and Proper Design

Arc-flash hazard analysis (AFHA) combines both electrical and safety engineering. Personnel performing AFHA must be aware of the proper methods of hazard and systems safety principles, as well as the power systems design. An AFHA consists of four distinct engineering functions, including [78]:

1. System modeling
2. Data entry and validation
3. System analysis
4. Reporting and recommendations

When conducting AFHA, one must first determine the amount of short circuit current (SCC) generated by the system during faulted conditions at each "node" (i.e., location, subsystem, device, etc.) in the facility [78]. This information is valuable for ensuring protective devices are properly rated to interrupt the available SCC and properly sizing grounding cables. The AFHA must take internal generation capabilities into account when performing a particular study, where one key output of the SCC analysis is a report known as the "protective device duty analysis," which compares the capabilities of protective devices (fuses, circuit breakers) to interrupt SCC to which it is subjected [78]. In cases where the SCC exceeds the interruption rating of the protective device, a "through-fault" results, which means the protective device operates but is unable to interrupt the flow of SCC. Because the result is the same effect as not having a protective device in the circuit, the SCC must then be interrupted by the next protective device in series with the system "upstream" toward the source, which can result in much slower arc clearing times. This in turn, translates into far greater incident energy exposure levels for electrical workers [78].

Additionally, coordination analysis involves evaluating the time current curves (TCC) of the protective devices to ensure that the electrical system will clear faults where a TCC corresponds to the speed at which a device will "clear" an SCC as a function of the amount of SCC to which it is exposed [78]. In general, the higher the SCC, the faster the protective devices will operate, which describes why systems with low SCC can actually have more incident energy because the arc duration time determines the amount of heat development. A coordination study performed the following tasks: 1. evaluates the coordination of the current system configuration, and 2. evaluates the system once the recommended engineering changes have been implemented. The recommended engineering changes that come from this analysis can involve any combination of the following [78]:

1. Reduced trip times on adjustable circuit breakers.
2. Use of current-limiting fuses.
3. Reducing fuse sizes of non-current-limiting fuses.
4. Replacing fuses with other styles of fuses that have different TCC characteristics.
5. Changing protective relay settings on systems where an electronic relay actuates a separate circuit breaker. Although these systems can be more expensive, they can provide maximum flexibility for engineering interventions because many different relays can be connected to a single circuit breaker. This indicates that the protective systems can be "smarter" than simply sensing magnetism or heat, as is the case in most simple thermal-magnetic circuit breakers found in residential applications. Additionally, lack of proper engineering studies may allow the installation of lesser expensive, yet ineffective types of protective devices.
6. Inserting additional protective devices in series with existing devices. Note: Often, the use of motor overloads in series with fuses can result in much lower values of incident energy because fuses can be set to interrupt only SCC while relying on the overload sensors to interrupt overloaded conditions.

It is a good design practice to perform all necessary electrical system designs in compliance with National Electric Code (NEC) compliance standards (including 110.16 Flash Protection and 240.12). As illustrated in Figure 5-1, safe operations can be facilitated by employment of both National Electric Code (NEC) and Occupational Safety and Health Administration (OSHA) protocols for both DC and AC systems [79]. It is also good practice to consider OSHA regulations (29-CFR, Part 1910) and customer safety standards in lieu of all breaker settings, all fuse types and coordination between all the protective devices [79]. Additionally, four separate industry standards focus on the prevention of arc flash incidents through design:

- NFPA 70-2005, National Electrical Code (NEC)
- NFPA 70E-2004, Standard for Electrical Safety in the Workplace
- IEEE Standard 1584-2002, Guide for Performing Arc Flash Hazard Calculations
- OSHA 29 Code of Federal Regulations (CFR) Part 1910 Subpart S.

NFPA 70E–2012, Annex D.8, includes a validated, conservative method for computing incident energy from DC arc-flash events, where available DC bolted fault current values are known. NFPA 70E was developed using several incident energy quantification methods, which included IEEE 1584. NFPA 70E–2012, Annex D.8, which includes a validated, conservative method for computing incident energy from DC arc-flash where the available DC bolted fault current is known. Here, the standard calls for quantified warning labels for equipment, where workers are exposed to live DC power can wear appropriate personal protective equipment [79].

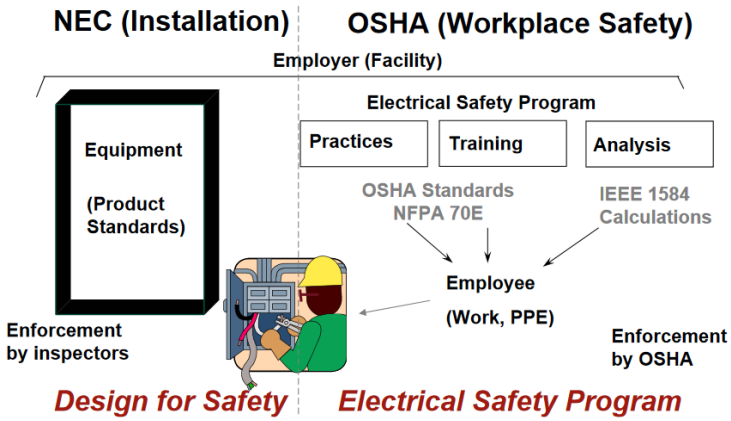

Figure 5-1. NEC and OSHA safe operations combined procedures [80].

Based on home wiring issues, the US Fire Administration estimates approximately 67,800 fires occur each year, resulting in 485 deaths annually, approximately 2,300 injuries annually and $868 million in property losses [81]. Consequently, arc-fault circuit interrupters were developed to address this issue whereby the National Electrical Code® was developed to provide codes and standards for these and other arc-discharge mitigation technologies. Currently, the NEC code requires arc-fault circuit interrupter (AFCI) devices on all residential and commercial structures as they provide an increased level of safety to the electrical wiring system [82]. The goal of arc sensing and extinguishing devices is to sense the arc-fault current and terminate the voltage in a timely manner before it develops into a serious arc-flash event [5]. Currently there are many circuit breaker arc-mitigating options like AFCIs that are available to reduce arc-flash energy levels. Using simple current-limiting breakers that will operate in the instantaneous and current-limiting regions will reduce incident energy levels. In addition, using breakers with solid-state trip units, which have adjustable long, short, and instantaneous settings is an effective method for reducing arc flash energy [37]. AFCI-type circuit breakers use magnetic sensing or other means to detect increases in current draw much more quickly. Without such protection, visually detecting arc-faults in defective wiring is very difficult, as an arc-fault can occur in a very small space. A problem with arc-fault circuit breakers is they are more likely to produce false positives due to normal circuit behaviors appearing to be arc-faults. For instance, lightning strikes on the outside of an aircraft mimic arc-faults in their voltage and current profiles. Recent advances in fault protection devices has been able to largely eliminate such false positives, providing the ability to quickly identify and locate necessary faulty electrical components [88].

Currently a number of companies are developing series arc-fault protection devices [28, 84]. Many AFCIs use elevated AC noise on the DC side of the DC-generating systems to detect series arc-faults. The difficulty comes in differentiating series and parallel arc-faults because the noise signatures are similar. In PV applications for example, many AFCIs are designed to be installed at the string or array-level [85] so if a parallel arc-fault causes the AFCI to trip, the arc will not be extinguished and may strengthen as more current is directed through the arc-fault path. As a result, it is imperative that AFCIs make the appropriate corrective action when an arc-fault occurs. To address this, UL 1699 [86] contains the requirements for listing AFCI devices. Each type of AFCI protects different aspects of the branch circuit and extension wiring. However, only the branch/feeder AFCI meets NEC requirements. AFCIs are not designed to prevent fires caused by series arcing at loose connections [10].

Overall, AFCI devices can be categorized by the following types, as described by Holt [10] and illustrated by Figure 5-2:

1. Branch/feeder AFCI–This device is installed at the origin of a branch circuit or feeder like a panelboard. It provides parallel arc-fault protection for branch circuit wiring, cord sets, and power supply cords. It's not UL-Listed to provide series-type arc-fault protection.
2. Combination AFCI–This device, which is typically a receptacle, provides parallel and series arc-fault protection for branch circuit wiring, cord sets and power supply cords downstream from the device. It doesn't, however, provide parallel arc-fault protection upstream.
3. Outlet circuit AFCI–This device is installed at a branch circuit outlet. It provides parallel and series arc-fault protection for the cord sets and power-supply cords plugged into the outlet. However, it doesn't provide arc-fault protection on feed-through branch circuit conductors, nor does it provide parallel arc-fault protection upstream from the device.

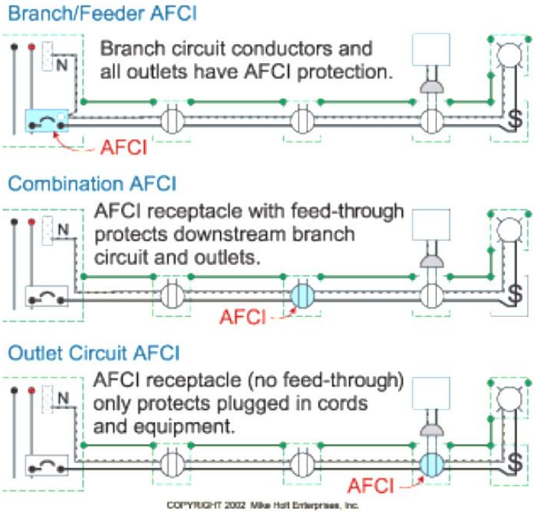

Figure 5-2. Types of arc-fault circuit interrupters [10]

Häberlin proposed having an AFCI open photovoltaic (PV) strings to extinguish series DC arc-faults, then, if arcing frequencies still existed, the string would be shorted to extinguish the parallel arc-fault [87]. This methodology would prevent most parallel arc-faults, but special attention would be needed for the case of cross-string parallel arc-faults because both strings must be shorted. The inverter company, SMA America, LLC has recommended isolation monitoring to prevent parallel faults [96], but they believe module-level shorting is required to stop a parallel arc-faults [97]. Johnson also suggested shorting the modules when parallel arc-faults were identified [15]. Although this could potentially leave the system energized at the short circuit current (I_{sc}), an AFCI can be quite effective in mitigating fires for parallel arc-faults. It is important to note that although most PV AFCIs are proficient, some protection devices are not always designed to prevent fires caused by series arcing at loose connections in devices like switches or receptacles [37].

A simple method to reduce the potential current that could fuel an arc-flash event is to reduce the fuse ampere size. If for example, a 400 A fuse is feeding loads that draw only 200A, then the 400 A fuse can be reduced, which will increase the chances that the fuse will operate in the current-

limiting region for an arcing fault [37]. However, it is important to check the inrush current of motors and transformers and verify that the fuse will not be damaged when these devices are energized. Several other ways to reduce fault current are the use of several smaller transformers and unit substations versus one large one. This also increases the system reliability by having several substations feeding equipment instead of one. Installing tie breakers will further increase the reliability should one of the substation services fail [37]. Another method for reducing fault current is the use of current-limiting reactors. These devices have been used in many facilities to reduce the fault current to levels below the equipment short-circuit ratings. Additionally, Current-limiting fuses operate extremely fast (if operated in the current-limiting range), reducing arc current and corresponding incident energy [37]. They are simple to install and have very little maintenance requirements. Additionally, arc flash energy can be reduced at locations where solid-state trip units are being used is to order the trip units with a zone interlocking feature. This feature adds communication between the main, tie, and feeder breakers. If a fault occurs downstream from the feeder breaker, a "restraint" signal is sent to the main and tie breakers to time out using their normal programmed LSI trip settings. If a fault occurs between the main and feeder breakers, a "no restraint" signal is sent to the main and bus tie breakers, which will then trip at a very low pickup and time delay [37]. A similar method is to employ differential protection. Zones of protection are set up using differential relays and current transformers. If a fault occurs within the zone, the relay trips at extremely low pickups and time delays, which can greatly reduce arc flash energy potential [37].

Another device used in arc-fault mitigation practices is an arc eliminator which can be employed as an efficient means to reduce arc duration as it is designed to extinguish an arc within a few milliseconds. Arc eliminators trip by optical open arc signal from an internal magnetic voltage transformer (VT) fault. The arc eliminator operates in 1-4 ms and creates a 3-phase short-circuit on another part of the system, typically upstream at higher voltages [37]. This device contains a fast contact pin that upon activation by an external relay, makes physical contact with the energized bus which then creates the short-circuit. The arc eliminator will protect a human if they are standing in front of the arc flash event and the relays detect the arc flash by diverting the arc flash to another location, however this may cause system failure at the location of the short-circuit [37].

Furthermore, some switchgear manufacturers have employed arc-flash venting technologies within their design. Here, during an arc-flash event, the blast energy is directed through a vent and outside to a safe area. However, this option can be expensive and should only be employed at main substations where the fault currents (and arc flash energy) can be extremely high [41]. If de-energizing the electrical equipment is not an option, then consideration should be given to the three items below, with the last item being the highest priority [37]:

- Lower the fault current
- Increase the work distances
- Reduce device clearing (trip) times

The fault current can sometimes be lowered by the elimination of paralleling of transformers, where in many facilities, double-ended substations or network faults are paralleled during normal periods. If the equipment is going to be worked on while energized, these paralleled transformers can sometimes be shut down, thus lowering the available fault current [37].

5.3 Preventative Maintenance and Reporting

Maintenance of electrical equipment, including protective devices, is critical to prevent arc-fault

events, where maintenance can employ NFPA 70E, and include infrared scanning and cleaning and ventilation of electrical spaces [78]. After infrared scan is completed, the engineer, electrician, or maintenance staff should replace the defective parts, tighten loose bolts and lugs, clean contacts, and clean coils and bushings, as well as keeping a log of the results for the life of the equipment [78]. Maintenance, should be performed every six months, depending on the area in which the electrical equipment is located.

Reporting and recommendations for an AFHA typically includes five major steps as outlined by Kolak et al. [78]:

1. Data analysis from a facility study–It is important to provide tabular data for each section of the report, because doing so allows critical review by other engineers and enables others to catch data entry mistakes in equipment labeling, etc.
2. Protective device duty analysis–Identifies devices at or near their interrupting duty ratings. Some software programs produce an "equipment duty report," which is synonymous with the protective device duty analysis.
3. Incident energy calculations–Highlights areas where incident energy levels exceed 10 cal/cm^2. We recommend using a 10 cal/cm^2 threshold because studies have shown that third-degree burns result from exposures to 10.7 cal/cm^2 (unprotected skin) or more.
4. Recommended engineering interventions–Provides revised breaker/relay settings when those changes will result in satisfactory outcomes. This section also includes a cost-benefit section for recommended interventions that necessitate either equipment replacement or significant retrofitting of equipment to lower incident energy exposure levels.
5. Equipment labeling–The NEC (110.16) requires that all equipment with arc flash hazard potential (>1.2 cal/cm^2) be field marked to warn electrical workers of the hazardous condition. This label normally includes the calculated incident energy value and other important safety information.

6. ARC-FAULT/ARC-FLASH PERSONNEL SAFETY

Unlike electrical shock incidents, a victim of an arc-flash event does not have to touch live components to sustain an injury. Other injuries from arc-flash incidents include blindness, hearing loss, nerve damage, and cardiac arrest. Because arc-flash events are rapid, they can cause injury including burns to immediate personnel, where serious or even fatal burns can occur when the victim is several feet from the arc [1]. Staged tests have also shown temperatures greater than 225°C on the neck and hands of a person standing close to an arc blast [1]. According to a study conducted by the US Bureau of Labor Statistics, 2,287 US workers died and 32,807 sustained lost-time injuries due to electrical shock or burn injuries over a 7-year period starting in 1992 [89]. The study showed that of the 32,807 non-fatal injuries involving lost time, 38% were classified as electrical burns. The report concluded that to decrease the number and severity of non-fatal electrical burn injuries, direct worker exposure to electrical arc energy must be reduced, where mitigation strategies are key to reducing the number of these incidents [89]. Therefore, proper quantification of incident energy is essential to assessing the potential burn hazard. After calculating the arc flash energy level, an appropriate selection of personal protective equipment should be made using Table130.7(C)(11) from NFPA 70E [40].

As Smith explained, the costs of electricity-generation downtime of electricity can be high where there is enormous pressure on electrical workers to perform their duties on energized systems that can be extremely hazardous even for well-trained and qualified personnel [29]. Therefore, a major hazard is the potential for injury due to electric shock, however there is also the potential for serious injury from electrical arc-flash incidents. Until now many recent injuries from electric shock were considered to be most common and serious hazard faced by electrical workers, but it is becoming more recognized that many of the burns suffered by victims of electrical accidents, which were once ascribed to being part of the conduction path of electric current, are actually caused by exposure to arc flashes and blasts [29]. It is generally accepted that arc flash events are not uncommon and constitute a significant portion of the 320 deaths and 4,000 major injuries that are caused by electrical accidents on average each year in the United States [90]. While the costs of individual accidents vary widely and are difficult to calculate, electrical accidents often have higher costs than other types of accidents, and one study by the Electric Power Research Institute (EPRI) in Palo Alto estimates the average total direct and indirect costs to be as high as 15 million dollars per case [90].

Section 110.16 of the 2008 National Electrical Code requires potentially hazardous electrical equipment be marked to warn personnel of arc-flash vulnerabilities [91]. While shock hazards can mostly be mitigated through safe work practices, training, permitting and use of PPE requirements are important for surviving an arc blast. Additionally, during operation, electrical safety guidelines consider specific zones of influence to energized equipment that could facilitate an arc-flash event. As shown in Figure 6-1, various approach and protection zones are considered, where their proximity are determined with respect to the voltage/current ratings and electric design of a respective circuit. It is typically assumed that the outer limit for the arc duration is no more than 2 seconds [4]. These boundaries account for the likelihood that arcing material within a respective arcing field will likely either be burned off or expelled by the force of a respective blast.

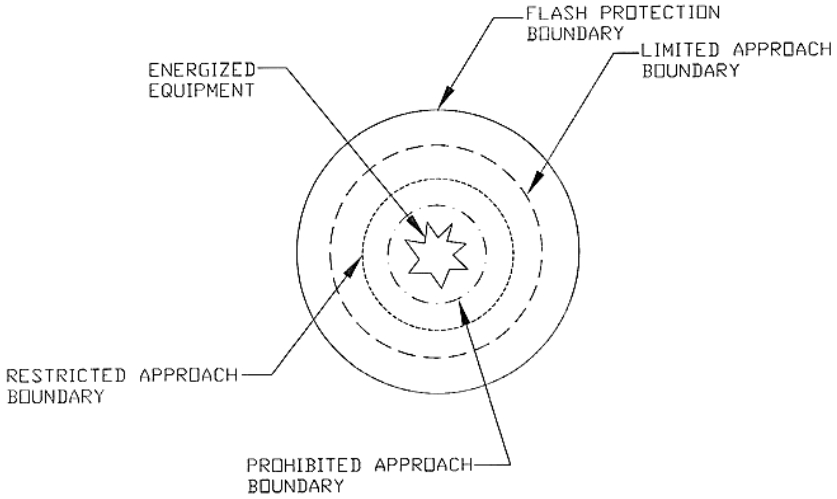

Figure 6-1. Generalized protection boundaries of an electrical system [4]

The energy released by an electric arc is capable of permanently injuring or killing a human being at distances of up to 6.1 m [92]. The distance from an arc flash source within which an unprotected person has a 50% chance of receiving a second degree burn is referred to as the "flash protection boundary." The incident energy of 1.2 cal/cm^2 on bare skin was selected in solving the equation for the arc flash boundary in IEEE 1584 [36]. The IEEE 1584 arc flash boundary equations can also be used to calculate the arc flash boundaries with boundary energy other than 1.2 cal/cm^2 such as the onset of second degree burn energy [93]. Personnel conducting flash hazard analyses must consider this boundary, and then must determine what PPE should be worn within the flash protection boundary. Figure 6-2 provides an estimation tool for determining appropriate PPE attire for both AC and DC electrical systems. Remote operators or robots can also be used to perform activities that have a high risk for arc-flash incidents, such as inserting draw-out circuit breakers on a live electrical bus. Remote racking systems are available which keep the operator outside the arc flash hazard zone [93].

Hazard / Risk Category and PPE	Calculated Incident Energy (Calories/cm²)	Minimum Arc Flash Rated PPE Required (arc rating value)
0	0 < IE ≤ 1.2	Non arc rated clothing, safety glasses, & rubber gloves
1	1.2 < IE ≤ 4	4 (2nd degree burn at 1.2)
2	4 < IE ≤ 8	8 Requires a face shield, safety glasses, and a balaclava be worn. Can cause 3rd degree burns on skin.
3	8 < IE ≤ 25	25
4	25 < IE ≤ 40	40 Between 25 and 40, you must wear the "Moon suit"
>4	IE ≥ 40	NFPA 70E does not go beyond 4 (not officially rated), but could exist by energy calculation method. Work de-energized!

Figure 6-2. PPE and HRC level and incident energy, for both AC and DC electrical systems [95]

7. CONCLUSION

The occurrence of arc-faults in electrical systems represents a major performance and reliability challenge for industrial, commercial and even residential systems. Fundamental understanding of arc discharges and their origin is important for mitigating risk and improving the robust utility of systems with high voltage. Arcing behavior is highly variable, and existing DC and AC models still require further development, especially in determining the duration of arc-faults in order to make accurate predictions of discharge energy. To do this, additional arc-fault, with subsequent arc-flash, testing is needed to develop more accurate V–I characteristics and improved arc resistance models. Extensive testing in a controlled environment is needed to study incident-energy levels associated with AC and DC arc-faults for varying types of equipment and power levels. A hazard risk assessment is also strongly needed to identify where potential arc-faults might be initiated within industrial power systems. The relative severity of the arc flash hazard posed by different types of power equipment must be identified [16] to provide sufficient recommendations for safety protocols.

Thanks to years of research by many individuals and the development of IEEE 1584 [36] as well as NFPA 70E [40], among other safety standards, good safety measures can be taken to prevent catastrophic failures that could lead to costly equipment damage, as well as injury or death to electrical workers. Although arc-flash calculations, in these standards address AC systems, there still are no widely-established standards for DC arc flash hazard analysis pertaining to DC power systems over a wide range of power levels [95]. However, some investigators have begun to formulate approaches for assessing DC arc-flash characteristics, such as that by D.R. Doan [42] who helped elevate the discussion of DC arc-flash calculations. The work by Ammerman et al., [16] provided a comparison study of the existing body of research into DC arcs and arc-flash modeling that has been conducted over the years. It also provided a series of calculation methods for determining incident energy from a DC arc-flash in open air as well as in a confined box space.

Overall, it is important that NFPA 70E [40] and IEEE 1584 [36] equations are applied appropriately. By using both sets of equations, a conservative set of values can be assembled. It is good practice to calculate arc-flash incident energy using both methods, and to use valid values (where only one set of equations may be valid) or to use the more conservative value (where both sets of equations are valid) [93]. Although some facility managers prefer to compare the NFPA 70E and/or IEEE 1584 calculated values, it is recommended here that to assess the safety of an electrical system, the reader is advised to consider a consolidated procedure between NFPA 70E and IEEE 1584, as recommended by Medich [93], in Appendix A3 that can prove to be a clearer and safer approach to arc-flash hazard analysis.

8. REFERENCES

[1] Augspurger Komm Engineering Inc., 2011, "Understanding arc flash hazards,," http://akeinc.com/news/understanding-arc-flash-hazards.

[2] Klipstein, D.L., "The great internet light bulb book, Part I," 2016, http://donklipstein.com/bulb1.html#wbs.

[3] IEEE Standards Association, "IEEE/NFPA arc flash collaboration research project prospectus," 2016, http://standards.ieee.org/esrc/arcflash/arcFlash_projectProspectus.pdf

[4] Chalhoub, N., "An arc fault primer," *Consulting-Specifying Engineer CFE Media*, 2016, http://www.csemag.com/industry-news/codes-and-standards-updates/single-article/an-arc-flash-primer/98d6872a3495868deac1baa59fa338f7.html.

[5] Pfeiffer, J.C., "What is Arc Flash," *National Electrical Code Internet Connection*, 2004, https://www.mikeholt.com/mojonewsarchive/NEC-HTML/HTML/What-is-Arc-Flash~20040512.php.

[6] C.W. Thurston, "Caution: fire, termites, poor performance," *PV Magazine*, 10 Aug. 2016, http://www.pv-magazine.com/archive/articles/beitrag/caution--fire--termites--poor-performance-_100015025/618/.

[7] J.L. Electrics, "Arc Fault," 2016, http://jlelectrics.com.au/products/solar-pv-arch-detection-unit-adu/.

[8] St. Pierre, C., "Putting arc-flash calculations into perspective," *EC&M Electrical Construction & Maintenance*, 2004, http://ecmweb.com/content/putting-arc-flash-calculations-perspective.

[9] Ammerman, R. F., Gammon, T., Sen, P. K., and Nelson, J. P., "Comparative study of arc modeling and arc flash incident energy exposures," *55th IEEE Petroleum and Chemical Industry Technical Conference*, pp. 1-12, 2008.

[10] Holt, M., "The basics of arc-fault protection," "Putting Arc-Flash Calculations into Perspective," EC&M Electrical Construction & Maintenance, 2002, http://ecmweb.com/content/basics-arc-fault-protection.

[11] Johnson, J., Montoya, M., McCalmont, S., Katzir, G., Fuks, F., Earle, J. and Granata, J., "Differentiating series and parallel photovoltaic arc-faults," Photovoltaic Specialists Conference (PVSC), 38th IEEE, pp. 720-726, 2012.

[12] B. Brooks, The Bakersfield Fire, SolarPro 4.2, Feb/Mar 20 II.

[13] B. Brooks, "Report of the results of the investigation of failure of the 1.1135 MW photovoltaic (PV) plant at the national gypsum facility in Mount Holly, North Carolina," Brooks Engineering Draft Report. 26 May, 2011.

[14] Schlumberger, A., Kreutzmann, A., "Brennendes problem - Schadhafte BP-module kiinnen feuer entfachen," Photon, August 2006, pp. 104-106 (in German).

[15] Johnson J. and Bower, W., "Codes and standards for photovoltaic DC arc-fault protection," Presentation for Solar American Board for Codes and Standards, Dallas, TX, 21 Oct., 2011.

[16] Ammerman, R. F., Gammon, T., Sen, P. K., and Nelson, J. P., "DC-arc models and incident-energy calculations," *IEEE Transactions on Industry Applications*, **46**, No. 5, pp. 1810-1819, 2010.

[17] Browne, Jr., T.E., "The electric arc as a circuit element," J. Electrochem. Soc., **102**, No. 1, pp. 27–37, 1955.

[18] Strom, A.P., "Long 60-cycle arcs in air," Trans. Amer. Inst. Elect. Eng., **65**, pp. 113–117, 1946.
[19] D. K. Sweeting and A. D. Stokes, "Energy transfers within arcing faults in electrical equipment," in Proc. 8th Int. Conf. Elect. Fuses Appl., Clermont-Ferrand, France, Sep. 2007, pp. 169–178.
[20] G. R. Jones, High Pressure Arcs in Industrial Devices. London, U.K.: Cambridge Univ. Press, 1988.
[21] Gammon, T., and Matthews, J., "Conventional and recommended arc power and energy calculations and arc damage assessment," *IEEE Transactions on Industry Applications*, **39**, No. 3, pp. 594-599, 2003.
[22] R. H. Kaufmann and J. C. Page, "Arcing fault protection for low-voltage power distribution systems—Nature of the problem," AIEE Trans., pp. 160–167, June 1960.
[23] R. L. Doughty, T. E. Neal, T. L. Macalady, V. Saporita, and K. Borgwald, "The use of low-voltage current-limiting fuses to reduce arc-flash energy," IEEE Trans. Ind. Applicat., vol. 36, pp. 1741–1749, Nov./Dec. 2000.
[24] IEEE Red Book, IEEE Standard 141-1993, 1993.
[25] Coleman, S. and Mohammed, A., "Arc flash hazard evaluation," EC&M Electrical Construction & Maintenance, 2012, http://ecmweb.com/arc-flash/arc-flash-hazard-evaluation.
[26] Wilkins, R., Lang, M., and Allison, M., "Effect of Insulating Barriers in Arc Flash Testing," *IEEE PCIC Conference Record*, pp 51-56, 2006.
[27] Lang, M. and Neal, T., "Arc flash basics: testing update," *Proceedings of the 8th International Conference on Electric Fuses and their Applications*, Clermont-Ferrand, France, 2007.
[28] J. J. Shea, "Identifying Causes for Certain Types of Electrically Initiated Fires in Residential Circuits," Fire and Materials, **35**, no. 1, pp. 19-42, 2011.
[29] Smith, D., "Arc flash hazards in AC and DC systems," Report, Dept. of Electrical & Computer Engineering, 2012.
[30] General Electric Application Information, "Short circuit current calculations," http://www.geindustrial.com/publibrary/checkout/GET-3550F?TNR=White%20Papers|GET-3550F|generic
[31] Thomas, R.E. and Rosa, A.J., "The analysis and design of linear circuits," 3rd Ed., John Wiley & Sons, Inc., 2001.
[32] Alexander, C. and Sadiku, M., "Fundamentals of Electric Circuits," 3rd Ed., *McGraw-Hill*. pp. 387–389, 2006.
[33] Papallo, T., "Arc flash calculations using a physics-based circuit model," *IEEE Transactions on Industry Applications*, **48**, No. 4, pp. 1230-1236, 2012.
[34] IEEE Buff Book, IEEE Standard 242-1986, 1986.
[35] Lee, R. H., "The other electrical hazard: electric arc blast burns," *IEEE Transactions on Industry Applications*, **3**, pp. 246-251, 1982.
[36] IEEE 1584-2002, IEEE Guide for Performing Arc-Flash Hazard Calculations, IEEE Std. New York, N.Y., 2004.
[37] Fuhr, R., "Ways to reduce arc flash energy," EC&M Electrical Construction & Maintenance, 2008, http://ecmweb.com/content/ways-reduce-arc-flash-energy.
[38] Stokes, A.D. and Oppenlander, W.T., "Electric arcs in open air," *J. Phys. D, Appl. Phys*., **24**, No. 1, pp. 26–35, 1991.

[39] Paukert, J., "The arc voltage and arc resistance of LV fault arcs," *Proc. 7th Int. Symp. Switching Arc Phenom*., pp. 49–51., 1993.
[40] NFPA 70E-2004, Standard for Electrical Safety in the Workplace, National Fire Protection Association, Quincy, MA., 2004.
[41] Mendenhall, W. P., "DC arc hazard mitigation design at a nuclear research facility," IEEE IAS Electrical Safety Workshop, pp. 1-4. IEEE, 2014.
[42] Doan, D. R., "Arc flash calculations for exposures to DC systems," *IEEE Transactions on Industry Applications*, **46**, No. 6, pp. 2299-2302, 2010.
[43] Fink, D.G., and Beaty, H.W., "Standard Handbook for Electrical Engineers," 12th Ed., Section 4, McGraw Hill, 1987.
[44] Das, J.C., "Power System Analysis: Short Circuit, Load Flow, and Harmonics," pp. 321-322, CRC Press, 2008.
[45] PowerGuru, "Interruption of DC fault currents," 2012, http://www.powerguru.org/interruption-of-dc-fault-currents/
[46] Cline, H.C., "Fuse protection of DC systems," *Proc. Annu. Meeting Amer. Power Conf.*, pp. 20–25, 1995.
[47] Van, A.R. and Warrington, C., "Reactance relays negligibly affected by arc impedance," *Elect. World*, **98**, No. 12, pp. 502–505, 1931.
[48] Hall, P.M., Myers, K. and Vilcheck, S.W., "Arcing faults on direct current trolley systems," *Proc. 50th WVU Conf. Coal Mine Electrotechnol.,* Morgantown, W.V., pp. 1–19, 1978.
[49] C. E. Sölver, Electric Arcs and Arc Interruption. Götenburg, Sweden: Chalmers Univ. Technol., 2006, EEK 195 High Voltage Technology, Lecture 7. [Online]. Available: http://193.140.122.139/high_voltage/elkraft/www.elkraft.chalmers.se/GU/EEK195/lectures/Lecture7.pdf
[50] Hsu, K.C., Etemandi, K. and Pfender, E, "Study of the free-burning high-intensity argon arc," J. Appl. Phys., **54**, pp. 1293, 1983.
[51] Tsai, M.C. and Kou, S. "Heat transfer and fluid flow in welding arcs produced by sharpened and flat electrodes," *Int. J. Heat Mass Transfer*, **33**, pp.2089-2098, 1990.
[52] Zhu, P., Lowke, J. J., and Morrow, R.H.N.R., "A unified theory of free burning arcs, cathode sheaths and cathodes," *Journal of physics D: Applied physics*, **25**, No. 8, pp. 1221, 1992.
[53] Lowke, J.J., "Simple theory of free-burning arcs," *J. Phys. D: Appl. Phys.*, **12**, pp. 1873-1886, 1979.
[54] Lowke, J.J., Kowitya P. and Schmidt, H.P., "Theory of free-burning arc columns including the influence of the cathode," *J. Phys. D: Appl. Phys.*, **25** pp. 1600-1606, 1992.
[55] Marrow, R. and Lowke, J.J., "A one-dimensional theory for the electrode sheaths of electric arc," *J. Phys. D: Appl. Phys.*, **26**, pp.634-642, 1993.
[56] P. Zhu, J.J. Lowke, and R. Morrow, "A unified theory of free burning arcs, cathode sheaths and cathodes," *J. Phys. D: Appl. Phys.*, **25**, pp. 1221-1230, 1992.
[57] Forsyth, W.E., "Smithsonian Physical Tables,," 9th Ed., Smithsonian Institution, Washington, D.C., 1954.
[58] Nottingham, W.B., "A new equation for the static characteristic of the normal electric arc," *Trans. Amer. Inst. Elect. Eng*., 42, pp. 302, 1923.
[59] Eze, M.N., "Electrical safety in power distribution," Presentation, *Institute of safety professionals of Nigeria*, 2014.

[60] Love, D.J., "Designing ground-fault protection for 480-V systems," *Specifying Engineer*, pp. 88–95, 1976.
[61] Stanback, H.I., "Predicting damage from 277-volt single phase to ground arcing faults," *IEEE Trans. Ind. Applicat*., **13**, pp. 307–314, 1977.
[62] Wilkins, R., "Simple improved equations for arc flash hazard analysis," *Proc. IEEE Elect. Safety Forum*, pp. 1–12, 2004.
[63] Lee, R. H., "Pressures developed by arcs," *IEEE Transactions on Industry Applications*, **4**, pp. 760-763, 1987.
[64] Capelli-Schellpfeffer, M., Miller, G. H., and Humilier, M., "Thermoacoustic energy effects in electrical arcs," *Annals of the New York Academy of Sciences*, **888**, No. 1, pp. 19-32, 1999.
[65] Uzelac, N., "Tools for the simulation of internal arc effects in MV and HV switchgear," *CIGRE A3.24 Working Group Presentation*, IEEE Switchgear Standards Meeting, 2014.
[66] BJØRTUFT, T. R., Granhaug, O., Hagen, S. T., Kuhlefelt, J. H., Salge, G., SKRYTEN, P. K., and Stangherlin, S., "Internal arc fault testing of gas insulated metal enclosed MV switchgear," *18th Int. Conf. Electricity Distribution*, Turin, Italy, 2005.
[67] Rodriguez, S., C. Mueller, and B. Merryman, "Lagrangian 3D CFD Simulation of Turbulent Aerosol Experiments," *American Nuclear Society Winter Meeting*, Las Vegas, NV, November 2016.
[68] Louie, D. et al., "NSRD-11: Computational Capability to Substantiate DOE-HDBK-3010 Data," Sandia National Laboratories, 2016.
[69] Robinson, A. C. et al., "ALEGRA-MHD User Manual," Sandia National Laboratories, *SAND2015-DRAFT*, July 2014.
[70] Louie, D. et al., "NSRD-11: Computational Capability to Substantiate DOE-HDBK-3010 Data," Sandia National Laboratories, 2016.
[71] Ireland, B., "Arc flash review–Industry update on arc flash studies and proposed revisions to safety standards," EC&M Electrical Construction & Maintenance, 2010, http://ecmweb.com/content/arc-flash-review.
[72] Longmire, Conrad L. Justification and Verification of High-Altitude EMP Theory, Part 1 LLNL-9323905, Lawrence Livermore National Laboratory. June 1986
[73] "The Early-Time (E1) High-Altitude Electromagnetic Pulse (HEMP) and Its Impact on the U.S. Power Grid," E. Savage, J. Gilbert, W. Radasky Meta-R-320, Prepared for Oak Ridge National Laboratory, January 2010
[74] "Project 2013-03 Geomagnetic Disturbance (GMD) Mitigation," Draft TPL-007-1, NERC GMD Task Force, June 2014
[75] "Meta-R-323. Intentional Electromagnetic. Interference (IEMI) and Its Impact on the U.S. Power Grid." William Radasky. Edward Savage. Metatech Corporation, 2010
[76] "Power Grid Geomagnetic Disturbance (GMD) Modeling with Transformer Neutral Blocking and Live Grid Testing Results," T.J. Overbye, F.R. Faxvog, W. Jensen, G. Fuchs, G. Nordling, D.B. Jackson, B.Groh, N. Ruehl, A.P. Vitols, T. L. Volkmann, D. Fromme, G. Edmiston, A. Walker, M.R. Rooney, 2013.
[77] Dargatz, M., "DC Arc-Faults and PV System Safety," Renewable Energy World White Paper, 2009, http://www.renewableenergyworld.com/articles/2009/12/dc-arc-faults-and-pv-system-safety.html.
[78] Kolak, J.J., "Arc flash hazard analysis primer–Proper implementation of arc flash hazard analysis can significantly reduce injuries from arc flash and arc blast events," EC&M

Electrical Construction & Maintenance, 2010, http://ecmweb.com/basics/arc-flash-hazard-analysis-primer.
[79] Wilhite, G., Durocher, D., "Implementing an Arc flash compliance program," EC&M Electrical Construction & Maintenance, 2007, http://ecmweb.com/content/implementing-arc-flash-compliance-program.
[80] Jones, E.F., "Understanding arc flash," *Engineering Services Presentation*, Schneider Electric, https://www.progress-energy.com/assets/www/docs/business/sqrd-progress-energy.pdf.
[81] NEMA, "The real impact of an electrical fire," National Electrical Manufactures Association, White Paper–Low voltage distribution equipment section, 2014.
[82] J. Johnson, K.M. Armijo, M. Avrutsky (Tigo Energy), D. Eizips (Tigo Energy), S. Kondrashov (Tigo Energy), Arc-Fault Unwanted Tripping Survey with UL 1699B-Listed Products, IEEE Photovoltaics Specialists Conference, June 2015.
[84] T. Zgonena, L. Ji, and D. Dini, "Photovoltaic DC Arc-Fault Circuit Protection and UL Subject I 699B," *Photovoltaic Module Reliability Workshop*, Golden, CO, 2011.
[85] J. Johnson, B. Pahl, c.J. Luebke, T. Pier, T. Miller, I. Strauch, S. Kuszmaul and W. Bower, "Photovoltaic DC arc fault detector testing at Sandia National Laboratories," *37th Photovoltaic Specialists Conference*, Seattle, WA, 2011.
[86] J. Johnson, "Suggestions for UL 1699B based on Arc-fault Testing at Sandia National Laboratories," private memo to UL 1699B Standards Technical Panel, 31 July 2012.
[87] H. Häeberlin, "Arc Detector as an External Accessory Device for PV Inverters for Remote Detection of Dangerous Arcs on the DC Side of PV Plants," *European Photovoltaic Solar Energy Conference*, Valencia, Spain, 2010.
[88] Stephenson, J. "Eliminating False Positives in the Detection and Location of sub 3ms Faults on AC/DC Lines," *Aircraft Airworthiness & Sustainment Conference*, 2011.
[89] Cawley, J. C., and Homce, G. T., "Occupational electrical injuries in the United States, 1992–1998, and recommendations for safety research," *Journal of safety research*, **34**, No. 3, pp. 241-248, 2003.
[90] Chicago Electrical Trauma Research Institute (CETRI), 2016, http://www.cetri.org/statistics.html.
[91] National Fire Protection Association., "National Electrical Code: 2008," NationalFireProtectionAssoc, 2007.
[92] Testguy, "NFPA 70E arc flash and shock hazard boundaries explained," vBulletin Solutions Inc., 2016, http://testguy.net/content/191-NFPA-70E-Arc-Flash-and-Shock-Hazard-Boundaries-Explained.
[93] Medich, B.O., "Calculating arc flash energy levels," *EC&M Electrical Construction & Maintenance*, 2007, http://ecmweb.com/content/calculating-arc-flash-energy-levels.
[94] Krywosz, M., "Case study of DC arc flash in 400 VDC 120 kW power system with VRLA battery," Intelec Presentation, 2014, http://www.emersonnetworkpower.com/documentation/en-US/Products/DCPower/Documents/INTELEC-2014_Case-Study-of-DC-Arc-Flash.pdf.
[95] Phillips, J., "Know your arc: DC arc flash calculations," Electrical Contractor Power & Integrated Building Systems, 2015, http://www.ecmag.com/section/safety/know-your-arc-dc-arc-flash-calculations.
[96] Bieniek, S., Behrends, H. Bettenwort, G., Bulo, T., Haring, A., Hopf, M. Kratochvil, M., Merz, C. and Wegener, T., "Fire prevention in PV plants using inverter integrated AFCI,"

26th European Photovoltaic Solar Energy Conference and Exhibition, Hamburg, Germany, 2011.
[97] Haring A. and Bieniek, S., "Prevention and Detection of Arc Faults in PV Systems," *Photon's 2nd PV Safety Conference*, Berlin, Germany, 2011.
[98] Freidman, A., "Plasma Chemistry," Cambridge Univ. Press, New York, NY, 2008.
[99] Julaihi, M.R.N., "Synthesis of metallic oxide nanoballs via submerged glow-discharge plasma and their photocatalytic effect," Ph.D. Dissertation, Hokkaido University, 2015.
[100] Calvert, J.B., "Electrical Discharges," 29 Sept 2005, http://www.physics.csbsju.edu/370/jcalvert/dischg.htm.html
[101] Cobine, J.D., "Gaseous Conductors," Dover, New York, USA, 1958.
[102] Burch, J.L., "Plasma physics of the local cosmos," The National Academies Press, Washington D.C., 2004.
[103] Miller, H.C., "Electrical discharges in vacuum: 1980-90." *IEEE transactions on Electrical Insulation*, **26**, No.5, 949-1043, 1991.
[104] Práce, D., "methods of preparation and characterization of experimental field-emission cathodes," Ph.D. Dissertation, BRNO University, 2013.
[105] Pfender, E., "Heat transfer from thermal plasmas to neighboring walls or electrodes," Pe & Appl. Chem., 1976, **48**, pp. 199-213.
[106] National Electrical Code, 2011 Edition, NFPA70, National Fire Protection Association, Quincy, MA.
[107] Hastings, J.K., Juds, M.A., Luebke, C.J., and Pahl, B., "A Study of Ignition Time for Materials Exposed to DC Arcing in PV Systems," 37th Photovoltaic Specialists Conference, Seattle, WA, 19-24 June 2011.
[108] Dini, A., and Brazis, P.W., "DC Arc Fault Testing to Support Photovoltaic Arc Fault Protection Device Requirements," UL Technical Document, Oct. 8th, 2013.
[109] K.M. Armijo, J. Johnson, M. Hibbs, A. Fresquez, "Characterizing Fire Danger from Low Power PV Arc-Faults," 40th IEEE PVSC, Denver, CO, 8-13 June, 2014.
[110] K.M. Armijo, J. Johnson, R.K. Harrison, K. E. Thomas, M. Hibbs, A. Fresquez, "Quantifying photovoltaic fire danger reduction with arc-fault circuit interrupters," Progress in Photovoltaics: Research and Applications, 2014, doi: 10.1002/pip.2561.
[111] J. Johnson, K.M. Armijo, "Parametric Study of PV Arc-Fault Generation Methods and Analysis of Conducted DC Spectrum," *40th IEEE PVSC*, Denver, CO, 8-13 June, 2014.
[112] J. Johnson, K. D. Blemel, F. Peter, "Preliminary photovoltaic arc-fault prognostic tests using sacrificial fiber optic cabling," Sandia National Laboratories Technical Report, SAND2013-1185, Feb. 2013.
[113] W.G. Essers, and R. Walter, "Heat transfer and penetration mechanisms with GMA and plasma-GMA welding," Weld J., 60(2): 37- 42, 1981
[114] K.H. Becker, U. Kogelschatz, K.H. Schoenback, and R.J. Barker, "Non-equilibrium air plasmas at atmospheric pressure," IOP Publishing Ltd, United Kingdom, 2005
[115] K. Samanta, M. Jassal, and A.K. Agrawal, "Atmospheric pressure glow discharge plasma and its applications in textile," *Indian J. Fibre & Textile Res.,* **31**, pp. 83-98, 2006.
[116] A. Seidel, "Characterization and analysis of polymers," Wiley & Sons, New Jersey, 2008.
[117] K.N. Pandiyaraj, V. Selvarajan and R. Deshmukh, "Effects of operating parameters on DC glow discharge plasma induced PET film surface," *J. of Phys. Conf.*, **208**, pp. 1-7, 2010.

[118] T. Morimoto, T. Mori and S. Enomoto, “Ignition properties of polymers evaluated from ignition temperature and ignition limiting oxygen index,” *J. App. Polymer Sci.*, **22**, pp. 1911-1918, 1978.
[119] AC Plastics Inc., “Multiwall polycarbonate” *Material Safety Data Sheet*, Retrieved from: http://www.acplasticsinc.com/techsheets/UACI_140005_GL_Multiwall_MSDS_HR.pdf
[120] X.T. Wang, "Optical spectroscopy of plasma produced by laser ablation of Ti alloy in air." J. Applied physics, 80, No. 3, pp. 1783-1786, 1996.
[121] I.L. Babich, V.F. Boretskij, A.N. Veklich, R.V. Semenyshyn, “Spectroscopic data and Stark broadening of Cu I and Ag I spectral lines: Selection and analysis,” *Adv. Space Res.,* **54**, pp. 1254-1263, 2014.
[122] S. Carroccio, C. Puglisi and G. Montaudo, “Mechanisms of Thermal Oxidation of Poly(bisphenol A carbonate)” Macromolecules, 35, p. 4297, 2002.
[123] K.M. Armijo, E. Schindelholz, M. Gordon, K. Holder, J. Grunlan, R.N. Sorensen and E.D. Spoerke, “Light it up: Passive suppression of arc faults with polymer clay”–***Submitted***
[124] Ayrton, H., “The Electric Arc,” London, U.K.: Electrician, 1902.
[125] C. P. Steinmetz, “Electric power into light, Section VI. The Arc,” Trans. Amer. Inst. Elect. Eng. 25, pp. 802, 1906.
[126] IEEE, “IEEE Standard Rating Structure for AC High-Voltage Cir- circuit Breakers Rated on a Symmetrical Current Basis,” ANSVIEEE Standard C37.04-1979, IEEE Product Number SH06288, 1979.
[127] IEEE, “IEEE Application Guide for AC High-Voltage Circuit Breakers Rated on a Symmetrical Current Basis,” ANSVIEEE Standard C37.010-1979, IEEE Product Number SH06569, 1979.

APPENDIX A1. ARC PLASMA THEORY

A1.1 Arc Plasma Physics

An arc-plasma discharge is generated when an electrical current is applied across a dielectric gas or fluid. Plasma is loosely described as an electrically neutral medium of positive and negative unbound particles (i.e. the overall charge of a plasma is roughly zero) [98]. When the charges move they generate electrical currents with magnetic fields, and as a result, they are affected by each other's fields. The plasma from an arc-discharge develops from a high-current, low-voltage event, which is in contrast with the lower-current, higher-voltage discharges such as dark and glow discharges as illustrated by Figure A1–1 [99].

For a breakdown in a plane gap d, between two current-carrying conductors by DC voltage V corresponding to an electric field $E = V/d$ occasional primary electrons near the cathode provide low initial current i_0, where the primary electrons drift to the anode, ionizing the gas and generating electron avalanches [98]. The ionization during the avalanches can be described by the Townsend ionization coefficient α, which indicates the production of electrons per unit length along the electric field:

$$\alpha = \frac{v_i}{v_d} = \frac{1}{v_d} k_i(E/n_0) n_0 = \frac{1}{\mu_e} \frac{k_i(E/n_0)}{E/n_0} \tag{A1.1}$$

where v_i is the ionization frequency, n_0 is the neutral gas density, $k_i(E/n_0)$ is the ionization rate coefficient and μ_e is the electron mobility, which is inversely proportional to pressure. The Townsend coefficient α is usually presented as a similarity parameter α/p depending on the reduced electric field E/p. Further dependences and theory for $\alpha/p = f(E/p)$ for different gases can be found in [98].

An arc-discharge is characterized by a relative negative-resistance V-I characteristic, and high temperatures. Electrons for the discharge are supplied by a cathode spot that is a much more efficient electron emitter than from a glow discharge cathode. The current density in the cathode spot is high and constant, so it adjusts its size to suit the discharge current [98]. The electrons are liberated either by thermionic emission, or by high-field emission, where it is traditionally assumed that the fixed cathode spot of refractory electrodes (such as carbon or tungsten) is thermionic [99], while the wandering cathode spot of low-melting-point cathodes (such as mercury) is high-field. A typical current density for a thermionic cathode spot is 470 A/cm^2, and of a high-field spot, 4000 A/cm^2 [100].

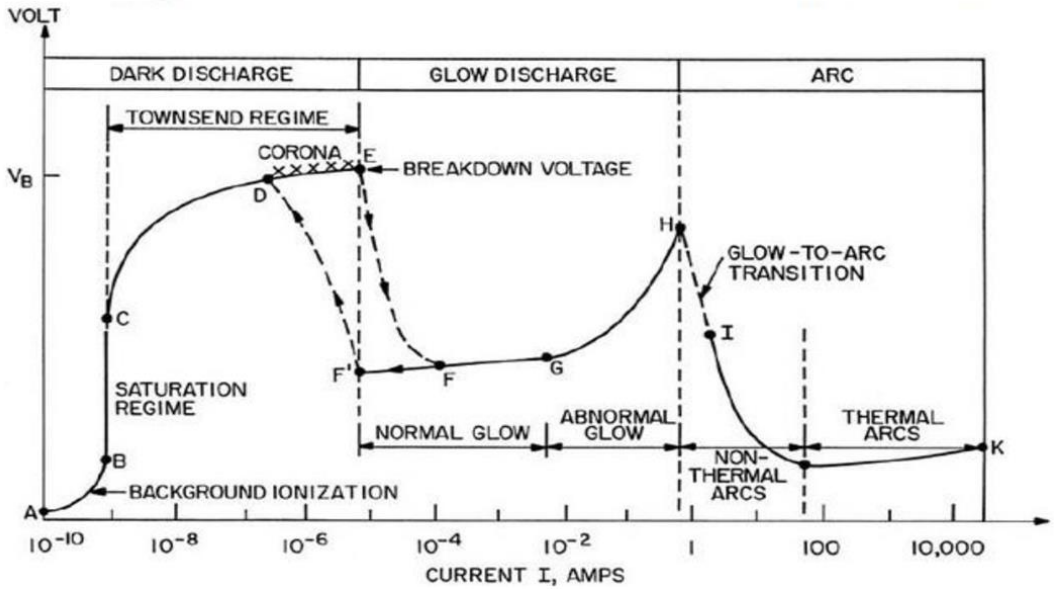

Figure A1–1. Plasma discharge phenomena characterized by current and voltage where the regime progression of dark discharge, glow discharge and arc discharge increases with current [99].

For a discharge to occur there must be a source of electrons at the cathode, where each ionizing collision produces a new electron, and a positive ion that moves in an opposing direction, which facilitate an ion pair [100]. An electron cannot do this unless it has acquired sufficient kinetic energy by being accelerated in an electric field by either accumulation or collision-induced excitation. Even if the electron doesn't experience any collisions, a small electric field will still allow it to accumulate energy in a long-enough run [100]. Electron energies (with units of electron-volts eV) are typically assessed during a discharge such that the energy U across the discharge length can be considered as the potential drop along a specified gap distance x. If the probability of collision of the electron over a distance dx is dx/L_e (where L_e is called the electron mean free path) then the speed of the electron is provided by $\mathcal{V} = KE$, where K is the electron mobility, in (cm/s) per (V/cm) [100]. The mean free path L is inversely proportional to the pressure; therefore, the pressure has a significant impact on energy gain of an electron under a voltage potential. The molecules of the gas also have a mean free path, although because molecules are larger, their mean free path L are shorter than L_e. Additionally, these electrons, ions and other neutral molecules may be present in a continual thermal motion due to their collisions being perfectly elastic [100]. In equilibrium, the velocities are distributed according to the Maxwell distribution:

$$f(v) = \sqrt{\left(\frac{m}{2\pi kT}\right)^3}\, 4\pi \mathcal{V}^2 e^{-\frac{mv^2}{2kT}} \tag{A1.2}$$

where m is the particle mass kT is the product of the Boltzmann's constant and thermodynamic temperature. Additionally, this probability density function provides the probability per unit speed of finding the particle with a speed near velocity $\mathcal{V}$. Any charged body attracts charges of the opposite sign that will ultimately neutralize its charge [100]. The energy required to excite a molecule or atom to its first excited state above the ground state is called the resonance energy,

which is less than its respective ionization energy. Inert gases, which have a closed shell of electrons in the ground state, tend to have very large resonance energies which can be metastable, where a transition to the ground state by radiation is difficult. Therefore, they typically retain their excitation energy for an extended period of time, or until they experience another collision with a surface wall, electron or atom. This makes cumulative ionization possible, where an atom can be ionized by multiple collisions in which the electrons have insufficient energy to ionize in a single collision [100].

Collision of a high-energy plasma electron with a neutral atom in a ground state can result in energy transfer from a free plasma electron to a bound state electron, which is the main source of electronically excited atoms in plasma. Here the growth of a bound electron during excitation can be due to an increase in the principal quantum number *n*, as well as with angular momentum [101]. This effect can be illustrated by the case of strong excitation of an atom to a relatively high potential quantum number *n*, where for one electron moving quite far from the nucleus, its energy can be described by the Bohr formula with a Rydberg correction factor Δ_i:

$$E = \frac{me^4}{2\hbar^2(4\pi\varepsilon_0)^2}\frac{l}{(n+\Delta_i)^2} \tag{A1.3}$$

High-energy plasma electrons can also provide excitation of molecules as well as atoms in electric discharges, where energy transfer from a free plasma electron to a bound electron in a ground-state molecule results in excitation. The electronically excited molecules can be metastable, having long lifetimes thus contributing to increased chemical kinetic activity and heat generation [100].

During arc discharges high-field emission of electrons also occurs, which can take place from a solid surface into air, a vacuum or any non-conducting or weakly conducting dielectric medium, induced by an electrostatic field [103]. According to Práce, high-field emission can be evaluated from the standpoint of quantum-mechanical tunneling, through the potential barrier at the surface of the cathode [104]. The current density of this emission is provided by the Fowler-Nordheim equation:

$$J = CE^2e^{-D/E} \tag{A1.4}$$

$$C = \frac{6.2\times10^{-6}}{\varphi+E_F}\left(\frac{E_F}{\varphi}\right)^{1/2}\frac{A}{V^2} \tag{A1.5}$$

where $D = 6.8 \times 10^9\varphi^{3/2}$ V/m, E_F is the Fermi energy in volts, φ is the work function in volts and E is the electric field in units of V/m. As an example by [100] for tungsten, $\varphi = 4.52$V and $E_F = 8.95$V, the fields required are very high. A field of 2×10^7 V/cm produces an emission of 1.7 μA/cm^2 in tungsten, where the current increases rapidly with field. With a field strength of 3×10^7 V/cm, the current density is 0.2 A/cm^2. At atmospheric pressure, the mean free path is about 10^{-5} cm in air, and if the cathode drop is 10V, the resulting electric field over one mean free path is 10^6 V/cm.

Thermionic emission occurs when free electrons are emitted from the surface of a metal when an external heat energy source is applied. During this process while heat energy is applied, free electrons gain enough energy to overcome the attractive force of the atomic nucleus, which holds the free electrons in the metal [100]. Thermionic emission occurs in metals that are heated to a very high temperature where the Richardson-Dushman equation has been previously used to

characterize the current density of this phenomena [103]:

$$J = AT^2 e^{-b/T} \tag{A1.6}$$

where T is the absolute temperature, k is the Boltzmann constant and the constant A, is prescribed by Eqn. A1.7.

$$A = \frac{m_e e k_B}{2\pi^2 \hbar^3} \approx 1.2 \times 10^6 \text{ [A/m}^2\text{-K}^2\text{]} \tag{A1.7}$$

Thermionic emission depends exponentially on temperature requiring respectively high temperatures depending on the medium gas. The Maxwell-Boltzmann distribution is applicable here because the number of electrons per state is very small for the energies at which the electrons can escape. Predictive modeling is further improved by inclusion of an additional electric field ε_{ext} term that drives electrons away from the surface of the solid, known as the "Schottky effect" [104]. The electric field has the approximate effect of lowering the work function value by the amount prescribed by Eqn. A1.8.

$$\varphi = \sqrt{\frac{e\varepsilon_{ext}}{4\pi\epsilon_0}} \tag{A1.8}$$

where ϵ_0 is vacuum permittivity. For relatively high electric fields significant numbers of electrons may also tunnel out due to their quantum uncertainty in position and field strength, which is commonly referred to as "field emission." [104]. Finally, thermionic emission may be used more generally to indicate the flow of charge carriers, either electrons or ions, over a potential barrier. Even for standard thermionic emission, it should be cautioned that the work function depends critically on surface conditions. For example, surface adsorption can significantly change it.

A1.2 Thermal Effects of Arc-Discharges

An effective exploitation for a particular plasma state requires a thorough understanding of the heat transfer process from a plasma to a solid structure. The existence of free electrons and positive ions in plasma as well as steep thermal gradients, particularly in the vicinity of walls or electrodes, can give rise to a number of thermal-physical effects, especially as a function of relatively strong radiation fields, which are typical for thermal plasmas [105]. Experimentally, electric arcs have been used as a convenient means for generating plasmas in a temperature range from approximately $7\text{x}10^3$ to $2\text{x}10^4$ K, with electron densities ranging from 10^{16} to 10^{18} cm^{-3} [105]. These plasmas can be described as continua thermal plasmas as they occur within atmospheric pressure conditions where the temperature is typically high enough to approach a state of local thermodynamic equilibrium (LTE). Analytical investigations in plasma heat transfer are traditionally restricted to laminar flow because the degree and nature of turbulence in plasma flows is still poorly known [105].

During a discharge the cathode is heated by positive ion bombardment, where there must be a sufficient number of ions to keep the cathode hot. Often the cathode is externally heated, at least until the arc is established. To further stimulate additional electron emission, cathodes can also be oxide-coated which can impact the work function [100]. With consideration of the positive-ion space charge, the field at the surface of the cathode can be estimated by:

$$E = \frac{4V}{d} \tag{A1.9}$$

where V is the cathode drop and d is the width of the cathode fall region. If for example V is approximately 10 V and d is approximately equal to one mean free path, then E is 10^5 to 10^6 V/cm, which is a high field that can facilitate electrons to discharge. Also, a superheated area may form at the surface of the cathode from adsorbed atoms [100]. When thermal plasmas have electrons and heavy particles at the same temperature this indicates thermal equilibrium. Electrical resistance along the continuous electric arc creates heat, which ionizes more gas molecules, and as per the sequence: solid-liquid-gas-plasma, the gas is gradually turned into a thermal plasma which must be in thermal equilibrium, where the temperature is relatively homogeneous throughout the heavy particles (i.e. atoms, molecules and ions) and electrons [103]. Plasma temperature is commonly measured in kelvins or electronvolts, and is a measure of the thermal kinetic energy per particle [100]. The degree of plasma ionization is determined by the "electron temperature" relative to the ionization energy. At low temperatures, ions and electrons tend to recombine into bound states atoms, [103] where the plasma will eventually become a gas. The electron temperature T_e is usually very different from the ion and neutral temperature T_n at low pressures because electrons receive more energy from electric fields during a discharge, and exchange kinetic energy with neutral particles with greater difficulty due to their weak contact. Due to their larger mass, ions and neutrals tend to move at much slower than electrons whose velocities, which are facilitated by electric fields are often much greater than thermal speeds, especially near the cathode where the electric field is very high [100]. These electrons, subsequently do not obey a Maxwellian distribution until they have lost most of their energy in inelastic collisions and ionization [100].

High electron temperatures and thus high values of electron energies in an electric discharge can provide high excitation rates for different electronically excited states of atoms and molecules for electron impact. Energy of electronically excited particles are typically high (above 5-10 eV) despite very short lifetimes (~10^{-8} to 10^{-6} s) [98]. If radiative transition to the ground state is forbidden by selection rules [98] the lifetime of the excited particles can be much longer due to the absence of transition which can facilitate metastable excited states for the particles. Their long lifetime with respect to radiation allows them to accumulate the necessary energy for discharge which contributes to the kinetics of various chemical reactions within the plasma. Radiative lifetime of metastable atoms can be as high as 1.4×10^5 s, where according to Friedman and Kennedy [98] the energy of excitation of these particles can be quite low (< 1 eV) which can facilitate high particle concentrations in electric discharges. Additionally, these metastable particles can also lose their energy by means of various collision/relaxation processes [100]. In hot air plasmas, oxygen and nitrogen are generally dissociated: $O_2 \rightarrow 2O$ (5.09 V) and $N_2 \rightarrow 2N$ (7.9 V), with the facilitated reaction $N_2 + O_2 \rightarrow 2NO$ and ionization potentials: NO=9.5V, O_2 = 12.2V, O = 13.614V, N = 14.54V, N_2 = 15.377V [100]. Additionally, it is also important to note that even when the electron and ion number densities and temperatures are roughly equal, electrons still carry the majority of the current because of their higher mobility [103].

The high-pressure positive column adjusts to a finite diameter D depending on the magnitude of the discharge current. It will not expand indefinitely if unconfined due to a balance between heat loss and heat generation within the conducting region. If the column expands, heat loss increases and ionization decreases, where the current tends to shift to a more conductive center, which raises the temperature in this region. This feedback tends to keep the column at a relatively constant diameter. The positive column is a cylindrical region in the ambient gas that can move about freely with respect to the gap distance and available voltage [100]. This positive column is accompanied by active convection that carries off its heat where its movement is sensitive to air currents as well

as magnetic forces. Its low density causes it to rise when surrounded by cooler air, hence its arc shape. As stated by Burch et al., [103] if the acceleration of gravity is zero, the longitudinal voltage gradient becomes zero because gravity drives convection. Therefore, in the absence of convection the column does not cool, and requires little approximated power to be sustained [103].

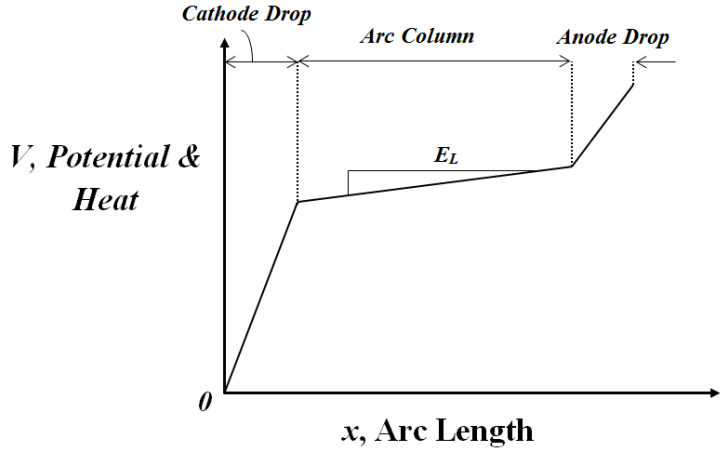

Figure A1–2. Qualitative potential distribution of an arc discharge between two electrodes.

Figure A1–2 illustrates the qualitative potential distribution for an arc, where for a short arc the potential is approximately the sum of the cathode and anode drops. Because of the large current, an arc has a small longitudinal voltage gradient E_L in the positive column, especially in a high-pressure arc. The gradient depends on the cooling rate of the positive column by the ambient atmosphere, and becomes small if cooling is low, while the current flowing through the cathode and anode drops generate large quantities of heat very close to the electrodes [100].

An arc can be initiated either by a transition from a glow discharge, or by separating contacts already carrying current. If the current in a glow discharge is increased, the width of the cathode fall decreases facilitating the ion energy to increase and the cathode to be heated. In arcs with thermionic cathodes, the transition is gradual as thermionic emission increases with temperature and the discharge voltage decreases [100]. The pressure can also be increased to start an arc if a glow discharge already exists.

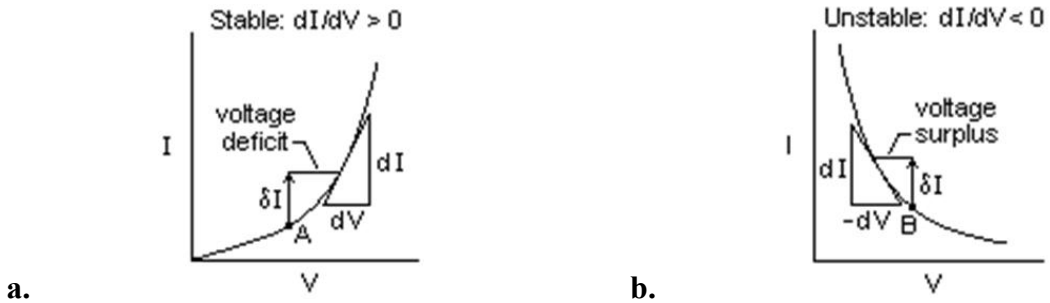

Figure A1–3. Stable and unstable voltage-current arc characteristics [100].

As shown in Figure A1–3 by [100] the distinction between stable and unstable voltage is generally apparent. For the case with a stable arc, Figure A1–3 a. the current increases monotonically with

applied voltage, where the slope $1/R = dI/dV$ is positive. If the current were suddenly less, then we would have a voltage surplus, and the current would then increase. Conversely, for an unstable arc, as illustrated by Figure A1–3 b., the current decreases monotonically with voltage where the slope $1/R = dI/dV$ is negative. In this case if there is a sudden current increase δI from point B, then more voltage will be available to increase the current, therefore a voltage surplus [100].

Finally, the emission of light is one of the principal characteristics of discharges. Light of a definite frequency is emitted when an excited atom falls to a lower energy level and if there is an electric dipole transition moment, then the transition typically occurs in approximately 10^{-8} s [100]. The collision frequency is approximately 10^{11} Hz at atmospheric pressure, so the excitation energy is typically lost in a collision before it can be radiated. Additionally, if the dipole transition moment is forced to be zero by symmetry then radiation may occur by other means, such as magnetic dipole or quadrupole radiation, though the radiative lifetime for these is much longer. At higher pressures, excited atoms are continually affected by collisions, which broaden the lines emitted. With further pressurization radiation begins to assume the characteristics of black-body thermal radiation [100].

APPENDIX A2. ARC-FAULT EXPERIMENTATION FOR PHOTOVOLTAIC APPLICATIONS

A2.1 Electrical Testing Setup

A PV simulator at Sandia National Laboratories was developed to provide power generation for the arc discharges, and to represent constant power I-V curves from a set of 1024 points, shown in Figure A2–1. From experimental observations, the arc power was nearly constant for any given curve regardless of the electrode gap spacing [110]. As a safety precaution, the PV simulator power was provided to the arc-fault generator through a power resistor so the simulator was never shorted. For reliable arc discharges this was found to be very significant. Additionally, the curves programmed into the PV simulator were limited to 600 V and 15 A.

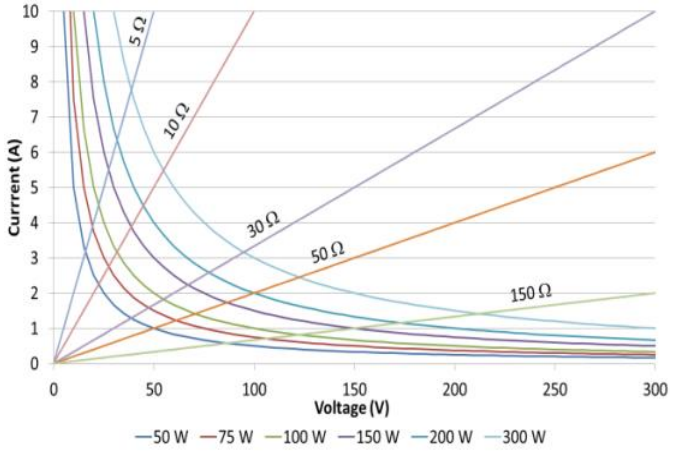

Figure A2–1. Constant Power Arc-Fault IV Simulation Test Curves [109].

The experimental setup used consisted of an arc-fault generator, with current and voltage probes, as well as a k-type thermocouple, which was placed on each respective polymer test sheath. The arc generator system Figure A2–2 was enclosed within a sealed chamber environment which could facilitate arc-discharges in atmospheres of inert and non-inert gases including those used for testing long-duration reliability. The chamber can also be operated under vacuum and pressurized environments. Humidity levels between 0 to 100% relative humidity can also be introduced within the chamber. Another feature of the generator is the electrode chucks that have a port to allow cabling to pass through to the current carrying circuit. The chucks are also capable of gripping current-carrying objects with characteristic dimensions of 100 μm to 7.5 cm. The electrode geometries that can be inserted consist of a variety of cylindrical and non-cylindrical objects.

The stage is capable of 3D movement and has safety controls to avoid pinch hazards. The fine resolution movement control is capable of facilitating stable arc-discharges across current-carrying conductors under both automated and manual control. Maintaining a stable arc discharge is necessary for successful testing and evaluation. The data from this robotic stage, as well as that of other sensed inputs (see below), are all obtained within a novel software algorithm with 100 Hz sampling resolution.

- Electrical Current
- Electrical Voltage

- Bulk Temperature Sensor
- Smoke Detection
- Camera Video and Fire Detection

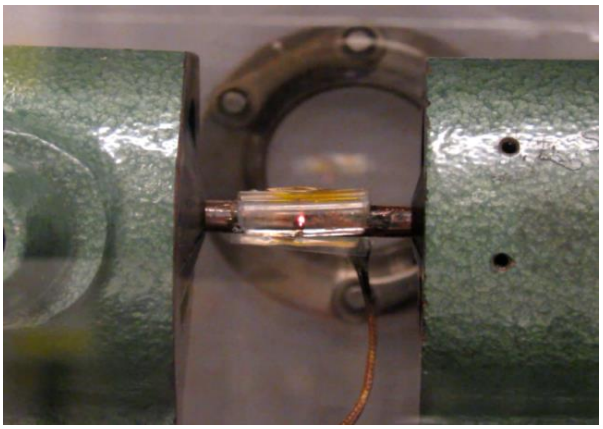

Figure A2–2. Arc-fault generator attachment holder with polycarbonate test specimen.

Additionally, the software algorithm is capable of obtaining FFT data of electrical current spectrum, using a novel sub-algorithm, with up to 5 MHz with 1 kHz resolution. This feature can be used to detect micro and macro-bulk arc discharges, as well as determine nuisance tripping and false-positive arc-faults in detection devices and systems. The system has all of the features to qualify PV materials, components and systems under certifying codes and standards, such as those by Underwriters Laboratory (UL), International Electrical Commission (IEC) and the National Electric Code (NEC) standards. Power to the arc-fault generator can come from either a DC or AC power source, where integrated safety engineering controls include five methods for disengaging the arc discharge, including two interlock controls.

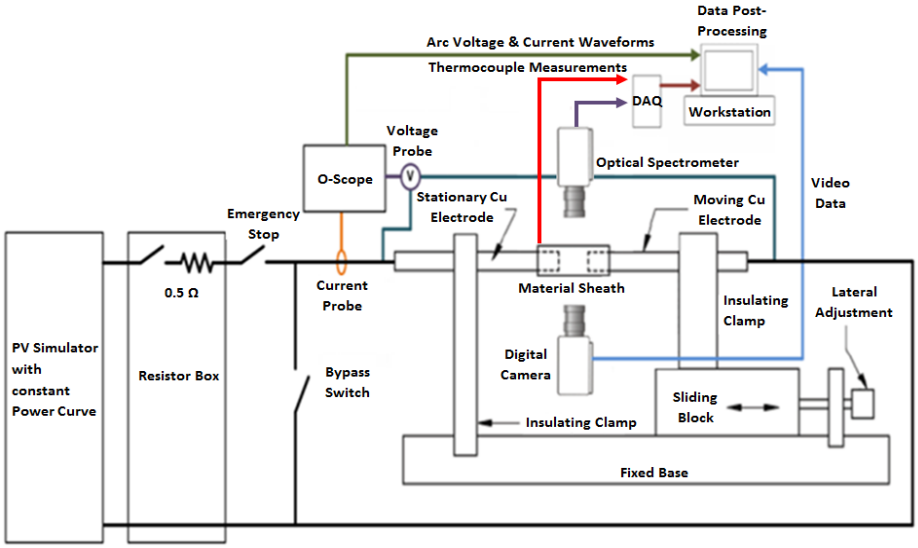

Figure A2–3. Arc-fault experimental configuration and data acquisition system.

Temperature and plasma composition measurements during discharges are important for analyzing material degradation mechanisms and internal physical phenomena of compounds. The arc-fault generator system incorporates a novel fundamental algorithm for determining electron and bulk

plasma temperature. The algorithm utilizes data from an optical spectrometer that is positioned in front of the conductors, Figure A2-3.

In addition to determining plasma temperatures through the algorithm, the spectrum information can also be used to identify material composition. This algorithm is based on novel fundamental spectral research developed at Sandia National Laboratories [110], which has applications in several fields such as Nuclear Energy/Weapons, thermal physics, electrical engineering and Material Science/Legal forensics to name a few. The arc-fault generator system also includes a high-temperature sensor for monitoring bulk temperatures of adjacently-positioned conductor materials, conductors and plasmas. This information can be used to determine a variety of physical and chemical phenomena of a degraded material.

In several experimental investigations 100 W and 300 W (with 900W possible) constant power curves were evaluated for the destructive testing of various polymer sheaths exposed to plasma discharges [109, 42]. These values were chosen to demonstrate the viability of low power discharges causing polymer ignition in common PV materials [109]. A partial list of arc-fault tests is shown in Table A2.1, where the entirety can be found by work by Armijo et al., [109]. Each test was performed at least 5 times to determine fire ignition times as well as to evaluate the ease of initiating and sustaining an arc [56]. For test purposes, each annular test piece (sheath), with a 0.125 inch wall thickness, 0.75-inch length, and 0.25-inch internal diameter was inserted over the two electrodes. For this apparatus, the electrodes–one moveable (anode) and one stationary (cathode)–were made of solid copper. The electrodes were separated using a lateral adjustment of the moveable electrode to the desired gap spacing.

Table A2–1. Summary of arc-fault experiments with PV simulator and arc-fault generator in a polycarbonate sheath [110].

Test Number	Arc Power	Electrode Diameter	Electrode Tip	Hole	Avg. Fire Ignition Time [Sec.]	Standard Deviation Fire Ignition Time [Sec.]
1 (UL 1699B)	300 W	1/4″	Flat	No	14.6	10.7
2	300 W	1/4″	Flat	Yes	11.8	5.9
3	300 W	1/4″	Flat	No	14.1	9.0
4	100 W	1/4″	Flat	No	69.0	41.1
5	100 W	1/4″	Flat	Yes	22.0	12.7
6	100 W	1/4″	Round	Yes	107.0	17.0
7	100 W	1/8″	Flat	Yes	21.7	4.5
8	300 W	1/8″	Flat	Yes	10.3	4.0

In addition, a set of test specimens were machined with a small centralized hole to assess combustion rates with an increased presence of oxygen. The hole simulated an arc-fault open to the atmosphere versus an arc-fault contained in the module, connector, or other self-contained area within the array. The polymer specimens were placed halfway over the stationary electrode and the moveable electrode was then adjusted to the appropriate gap distance from the stationary electrode. During each test, power was applied until the sample pyrolyzed by setting the electrode

gap appropriately to sustain the arc. A UL-listed smoke detector was also installed just above the arc-fault generator and high-speed video recordings were collected to determine the first instance of smoke and subsequent combustion of the sheath material.

A2.2 Degradation of Materials with Plasma Exposure

More than 100 parameterized arc-fault experiments were performed using the test system, though for this paper results will be presented that cover just tests for polycarbonate materials. A sample of one of the experimental results can be seen in Figure A2–4 for a 100 W arc with a 0.25 inch diameter polycarbonate sheath, containing a 0.25 inch hole for air ingress. The data indicates steadily increasing temperatures as the polycarbonate sheath reacts to the plasma arc.

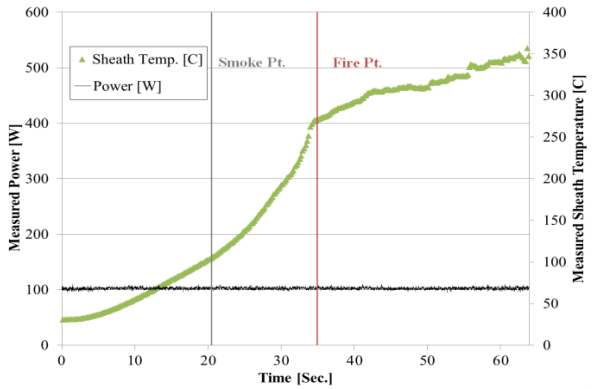

Figure A2–4. 100 W arc-fault test results using a 0.25-inch diameter polycarbonate sheath that includes a 0.125-inch hole. The arc-fault was established at time = 0 s [110].

The arc-fault videos obtained from the digital camera were converted into a series of frames so the time to polymer melting, smoke formation, and fire were either validated or determined from measurements (i.e. thermocouples and smoke detector), Figure A2–5. In the majority of the 100 W arc-fault tests the time to reach smoke and fire combustion was greater than 20 seconds. While a small number of tests did not reach the fire ignition point, it was clear that 100 W arc-faults are capable of causing fires in PV systems. Additional parametric results for other tests can be found in Armijo *et al.* [109].

For the tests with polycarbonate sheaths, the average time to detect smoke was 9.4 s with a minimum value of 2.5 s, while the average time to detect fire combustion was 33.8 s. In situations where the polymer did not combust, the sheath and electrodes heated up to the point that the sheath melted off the hot electrodes.

Figure A2–5. Polycarbonate tube with no hole example test. Possibly fire ignition at 7.26 s, but no sustained external flame until after 92.04 s.

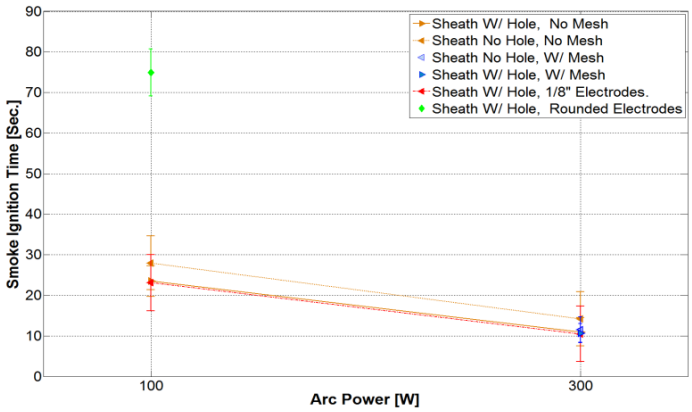

Figure A2–6. Parametric arc-fault tests using 0.125 inch and 0.25 inch diameter copper electrodes, for 100 W and 300 W arc discharges, with and without oxidation holes and arc initiation wire mesh [110].

The results in Figure A2–6 indicate that a difference of 1.7% and 4.7% in smoke ignition times between electrode diameters of 0.25 inches and 0.125 inches, for respective 100 W and 300 W power levels. Reducing the electrode diameter constrains the air volume for plasma discharge, which impacts off-gas concentrations of reactive species, surface chemical reactivity [115], as well as the respective ionization potential [116] to initiate the arc.

The results between the flat and rounded-tip electrodes found a 17.4% reduction in smoke ignition time, as well as a 26.6% decrease in measured smoke ignition sheath temperatures, respectively [109]. An example arc-fault test with thermocouple data is shown in Figure A2–7. The rounded-tip increased arc stability because the plasma stream remained at the minimum gap distance at the

center of the electrodes; whereas with the flat electrodes the arc would jump to different locations on the coplanar electrode faces. This effect was associated with an increase in the visible ignition time by as much as 35.5% and average external sheath ignition temperature as high as 260.6 °C, shown in Figure A2–7 [109]. It is postulated that the rounded-tip electrodes constrain the arc plasma stream to the radial center of the electrode cavity and therefore the polymer is exposed to lower initial temperatures during arc-fault tests due to reduced contact with the plasma stream. These types of electrodes were found to have more uniformly distributed heating of the electrodes and polymer material, which would eventually melt into the arc gap and induce fire ignition. For flat electrodes, the arc was often found to be located against the surface of the polymer which intensified localized heating and polymer degradation, often with higher temperatures [109].

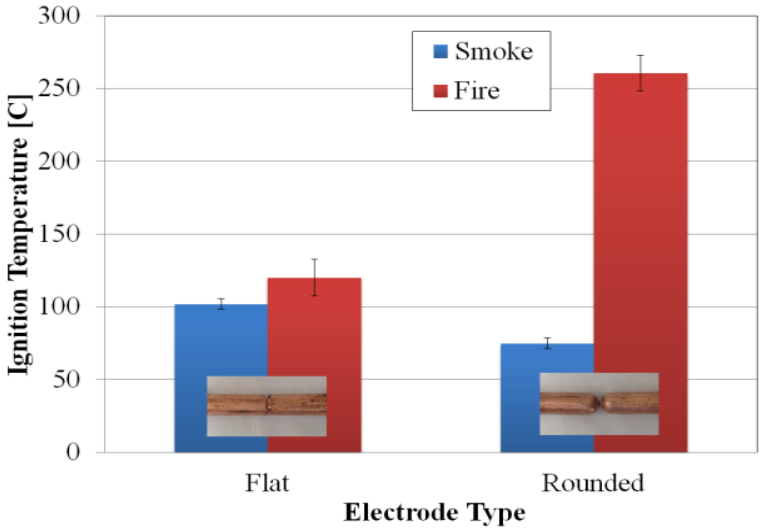

Figure A2 –7. 100 W rounded-tip electrodes arc-fault test with a polycarbonate sheath, with a 0.125-inch hole, and no steel wool tuff [109]

Additionally, the inclusion of a small centrally-located 0.125-inch hole suggested improved arc sustainability for both 100 W and 300 W power levels. The results showed a 16.1% and 22.9% decrease in ignition times for the respective 100 W and 300 W polycarbonate tests with the inclusion of the hole. Previous research by Pandiyaraj et al., [117] also found increased oxygen levels increased plasma/surface interfacial chemical potentials, which influence ionization potentials and the capability for ignition [118].

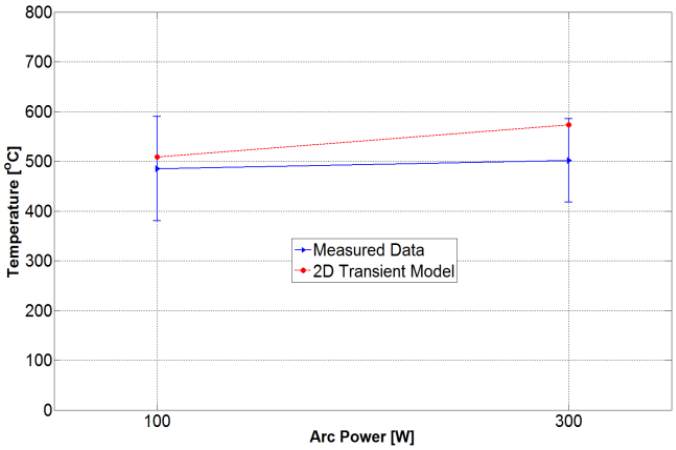

Figure A2–8. Outer polycarbonate sheath temperature comparison between simulated and the average of the measured data for 100 and 300 W arc-faults after the average arc-extinguish time period [110]

As shown in Figure A2–8, analysis of the transient 2D model revealed good agreement with experimental data with a uniform polycarbonate sheath, without the inclusion of a hole or arc ignition mesh. The 100 W input power-level exhibited a 4.9% uncertainty and the 300 W case had 14.2% uncertainty after 69 s which was the average arc-extinguish time period.

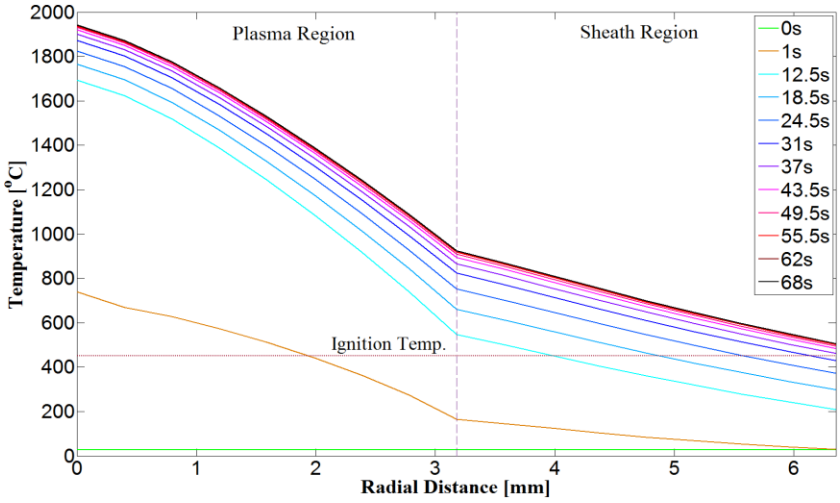

Figure A2–9. Simulated plasma and polycarbonate sheath region temperatures for a 100 W input power level, within air ambient conditions and a pressure of 1 atm [110]

Due to the approximation of a constant electric field across the electrode gap, average low temperature variations of 0.87% and 0.68% were found across the respective plasma and sheath regions. However, larger radial variations were found, where average temperatures of 788.7 °C and 346.7 °C were observed across the plasma and sheath regions respectively.

In this analysis the time duration of the simulation was based on respective experimentally recorded times. Overall, in an unmitigated arc-fault, without an AFCI device, the results indicate a significant danger as the predicted outer sheath temperatures can rise above the polycarbonate

auto-ignition temperature of 450 °C [119]. The model suggests that these temperatures can be as high as 508.96 °C after approximately 60 s for a low 100 W power level. Experimental observations confirm the polymer fires after this time period, and in some cases much quicker if the interior polymer material melted into the plasma stream.

Table A2–2. Model of predicted transient polycarbonate material temperatures (°C) for increasing power levels, 100-1200W [110].

Arc Power [W] \ Arc Duration Time [sec.]	0.20	0.40	0.63	0.83	1.15	1.50	2.00	4.00	6.00	8.00	10.00
100	25.79	27.03	33.06	41.94	61.23	86.90	128.03	297.40	425.27	499.96	538.53
300	25.91	28.87	40.87	58.66	98.42	153.16	242.46	556.19	694.35	743.50	760.65
500	26.05	30.78	49.15	76.87	140.46	229.68	372.76	754.14	861.42	890.81	898.93
650	26.13	32.00	54.49	88.81	168.60	280.93	455.90	846.23	936.74	958.79	964.23
900	26.27	33.99	63.38	108.97	216.57	367.08	584.86	961.27	1031.54	1046.20	1049.29
1200	26.44	36.37	74.23	133.93	276.20	470.04	719.73	1062.64	1116.78	1126.49	1128.25

Material Under Non-Destructive State
Material Undergoing Melting
Material Undergoing Fire Ignition

UL 1699B AFCI Maximum Trip Time
T_{melt} = 155°C
$T_{ignition}$ = 450°C

After validating the model with the experimental data from the 100 and 300 W arc-faults, the simulation was used to predict the burn times for higher power arc-faults. These arc-faults may occur on the output circuits of PV systems either after the combiner or recombiner box where currents can be between 15 and 500+ amps. In these locations, if there is a failure in the conductor or connector, either an arc flash will explosively damage the faulted region or—for lower currents—a sustained arc-fault will occur. UL 1699B only requires tests from 300-900 W, but the model was used to more broadly predict fire risk for 100–1200 W arc-faults. To evaluate this risk, the outer sheath temperature was calculated and compared to the ignition temperature for polycarbonate. The temperatures shown in Table A2.2, are the average (bulk) polymer temperature, which the median radial temperature through the sheath. As the arc power increases there is less time before the polymer reaches the ignition temperature. Also, these results suggest increasing arc-power levels can have impacts on ignition time scales, which requires rapid and accurate AFCI responses. UL 1699B defines the maximum AFCI trip time according to Eqn. A3.1.

$$t_{trip} = min\left(2, \frac{750}{i_{arc} \cdot V_{arc}}\right) \quad \text{(A3.1)}$$

These trip times have been included in the table to determine polymer temperatures at the point when AFCIs must de-energize the arc-fault. As can been seen in the table, the trip times are sufficient to prevent the combustion of polycarbonate. The burn times of other PV polymer materials will differ based on their heat transfer properties and ignition temperature. If the AFCI fails to trip within the required period, the temperature of the polymer quickly reaches the combustion point so it is critical for these devices to effectively detect and mitigate the arc-fault.

A2.3 Optical Emission Spectrum Analysis

To further validate the model, understand the plasma discharge process, and predict material degradation mechanisms, measurements of the plasma electron temperature are necessary. Recent work indicates the optical emission spectrum of plasmas can be analyzed to calculate the electron plasma temperature [120]. This analysis was used to develop a method for validating the electron

temperature of the plasma as well as the plasma thermal model, which could provide insight into the destructive nature of the arc plasma discharge. For this study, optical spectra of the arc plasma were acquired using an Ocean Optics S2000 fiber spectrometer, which consisted of an integrated linear silicon CCD array and miniaturized optical bench. The spectrometer had a resolution of 0.33 nm, and a spectral measurement range of 340-1019 nm. The plasma spectra were optically coupled to the spectrometer using a diffusive cosine corrector free-space to fiber adapter. The position of the detector was adjusted relative to the arc to avoid saturation. A spectrum integration time of 100 ms was used, with a series of over 100 spectra captured per arc discharge trial to examine the change in emission and plasma conditions as a function of time.

Spectra were analyzed for 100 W and 300 W arcs using a polycarbonate sheath with and without a hole. From Figure A2–10 the optical spectra for both arc discharge power levels correspond to atomic emission lines from singly ionized copper ions, which emanate from the electrodes. However, further study is needed to validate the degree of ionization and dissociation of ions in the plasma, which could affect the temperatures and optical emission for varying plasma conditions.

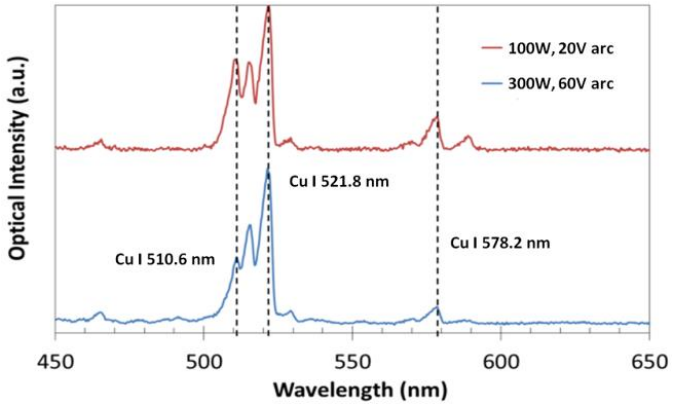

Figure A2–10. Optical intensity emission spectra analysis for 100 W & 300 W arc power levels [110]

Changes in the emission line ratios were observed for the 522, 515 and 511 nm peaks between the two electrical power levels. It is postulated that these changes could correspond to differences in the plasma equilibrium and mean excitation levels of the copper ions, as would be expected for different excitation voltages that were employed, which were 20 and 60 V respectively.

An examination of the plasma emission for the 100 W power level as a function of time was also performed, with the results shown in Figure A2–10. The chorological spectrum numbers contain information for 100 ms time bins. Interestingly, the emission line ratios provide a clear indication of arc discharge characteristics. For the 300 W case, the emission line ratios were roughly constant as a function of time during the arc. During the 100 W arc discharge increases of 24% and 30% were observed for the 511/522 and 511/515 ratios, respectively. These increases indicate rising plasma temperatures as a function of time, but further investigations are needed for quantitative analysis.

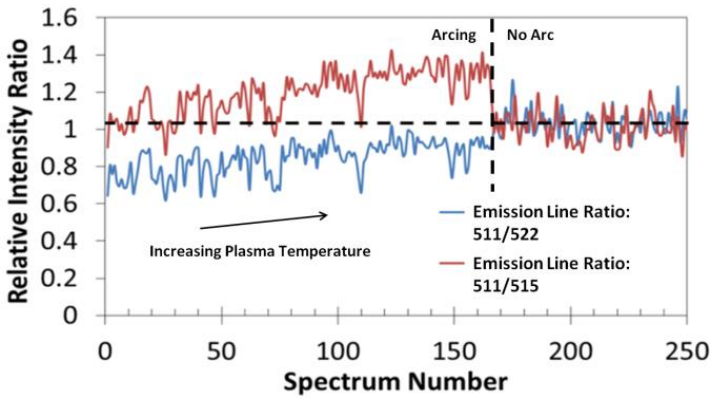

Figure A2–11. Emission line ratio analysis for a 100 W arc power level, with emission line ratios evaluated for 511 nm/522 nm and 511 nm/515 nm peak pairs [110]

An examination of the plasma emission for the 100 W power level as a function of time was also performed, with the results shown in Figure A2–11 provided as a spectrum number in the sequence of acquisition. Interestingly, the emission line ratios identified provide a clear indication of arc discharge by their correlation. For the 300 W case, the emission line ratios were roughly constant as a function of time during the arc. During the 100 W arc discharge increases of 24% and 30% were observed for the 511/522 and 511/515 ratios, respectively. These increases suggest potential rise in plasma temperatures as a function of time, however further investigation is needed for thermal validation. The detected emission lines correspond to singly ionized copper ions in the arc column, but further testing and analysis will be needed to evaluate the degree of dissociation and ion excitation, which can impact the plasma composition and temperature.

During these tests, the acquisition of optical spectra was stopped after the arc self-extinguished. The extinction of the arc is clearly seen in the data when the emission line ratios fall to random correlation oscillating around one corresponding to the background electrical and optical noise.

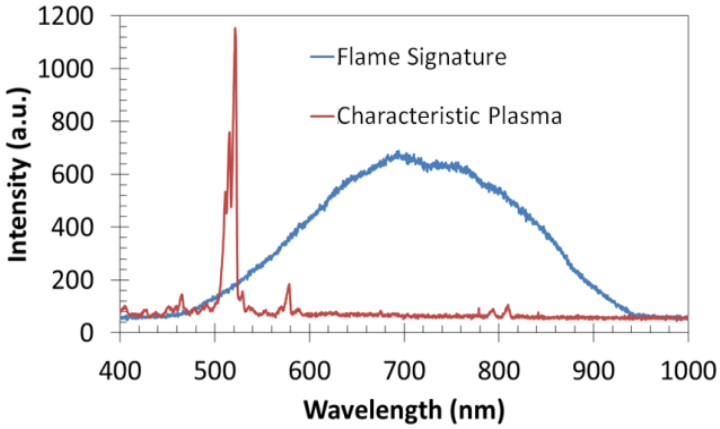

Figure A2–12. Optical intensity emission spectra analysis for 100 and 300 W arc-faults [110]

Finally, optical emission spectra were compared for the 300W arc discharge of copper electrodes surrounded by a sheath with and without a hole, shown in Figure A2–12. For the arc discharge utilizing a continuous sheath, optical emission corresponding to a flame signature was observed after the arc was extinguished and when the fire ignition point was reached. Here, we see a dramatic difference between characteristic plasma emission from the sheath containing a hole (red line), and the blackbody optical emission corresponding to the burning plastic sheath (blue line).

These signals could provide an additional metric for identifying the onset of arc discharge or fire.

For the arc discharge utilizing a continuous sheath, optical emission corresponding to a flame signature was observed after the arc was extinguished and when the fire ignition point was reached. Here, we see a dramatic difference between characteristic plasma emission from the sheath containing a hole (red line), and the blackbody optical emission corresponding to the burning plastic sheath (blue line). These signals could provide an additional metric for identifying the onset of arc discharge or fire.

A deeper analysis of the plasma emission from bare copper electrodes revealed that plasma temperatures can be determined from arc discharge optical emission spectroscopy using a Boltzmann plot of the measured line emission intensities against the transition ionization energies [121]. The slope of this plot is the temperature of the plasma. Figure A213 shows an example of a derived temperature using the Boltzmann plot method.

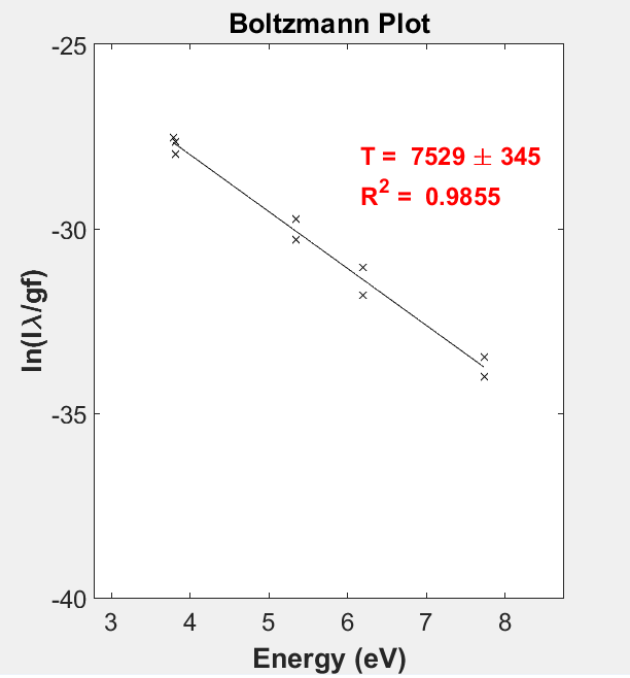

Figure A2–13. Boltzmann plot and derived temperature for a copper plasma arc-discharge.

Figure A2–14 shows an example of a measured spectrum from a bare copper atmospheric pressure arc discharge and the plasma temperature determined from the relative peak intensities for copper emission as a function of time.

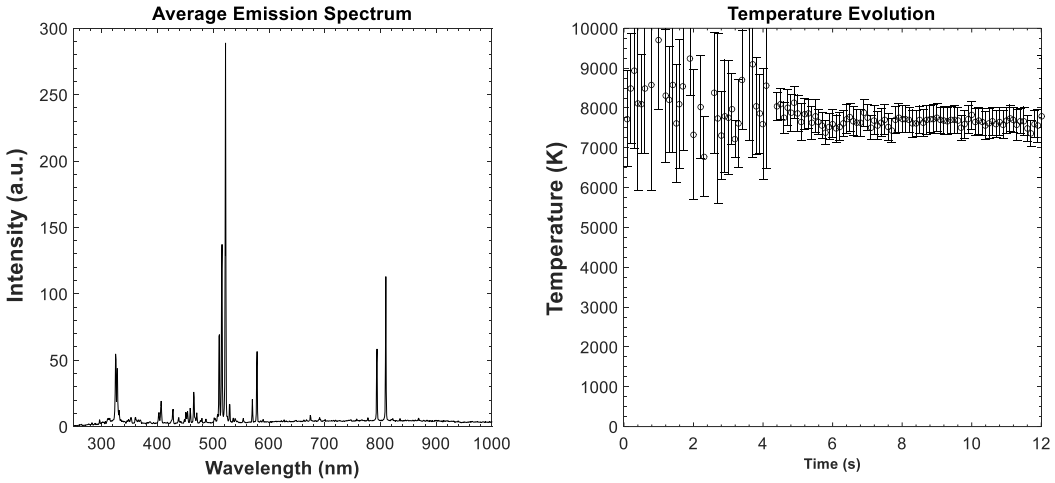

Figure A2–14. Optical intensity emission spectrum and derived temperatures for a copper plasma arc-discharge

The measured optical emission spectrum can also be used to identify the elements in the arc discharge plasma. Indeed, plasma optical emission spectroscopy is a commonly used method in materials analysis. Figure A2–15 shows the identification of iron and chrome emission lines in an arc discharge from nickel alloy steel electrodes.

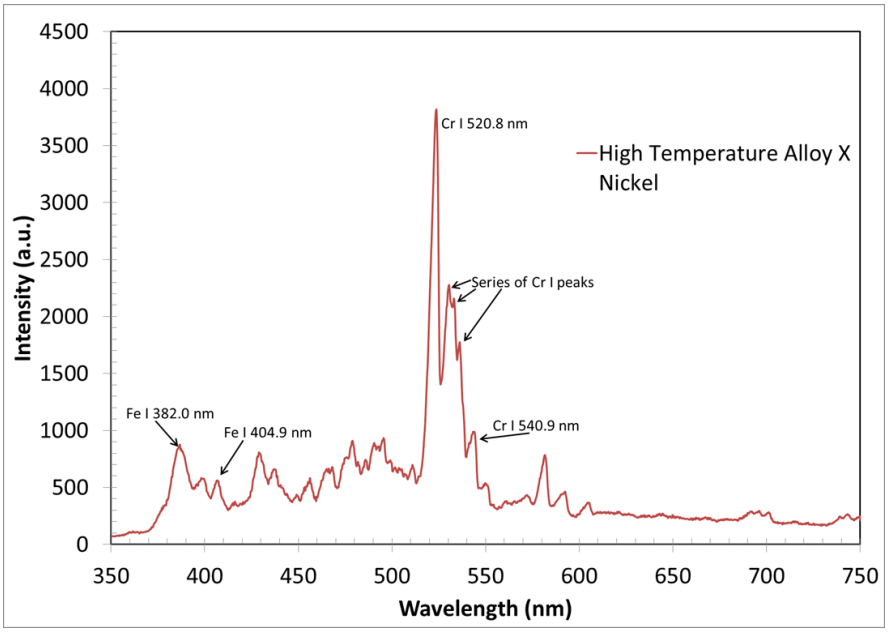

Figure A2–15. Optical intensity emission spectrum for a nickel alloy steel arc discharge showing the emission from constituent elements in the plasma

A2.5. Chemical Degradation Analysis

To further understand the degradation mechanisms of the varying polycarbonate geometries exposed to the arc plasma, the samples were cut open and subjected to Attenuated Total Reflection Fourier Transform Infrared Spectroscopy (ATR FTIR) analysis. ATR FTIR experimental results of the polycarbonate samples exposed to arc-faults each showed markers in the IR spectra, identified as indicators of thermal polymer decomposition. These markers were specific peaks in

the spectra that either corresponded to a reduction of a functional group in the control polymer (unburned sheath), or the appearance of new functional groups found in well-established decomposition products.

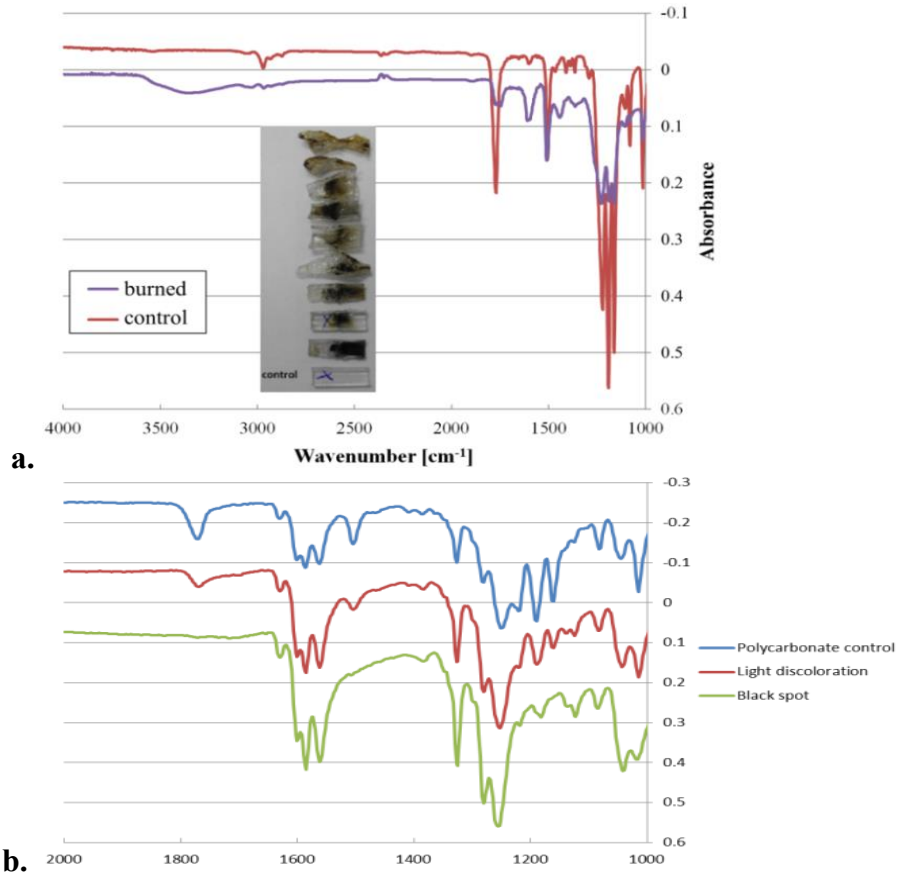

Figure A2–16. IR spectral analysis of polycarbonate (PC) experimental and control sheaths [110]

IR spectra were taken at several spatial positions on the samples with varying discoloration in order to determine the extent of the thermal oxidation reactions. Figure A2–16 shows IR spectra from an unburned polycarbonate control sample and a polycarbonate sample exposed to an arc-fault. The two most obvious changes in these samples are:

1. The appearance of a broad peak between 3100 and 3500 cm^{-1}.
2. The diminishment of the sharp peak at 1772 cm^{-1}.

The former is indicative of O-H stretching and the latter is due to reduced C=O stretching in a carbonate group. In the top reaction, polycarbonate was oxidized to give a phenol and a methyl ketone as products. In the bottom reaction, polycarbonate undergoes a loss of carbon dioxide to give an aryl ether product [122].

This chemical analysis shows that oxidation reactions (combustion) occur during the arc fault tests and changes in the appearance of the polymers are not only from melting. From Figure A2–17, it

is postulated that excess air enabled a fast, hot burn, while the closed-sheath tests ignited much slower. The products formed from the faster burn time typically had a narrower range of products than if the combustion took place over a longer period of time. Therefore, extra oxygen would provide a different reaction pathway from a closed-sheath. These results indicate two of these potential degradation pathways the polycarbonate sheaths may have undergone during testing which may explain the optical emission differences in signatures.

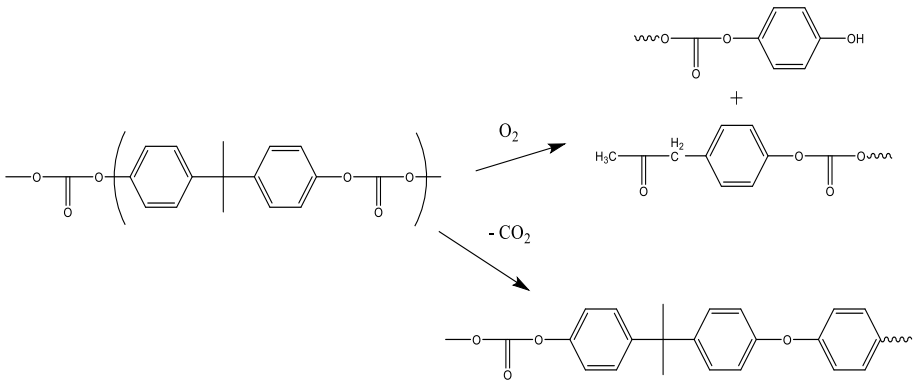

Figure A2–17. Thermal decomposition pathways for polycarbonate [110].

A2.6. Self-Extinguishing Materials

Although attempts have been made to develop devices and compounds for rapid extinguishment of fires, none have been developed to extinguish fires and even high-temperature thermal arc plasmas. Very few polymers are naturally self-extinguishing, and most ignite quite easily when exposed to a flame. In particular acrylates, which are commonly used for molded or extruded sheets, paints and shellacs, are highly combustible and very difficult to render flame retardant, even with the addition of large amounts of conventional flame retardant (FR) agents, such as halogenated compounds, phosphorus and inorganic materials. Additionally, reducing annual electrical device and system degradation rates and eliminating potential safety hazards attributable to inadequate existing encapsulant or potting technologies are critical objectives for many initiatives that would improve safety and reliability to help promote ubiquitous deployment of PV systems. Research by Spoerke et al. [123] has been to incorporate transparent layered composite thin film (LCTF) encapsulant materials to address several significant challenges to functional electrical device lifetime and safety, both factors that directly affect ultimate electrical system costs. Formed through a deliberate, layer-by-layer process, these highly organized, anisotropic materials have remarkable oxygen and moisture barrier properties that exceed those of currently utilized encapsulants. In addition to the improved barrier properties of such new encapsulants, these composite thin films exhibit remarkable flame retardant properties. With the increased deployment of outdoor systems such as PV, there is a very real need to address the hazards of electrical system-related fires, such as those resulting from arc-faults in these high voltage systems. The Sandia team is currently investigating various approaches for leveraging these LCTF barrier films to not only improve reliability through moisture-barrier enhancement, but to also dramatically improve system resistance to arc-fault fires. Initial demonstrations conducted at Sandia on composite films produced at Texas A&M have already shown a remarkable resistance to ignition in simulated electrical arc-plasma tests. For initial materials studies, annular test substrates modified with LCTF coatings were placed over two solid copper electrodes. With power applied to

the system, plasma arcs (300 W) were exposed to test substrates. Sample temperatures were measured and high-speed video recordings were used to characterize time to smoke and time to ignition of test samples. The test module structures were systematically cut or broken and arranged to simulate arc-fault initiation in realistically arc-susceptible PV elements, such as a failed bus bar. This approach provides direct insight into the ability of LCTFs to prevent arc-fault initiation in a functioning electrical, high-voltage system. Preliminary tests on annular test samples have shown that time to flame more than doubles for LCTF films on polyethyleneterephthalate (PET) relative to the uncoated PET substrate. By optimizing these materials through modification of clay content, composition, and organization in the LCTF films, the Sandia team has built on these promising results, targeting a 10-fold increase in time to flame over extinction of the arc by melted substrate to ensure significant improvements in arc-fault-related safety, Figure A2–18.

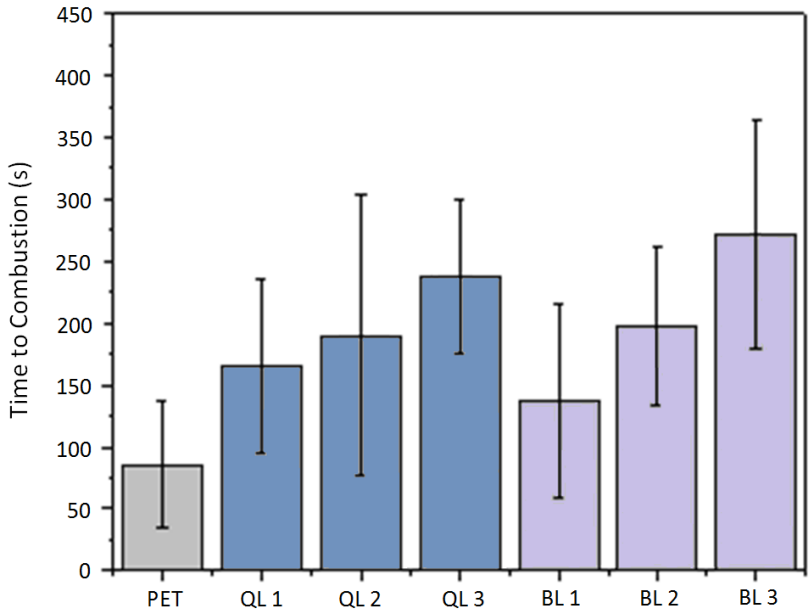

Figure A2–18. Arc-Fault combustion time for seven different polymer test configurations [123].

APPENDIX A3. A CONSOLIDATED PROCEDURE FOR PERFORMING AN ARC-FLASH ANALYSIS

The following steps outline a suggested procedure for performing an arc flash analysis of a facility. Although this is not the only possible procedure, it does cover a wide range of conditions, and takes a conservative approach to the application of both IEEE 1584 and NFPA 70E equations.

1. *Assemble existing as-built documentation* — Start by collecting all of the relevant, existing as-built documentation. Include power floor plans showing locations of electrical equipment, and single-line diagrams indicating the overcurrent protective devices and cable sizes for all relevant areas.
2. *Field verify existing conditions* — Because conditions may have changed because the original installation, it is critical that the existing conditions be field verified to ensure that the arc flash analysis is performed using accurate breaker settings and field conditions.
3. *Obtain the available utility fault current (range) and X/R ratio* — The serving utility should be able to provide this information. Note that the utility normally guarantees a range of short-circuit current, and that the highest arc flash energy value may occur anywhere within the range of available short-circuit current values.
4. *Perform a short-circuit analysis* — The short-circuit analysis must be performed to obtain the available bolted-fault and arc-fault currents at each point in the system.
5. *Perform an NFPA 70E arc flash analysis* — Perform the arc flash analysis using the NFPA 70E equations and parameters.
6. *Perform an IEEE 1584 arc flash analysis* — Perform the arc flash analysis using the IEEE 1584 equations and parameters.
7. *Repeat steps 4 through 6 for the entire range of possible values* — The short-circuit and arc flash studies must be repeated over the entire range of valid utility fault capacities. The studies may be performed in a range of fault increments to ensure that the highest arc flash energy value is captured at each component. For example, a system that has a fault value ranging from 3,000A through 12,000A may be run in 1,000A increments.
8. *Repeat steps 4 through 7 for all likely operating conditions* — The report must be run for all likely operating conditions for the facility, including normal operation, load shedding modes, parallel operation, tie breakers open and closed, and operating on standby power. It is important that all configurations be fully evaluated to ensure that the worst-case scenario is developed for each piece of equipment.
9. *Eliminate invalid data* — Export the arc flash reports to spreadsheet software, and delete invalid values because they do not fall within the range of valid conditions for the equation set used (i.e. NFPA 70E values calculated from short-circuit currents that are not between 16kA and 50kA as required).
10. *Sort the worst-case values for each component or bus* — Using a spreadsheet, the remaining valid values may be sorted and the worst-case extracted for each component within the system. This value will be considered the available arc flash energy at its associated point in the system.
11. *Assemble the comprehensive report* — The final report should indicate the available short-circuit current used at each component, the available arc flash energy, the

category of PPE required to safely work on the equipment, and which set of equations was used to determine the available energy. The report should also include the working distance used in the calculation, and the flash protection boundary (generally the threshold where the available energy exceeds 1.2 cal/cm2). In addition, any information that your specific client requires (duration of arc, closing time of breaker, equipment required for safe operation, etc.) should be included in the report.

APPENDIX A4. ARC-FAULT/ARC-FLASH DEFINITIONS AND TERMINOLOGY

1. **Arc-flash hazard:** A dangerous condition associated with the release of energy caused by an electric arc.
2. **Arc-fault current:** A fault current flowing through electrical arc plasma, also called arc-fault current and arc current.
3. **Available fault current:** The electrical current that can be provided by serving utility and facility-owned electrical generating devices and large electric motors, considering the amount of impedance in the current path.
4. **Bolted fault current:** A short circuit or electrical contact between two conductors at different potentials in which the impedance or resistance between the conductors is essentially zero.
5. **Circuit:** A conductor or system of conductors through which an electric current is intended to flow.
6. **Electrical hazard:** A dangerous condition in which inadvertent or unintentional contact or equipment failure can result in shock, arc-flash burn, thermal burn, or blast.
7. **Electric Shock:** Physical stimulation that occurs when electrical current passes through the body.
8. **Energized:** Electrically connected to or having a source of voltage.
9. **Exposed (live parts):** It is applied to parts that are not suitably guarded, isolated, or insulated.
10. **Fault current:** A current that flows from one conductor to ground or to another conductor due to an abnormal connection between the two.
11. **Flash hazard analysis** A method to determine the risk of personal injury as a result of exposure to incident energy from an electrical arc flash.
12. **Flash-protection boundary:** An approach limit is a distance from live parts that are un-insulated or exposed within which a person could receive a second degree burn.
13. **Incident energy:** The amount of energy impressed on a surface, a certain distance from the source, generated during an electrical arc event. Incident energy is measured in joules per centimeter squared.
14. **Shock hazard:** A dangerous condition associated with the possible release of energy caused by contact or approach to live parts.
15. **Arc Blast:** The explosive result of an arcing fault. As current begins passing through ionized air, large volumes of ionized gases, along with metal from the vaporized conductors, are rapidly expelled, creating such hazards as intense heat, thermoacoustic shock wave, molten metal, shrapnel, blinding light, toxic smoke and contact with energized components.
16. **Current limiting fuse:** A UL Listed, current-limiting fuse must clear a short circuit current in less than one half cycle. By isolating a faulted circuit before the fault current has sufficient time to reach its maximum value, a current-limiting fuse tremendously limits the total electrical energy delivered to the fault, reducing both the magnitude and duration of a fault current.
17. **Short circuit:** An electrical malfunction where current takes the path of least resistance to ground, Current flow is excessive from low resistance resulting in a blown fuse.
18. **Interrupting capacity:** The interrupting capacity is the maximum value of current that

a contact assembly is required to successfully interrupt at a specified voltage for a limited number of operations under specified conditions.

19. **Arc clearing time:** The time from the onset of the arcing current to the moment the arc is extinguished. The clearing time is comprised of three separate variables: the time it takes for the protective device to "sense" the fault, the mechanical operating time of the protective device (circuit breakers or fuses), and the time it takes for the protective device to extinguish the arc.
20. **Arcing fault current:** A fault current flowing through an electrical arc plasma, also called arc-fault current and arc current.
21. **Arc-in-a-box:** The estimated incident energy for an arc in a cubic enclosure with sides of 20 in.
22. **Arc rating:** The maximum incident energy resistance demonstrated by a material (or a layered system of materials) prior to break-open or at the onset of a second-degree skin burn. Arc rating is normally expressed in calories per square centimeter.
23. **Available fault current:** The electrical current that can be provided by a serving utility and facility-owned generation devices and large electrical motors, considering the amount of impedance in the current path.
24. **Bolted fault current:** A short circuit or electrical contact between two conductors at different potentials in which impedance between the conductors is essentially zero.
25. **Electrical hazard:** A dangerous condition in which inadvertent contact or equipment failure can result in shock, arc flash burn, thermal burn, or blast.
26. **Exposed:** Capable of being inadvertently touched or approached nearer than a safe distance by a person. It is applied to parts that are not suitably guarded, isolated, or insulated.
27. **Fault current:** A current that flows from one conductor to ground or to another conductor through an abnormal connection (including an arc) between the two.
28. **Flame-resistant (FR):** The property of a material whereby combustion is prevented, terminated, or inhibited following the application of flaming or non-flaming source of ignition — with or without removal of said flaming source.
29. **Flash hazard analysis:** A method to determine the risk of personal injury as a result of exposure to incident energy from an electrical arc flash.
30. **Flash protection boundary*:*** An approach limit at a distance from live parts that is un-insulated with which a person could receive a second-degree burn. This is defined as incident energy levels of 1.2 cal/cm^2 or more.
31. **Incident energy:** The amount of energy impressed on a surface, a certain distance from the source, generated during an arc event. Incident energy is measured in joules per square centimeter or calories per square centimeter.

DISTRIBUTION

1 Kenneth Hamburger
U.S. Nuclear Regulatory Commission
RES/DRA/FXHAB
Mail Stop: TWFN 10A12
Washington, D.C., 20555-0001

1	MS0748	Chris B. LaFleur	06231
1	MS0748	Alice B. Muna	06231
1	MS0889	Eric J. Schindelholz	01852
1	MS0968	Richard K. Harrison	05754
1	MS1033	Abraham Ellis	06112
1	MS1033	Jay Johnson	06112
1	MS1127	Kenneth M. Armijo	06123
1	MS1127	Clifford Ho	06123
1	MS1136	Olga Lavrova	06112
1	MS1136	Salvador Rodriguez	06221
1	MS0899	Technical Library	09536 (electronic)


Sandia National Laboratories